Université du Québec en Outaouais

Département d'informatique et d'ingénierie

Développement de Nouveaux Types de Ligne de Transmission à Base d'Inclusions/Cellules Métamatériaux et leurs Applications Potentielles

Par

Ousama Abu Safia

Thèse présentée au Département d'informatique et d'ingénierie

Pour l'obtention du grade de

PHILOSOPHIAE DOCTOR (Ph.D)

En sciences et technologies de l'information

Jury d'évaluation

Président du jury:	Prof. Luigi Logrippo, Ph.D
Directeur de recherche:	Prof. Larbi Talbi, Ph.D
Co-directeur de recherche:	Dr. Khelifa Hettak, PhD
Examinateur interne:	Prof. Michael Korwin-Pawlowski, PhD
Examinateur externe::	Dr. Nouredine Outaleb, PhD
Examinateur externe:	Prof. Abdel Razik Sebak, PhD

Gatineau, Québec, Canada, 2014

Résumé

Développement de Nouveaux Types de Ligne de Transmission à Base d'Inclusions/Cellules Métamatériaux et leurs Applications Potentielles

Par

Ousama Abu Safia

Les métamatériaux sont des matériaux artificiels qui ont des propriétés physiques et électriques inexistantes dans les matériaux conventionnels. Il existe deux approches principales de conception des composants micro-ondes à base de métamatériaux: l'approche de type résonance et l'autre approche de type ligne de transmission artificielle. Dans cette thèse, de nouvelles cellules et inclusions métamatériaux basées sur les deux approches de conception mentionnés sont proposées. Ces inclusions et cellules ont de nombreux avantages par rapport aux implémentations conventionnelles et remédient à de nombreuses limitations inhérentes à des inclusions et cellules bien connues de la littérature.

L'avantage d'utiliser des lignes de transmission de type coplanaires (CPW) et leurs discontinuités associées génèrent de nouvelles inclusions métamatériaux résonantes. Ces nouvelles inclusions sont simulées, fabriquées, testées et appliqués dans plusieurs circuits micro-ondes afin de valider leurs potentialités. De plus, ce travail propose une nouvelle inclusion métamatériau bi-bande basé sur une technique hybride qui consiste à combiner les deux techniques précitées.

Enfin, de nouvelles lignes de transmissions artificielles basées sur les éléments distribués ayant des réponses non dispersives et/ou contrôlables en fonction de la

fréquence sont introduites. Ces nouveaux éléments sont implémentés dans trois circuits micro-ondes, à savoir, anneau résonateur bi-bandes, filtre passe bande large bande, et coupleur hybride bi-bandes. Les trois applications montrent en evidence le potentiel de ces nouveaux éléments.

University of Quebec in Outaouais

Department of Computer Science and Engineering

Development of New Types of Transmission Line-Based Metamaterial Inclusions/Cells and Their Applications

by

Ousama Abu Safia

A thesis presented to the University of Quebec in Outaouais in fulfillment

of the thesis requirement for the degree of Doctor of Philosophy in

Science and Information Technologies

(Emphasis: Microwave Engineering)

Committee members

Chairman:	Prof. Luigi Logrippo, Ph.D
Research advisor:	Prof. Larbi Talbi, Ph.D
Research co-advisor:	Dr. Khelifa Hettak, PhD
Internal examiner:	Prof. Michael Korwin-Pawlowski, PhD
External examiner:	Dr. Nouredine Outaleb, PhD
External examiner:	Prof. Abdel Razik Sebak, PhD

Gatineau, Quebec, Canada, 2014

Abstract

Development of New Types of Transmission Line-Based Metamaterial Inclusions/Cells and Their Applications

By

Ousama Abu Safia

Metamaterials are artificial materials which have physical and electrical properties not existing in natural materials. There are two main design approaches for metamaterial-based microwave devices: the resonance-type approach and the artificial transmission line approach. In this thesis, new metamaterial cells and inclusions based on the two aforementioned design approaches are proposed. These inclusions and cells have many advantages over conventional implementations and overcome many limitations related to well-known inclusions and cells found in the literature. The advantage of using coplanar waveguide (CPW) transmission lines and their discontinuities are utilized. These new inclusions are modeled, simulated, fabricated, tested, and applied into several microwave circuits and antennas to validate their potentiality. Also, this work proposes a novel dual-resonant metamaterial inclusion based on a new hybrid technique that combines the two aforementioned approaches for the first time. A detailed design procedure, and a semi-distributed model for the inclusion were proposed. Several applications to filters and antennas design were presented in order to validate the new inclusion and the hybrid technique.

Acknowledgments

I would like to acknowledge the support and cooperation I received throughout the time I have spent on this thesis:

First of all, I would like to gratefully acknowledge my promoters and supervisors, Prof. Larbi Talbi, and Dr. Khelifa Hettak for their excellent guidance and encouragement. Prof. Talbi was very generous with me in the last three years. Besides his academic supervision, he has been supporting me financially during my PhD study. Also, he gave me the opportunity to attend several national and international conferences. Moreover, Prof. Talbi supported my applications for many national scholarships, and several internal scholarships from UQO. He was very flexible and understandable to my personal life situations and circumstances. I will always be inspired by his nobility.

On the other hand, Dr. Khelifa's comments, suggestions and corrections were very valuable to my research progress. Also, he gave me an excellent course in RF technologies and systems. This course helped me to set strong theoretical and technical bases for this dissertation.

I would like also to thank my colleagues in the laboratory: Dr. Tahar Haddad, Dr. Mohammad Ghaddar, Vincent Fono, Betty Savitri, Dr. Ismail ben Mabrouk, and Jamal Abdali for the long hours of pleasant talks and discussions.

I would also like to thank Professor Michael Korwin-Pawlowski for correcting the written English of my proposal precisely. In the same way, I would like to thank Dr. Nouredine Outaleb, Prof. Luigi Logrippo, and Prof. Abdel Razik Sebak for

Dedication

to my country, the Levant (Bilad al-Sham, Arabic: بلاد الشام)
the land of the most ancient and brilliant civilizations on earth,

and those who have been giving their lives to flourish the Arab
Spring.

"Investigate what is, and not what pleases"

Johann Wolfgang von Goethe

Contents

List of Publications

A. Published refereed journal

1. **Abu Safia, O**.; Talbi, L.; Hettak, K., "A New Type of Transmission Line-Based Metamaterial Resonator and Its Implementation in Original Applications," *IEEE Transactions on Magnetics* , vol.49, no.3, pp.968,973, March 2013.

B. International conference papers

2. **Abu Safia, O.;** Talbi, L.; Hettak, K., "Dual-Band Split-Ring Resonator Using Composite Right-/Left-Handed Coplanar Waveguide Transmission Line-Based Elements," *2014 27th IEEE Canadian Conference on Electrical & Computer Engineering (4-7 May 2014).*

3. **Abu Safia, O.**.; Talbi, L.; Hettak, K., "A novel artificial magnetic material based on a CPW series-connected resonator and its implementation in original applications," *Antennas and Propagation (EuCAP), 2013 7th European Conference on* , vol., no., pp.2756,2760, 8-12 April 2013

4. **Abu Safia, O.;** Talbi, L.; Hettak, K.; Kabiri, A., "CPW discontinuities-based metamaterial inclusions," *Antennas and Propagation Society International Symposium (APSURSI), 2013 IEEE* , vol., no., pp.1176,1177, 7-13 July 2013

5. **Abu Safia, O**.; Talbi, L.; Hettak, K., "A new class of artificial magnetic materials based on a modified uniplanar series resonator and their implementation in original applications," *IEEE International Conference on Microwave Magnetics, Kaiserslautern Germany* 26-29 August 2012.

6. **Abu Safia, O**.; Talbi, L.; Hettak, K.; Kabiri, A., "Dual-band SRR using CRLH TL based elements," *IEEE Antennas and Propagation Society International Symposium (APSURSI), Memphis, USA July, 2014.*

C. In progress works

7. **Abu Safia, O**.; Talbi, L.; Hettak, K., "CPW-fed single folded slot antenna based on a Dual-Resonat Metamaterial Inclusion   having composite right/ left-handed Transmission Lines elements ", *Microwaves, Antennas & Propagation, IET*

8. **Abu Safia, O.**., Talbi, L.; Hettak, K.,"Dual-band HBLC using dual-band CPW CRLH cells," *Electronics Letters*.

D. Other journal publications

9. **O. Abu Safia**, A. A. Omar, and M. C. Scardelletti, "Design of dual-band bandstop coplanar waveguide filter using uniplanar series-connected resonators," *Progress In Electromagnetics Research Letters*, Vol. 27, 93-99, 2011.

10. Omar, A. A., **Abu Safia, O. H**., and Scardelletti, M. C. (2011). "Design of dual-band bandpass coplanar waveguide filter," International Journal of Electronics, 98, 311–322. 2011.

List of Abbreviations

CPW	coplanar waveguide
HBLC	hybrid branch line coupler
LH	left handed
MTM	metamaterial
CRLH	composite right/left handed
TL	transmission line
AMM	artificial magnetic material
SRR	split ring resonator
RF	radio frequency
GSM	global system for mobile communications
WCDMA	wideband code division multiple access
RH	right handed
SMT	surface mount technology
S-SRR	square split ring resonator
EMT	effective medium theory
IDC	interdigital capacitors
SSI	short-circuited stub inductors
MS	microstrip
TW	thin wire
BWs	backward waves
p.u.l	per unit length
SDIE	space-domain integrated equations
DB	dual band
BPF	band pass filter
BSF	band stop filter
LE	lumped element
SIW	substrate integrated waveguide

List of Symbols

c	speed of electromagnetic waves in vacuum
λ_0	wavelength of electromagnetic waves in vacuum
ω	angular frequency of an electromagnetic wave
ε_{eff}	effective permittivity
μ_{eff}	effective permeability
$\mathbf{k}$	wave vector
$\mathbf{E}$	electric field intensity
$\mathbf{H}$	magnetic field intensity
ε_r	relative permittivity of a material
μ_r	relative permeability of a material
χ_m	magnetic susceptibility
M	mutual inductance
σ	conductivity
C_0	capacitance per unit length of an inclusion
L_0	inductance per unit area of an inclusion
β	propagation constant
Z_c	characteristic impedance
ε_0	permittivity of the free space
μ_0	permeability of the free space
α	dissipation factor
φ	phase shift
ω_0	Resonant angular frequency
Ω	normalized frequency with respect to the resonant frequency
BW	frequency bandwidth
Re	real part of a complex function
Im	imaginary part of a complex function
η	radiation efficiency

LIST OF FIGURES

LIST OF TABLES

CHAPTER 1

Preface

1.1. Thesis

Metamaterials are composite human-made materials that have properties not found in natural materials. Metamaterials are realized by embedding electrically small metallic inclusions aligned in parallel to a host dielectric medium. In the presence of a magnetic field, an electric current is induced within the inclusions leading to the emergence of an enhanced magnetic response inside the medium at their resonant frequencies.

Two main design approaches are used to produce metamaterial-based devices at microwave frequencies. Firstly, the resonance-type (split ring resonators) approach, and secondly, the composite right/left-handed (CRLH) transmission line (TL) approach.

The resonance-type approach is based on loading conventional host transmission lines with artificial magnetic material (AMM) inclusions, such as split ring resonators. Etching a transmission line with AMM inclusions enables the generation of current loops inside the inclusions. This magnetic coupling phenomenon produces a stopband response around the AMM's resonant frequency. The stopband response can be physically interpreted as a result of the negative effective permeability of the host TL around the inclusion's resonant frequency.

The second metamaterial design approach is the composite right/left-handed transmission lines approach. These lines consist of two parts: a right-handed part; usually realized using conventional transmission line segments, and a left-handed part which consists of a chain of series-connected capacitors separated by shunted connected inductors (the dual configuration for the lumped element model of a conventional TL).

CRLH TLs have a nonlinear phase-frequency curve response, and hence, the frequency offset and phase slope can be controlled to obtain a similar response at two different frequencies. On other words, these lines support dual-band operations which allow producing arbitrary dual-band circuits.

This dissertation focuses particularly on: firstly, utilizing several coplanar waveguide (CPW) transmission lines discontinuities and elements to produce a new type of TL-based single-resonant metamaterial inclusions, and secondly, producing a dual-resonant metamaterial inclusion derived from the single-resonant inclusions by using a new hybrid approach that combines the two main metamaterial design approaches.

First, the composite right/left-handed transmission lines approach is investigated theoretically, then, a CPW-based implementation for these artificial lines is proposed. The well-known dual-band property for these lines is validated by designing a dual-band hybrid branch line coupler.

Second, a new single-resonant transmission line-based metamaterial resonator that has many advantages over conventional split ring resonators (SRRs) is proposed. The structure is based on a modified coplanar waveguide series-connected resonator folded to form a square loop layout. The resonant frequency for the inclusion is calculated and compared with simulations and measurements results.

Third, in order to illustrate the potentiality of the proposed inclusion, two inclusion-based microwave devices are designed: a dual-band bandstop filter, and a miniaturized hybrid branch line coupler (HBLC). Miniaturizing the size of the HBLC is based on a new proposed loading technique which allows decreasing the electric length of the host transmission lines.

Fourth, a new hybrid technique which combines the two previous metamaterial design approaches is proposed, resulting in a dual-resonant response. CPW CRLH TLs

are used to replace the conventional lines in the single-resonant prototype inclusion to obtain a dual-resonant metamaterial inclusion. Hence, the new inclusion contains composite right/left-handed transmission line-based passive elements.

Finally, to validate the new hybrid approach and the resultant dual-resonant inclusion, two antenna designs which are based on that inclusion are proposed: a dual-band CPW-fed single folded slot antenna, and a dual-band notched ultra wide-band antenna.

1.2. Organization

The thesis contains seven chapters including preface and afterword. This thesis is organized as follows:

- *Chapter 2* presents the introduction, research question, objectives, methodology and the state of the art.

- *Chapter 3* presents the method used to synthesize composite right/left-handed transmission lines. Then, these lines are used to produce a simple bandpass filter. In addition, the dual-band property found in these lines is validated by proposing CPW dual-band hybrid branch line couplers.

- *Chapter 4* introduces new TL-based single-resonant inclusions that utilize series-connected CPW passive elements patterned in its the center conductor. Also, a lumped element model that predicts the inclusions' resonant frequencies is introduced.

- *Chapter 5* proposes two applications for the new inclusions: a dual-band bandstop filter and a compact hybrid branch line coupler. Also, a thorough investigation of the effect of loading our inclusions in increasing the electrical length of the host TLs is

introduced. This phenomenon explains the ability to produce compact microwave circuits using our inclusions.

- *Chapter 6* introduces a new technique in which CRLH TLs replace the conventional lines in the single-resonant prototype inclusion. This technique allows producing a dual-resonant metamaterial inclusion. The designed inclusion is deployed into two antenna designs to verify its dual-resonant response impact.

- *Chapter 7* draws the major conclusions and contributions, and addresses the recommended future work.

CHAPTER 2

Introduction

2.1 Introduction

Metamaterials are artificial materials which have electromagnetic properties not readily available in nature. These materials are synthesized to provide specific permeability and permittivity values over microwave frequency ranges [1]. The material medium of metamaterials contains electrically small inclusions arranged periodically in the host medium [1]. These inclusions change the electromagnetic properties of the host medium due to the inclusions' resonance behavior in the presence of an electromagnetic excitation [1]. When the host medium is excited by electromagnetic waves having wavelengths much larger than the maximum dimension of the metamaterial structure, the medium exhibits new physical and electrical features not covered by natural materials. At this point, the non-homogeneous artificial structures of metamaterials can be characterized as homogenous mediums described by effective permittivity and effective permeability parameters. This condition ensures that the electromagnetic wave is refracted and not diffracted in the material medium of metamaterials [2].

Artificial magnetic materials (AMMs) are small metallic looped-shape inclusions, aligned in parallel planes perpendicular to the direction of incident magnetic field. The incident electromagnetic field induces an electric current on the inclusions leading the emergence of a magnetic response inside the medium at the inclusions' resonant frequencies. The resonant frequency of any AMM is determined by the size and geometry of its layout.

One main target for microwave circuits designers is to decrease the size of AMM-based devices. This can be simply achieved by decreasing the size of these conventional inclusions [3]. However, due to the limited lateral resolution of standard fabrication systems, it is difficult to drive conventional AMM dimensions below one-tenth of a wavelength at resonance, and hence, new AMM inclusions having more compact topologies need to be considered [4]-[6].

To estimate and characterize the performance of AMM, several related lumped element (LE) models have been introduced. For instant, a lumped element model of a host conventional transmission line loaded by SRRs has been proposed in [3]. The model contains a series-connected shunt LC resonator attached to the LE model of the host TL. However, accurate LE models that reflect the magnetic coupling between the host TL and the AMMs need more investigations.

Recent wireless communication systems demand radio frequency (RF) devices operating at multiple frequency bands. For example, in the second and third generation cellular mobile systems (GSM and WCDMA, respectively) the RF transceivers must be able to transmit and receive signals at 900 and 1800 MHz, respectively. Therefore, microwave devices such as filters, power dividers and branch line couplers used in these systems should operate at multiple frequency bands. The second design approach of metamaterials, namely the composite right/left-handed transmission lines approach, provides the dual-band response needed to produce such dual-band devices [7], [8]. By controlling the slope of the phase-frequency dispersive curve of a CRLH TL, several dual-band devices can be designed [8]-[11].

In CRLH TLs, there are right-handed (RH) and left-handed (LH) transmission line parts attached together in order to get several new appealing properties [7],[8]. A balanced combination of the left-handed and right-handed parts permits backward

waves propagation (passband response) for a wide range of frequencies [7]. The right-handed section is usually realized using microstrip or coplanar waveguide (CPW) transmission lines. These host lines introduce parasitic elements that cannot be neglected, and they should be taken into account to describe the propagation characteristics of these lines accurately. On the other hand, the LH part is realized using a chain of series-connected capacitors and shunt-connected inductors. These capacitors and inductors are implemented using either distributed elements or surface mount technology (SMT) components [7], [8].

SMT components have many advantages such as their small size, and their relatively frequency independent lumped element values within a specific range of frequency. Moreover, these components can be deployed and integrated easily into microwave circuits. However, SMT elements operate in a limited frequency range due to the parasitic effects that cause self-resonance [12]. In addition, their nominal values are restricted to those provided by manufacturers, and finally, SMT elements are relatively expensive; soldering is necessary and it goes against the full integration of microwave components [12].

On the other hand, using distributed elements overcomes the aforementioned disadvantages. However, one main limitation of using distributed elements is their frequency-selective response; therefore, new techniques to overcome this problem have to be investigated.

2.2 Research question

In spite of the large number of AMM inclusions introduced in the literature, most of these inclusions have similar geometrical structures and electrical behavior to conventional split ring resonators. Moreover, these inclusions have many common

limitations. For example, they have complex expressions for their LC elements. This leads to complex expressions for their resonant frequencies. Therefore, it is important to produce new AMMs that overcome such limitations, and to have new properties such as the dual-resonant response, in addition to have accurate and simple LE model to estimate their resonant frequencies.

Utilizing distributed passive elements to design CRLH TLs has several advantages over lumped elements. However, their frequency-selective behavior represents a major disadvantage especially when they are implemented in dual-band frequency circuits. Hence, new techniques to overcome this problem should be considered.

CPW TL discontinuities have not been utilized to produce AMM inclusions. These structures are expected to share the same appealing properties with conventional CPW TLs

A well-designed dual-resonant inclusion having a controllable resonant frequency can replace the need for two AMM inclusions having different sizes. Also, this inclusion can be applied into dual-band microwave (MW) applications and antennas.

2.3 Objectives of the proposed research

Series-connected resonators based on special stubs patterned in the center strip of a CPW TL have been introduced in [13]. These resonators can be modified and reshaped in order to produce new AMM inclusions. The new inclusions, which consist of open-ended and short ended stubs, are designed to operate at the ultra-high frequency range. Because the passive elements within the new inclusion are based on TLs, the new inclusion overcomes many limitations and disadvantages found in the conventional inclusions. For example, it has the ability to control the quality and reduction (compactness) factors in MW devices. Unlike conventional inclusions, the proposed

inclusions have independently controllable distributed elements (the inductive and capacitive elements are approximately frequency independent). This can simplify controlling and estimating the resonant frequency and the quality factor. In addition, special CRLH TLs can replace the conventional TLs in the proposed single-resonant inclusion in order to have dual-band AMMs, and hence, new compact dual-band MW circuits can be produced.

The aforementioned technique in which CRLH lines replace conventional TL can be used to design new CRLH TL-based passive distributed elements having constant equivalent lumped element values at two different center band frequencies. Therefore, the responses of dual-band components based on these artificial lines can be enhanced. The proposed techniques and structures are validated by designing and fabricating several dual-band filters, and branch line couplers and antennas.

2.4 Methodology

High quality distributed capacitors and inductors based on open-ended and short-ended stubs, respectively, patterned in the center conductor of CPW TLs, are designed and simulated using a full-wave electromagnetic simulation tool [14]. Several proposed miniaturization techniques are utilized [15]-[17]. The simulated results are compared to the theoretical results of the equivalent lumped-element model. The LE model is adjusted to consider the CPW discontinuities effect [18]-[20]. After that, special CRLH TLs are designed to replace the distributed passive elements, in order to get the dual-band response. From the simulated scattering parameters values the capacitance and inductance within the CRLH TLs are extracted and compared with the designed values. Optimizing the physical dimensions of these artificial TLs is considered to enhance their response, and later, these meta-lines are deployed into the new proposed AMM

inclusions. A theoretical model based on simple TL theory to calculate the resonant frequency of the proposed AMMs is introduced. After validating the responses of the proposed AMMs and CRLH cells by fabrication and measurements, several dual-band, high performance and ultra-compact MW circuits are produced. Finally, the novelty of the proposed techniques and designs is evaluated and compared with the existing MW circuits of the literature [21]-[26].

2.5 State of the art

Split ring resonators (SRRs) were first introduced by Pendry *et al.* [1]. Since then, numerous SRRs having various geometrical configurations have been proposed [27]-[31]. However, most of these SRRs are derived from the prototype structure proposed in [1]. For example, in [27] a square split ring resonator (S-SRR) was proposed which has more degrees of freedom from a design point of view, and more magnetic coupling with the host transmission line, than SRRs. Saha *et al.* built a theoretical model for S-SRRs to estimate their resonant frequency and their magnetic polarization in [28]. They also investigated the bandstop behavior of these resonators when loaded into CPW. In [29], bandstop filters based on SRRs placed on the back side of CPW substrate were first introduced. These filters give significant insertion loss in the rejection band with very good frequency selectivity near the resonant frequency. Baena *et al.* proposed many SRR topologies with different broken-loop shapes, and their equivalent lumped element models [3]. Although the number of capacitors and inductors varies in each topology, it can always be simplified to a series-connected LC resonator mutually coupled with the host TL. In [30], a spiral resonator of one metallic planar piece is proposed in order to facilitate the fabrication process because of the absence of the narrow slots between the

strips. In [31], a modified broadside coupled SRR was proposed by Marques *et al.* as an alternative to a conventional SRR in order to avoid the bi-anisotropic effects.

The resonance behavior in artificial magnetic materials (AMMs) results from the perpendicular excitation of the time varying magnetic field through their sectional areas; therefore, induced resonating currents flow inside the broken-loops which act as magnetic dipole moments. This physical phenomenon can be modeled as a series-connected LC resonator, mutually coupled with the host TL [29]. The real part of the effective permeability (μ_r) within the host dielectric substrate medium encounters a bipolar impulse response in the vicinity of the resonant frequency (f_c), i.e., μ_r increases positively just before f_c then it falls down to negative values with high slope rate after that [32]. Mapping this phenomenon to filter applications, it can be concluded that a bandstop response can be detected in the resonant frequency range.

The resonance and dispersive behavior in SSRs are entirely determined by the geometry and the size of the metallic broken-loop inclusions [1]. For all the proposed geometries which are driven from conventional SRRs there are some advantages and disadvantages.

AMMs are suitable for compact microwave devices such as filters and diplexers due to their resonance nature, and due to the controllability of the electrical properties in AMM-based TLs which include the dispersion diagram and the characteristic impedance of such artificial lines. It is possible to design components with smaller size and superior performance compared to conventional implementation (such as enhanced bandwidth devices), and devices based on new functionalities such as dual-band circuits.

Several numerical and analytical methods were introduced to characterize the constitutive parameters for AMMs [33]-[37]. In [33], Smith and Pendry proposed a field

averaging method in order to homogenized a periodic structure that contains several metamaterial cells with different geometries. The electric and magnetic fields were averaged and calculated at the edges of two successive cubic lattices. In [34], the effective parameters of a transmission line loaded with asymmetrical SRRs were calculated by proposing an equivalent bianisotropic medium, which imitates the effect of asymmetric unit cells. In [35], analytical expressions for the relative permittivity and permeability of SRRs were introduced based of a simple transmission line theory. The two parameters were extracted from the derived expressions of reflection and transmission coefficients. In [36], effective material parameters in metamaterial were calculated using a modal approach combined with the Finite Integration Technique (a generalized FDTD method). The parameter fitting of dispersive models (PFDMs) method was used in [37] to extract the effective material parameters from the scattering parameters of a double negative metamaterial structure.

Many lumped element models are proposed to model SRRs and their interaction with transmission lines. [3],[38]-[41]. For example, In [38], successive transmission line sections connected in series with two capacitive π networks that represent the split gaps were used to represent a microstrip double SRR geometry. In [39], an equivalent circuit model for a singly split ring resonator (SSRR) based on bulk and distributed elements was proposed. A set of differential equations with boundary conditions imposed at the position of the split was solved to find the voltage and current variations in the inner and outer rings. In [40], a new equivalent circuit model for two-dimensional cross embedded SRR was proposed. Each column of the SRRs array was modeled as a quasi-solenoid under magnetic induction. Moreover, electromagnetic coupling between each column was considered. The quasi-analytical model used to compute the polarizabilites of the edge- and broadside-coupled SRRs in [41] was also used to find the lumped LC

values for several other SRR configurations and their complementary topologies [3]. From these models, the stopband and passband characteristics can be easily explained.

The second approach to produce metamaterial-based components and circuits is a non-resonant artificial transmission lines-based approach called composite right/left handed transmission lines [42]. Their nonlinear phase slope response makes them convenient to produce arbitrary dual-band circuits by simply replace the conventional lines in prototype circuits [43], [8]. A two-dimensional (2-D) CRLH TLs have been investigated in [44]. Their dispersive diagram has been derived analytically in [45]. Similar planar cells were utilized to produce infinite wavelength resonant antennas with monopolar radiation patterns in [46]. Other 2-D planar resonant-type distributed structure based on complimentary split ring resonators and series gap capacitors has been proposed in [47]. In [48], a leaky-wave antenna with tunable radiation angle and beamwidth based on CRLH microstrip structure was proposed. The antenna has varactor diodes to tune its resonant frequency. In [49], a compact four unit cell antenna based on a CRLH cell was produced. The antenna utilizes the anti-parallel phase and group velocities of CRLH cells at their functional mode where the propagation constant increases as the frequency decreases, and hence, a small size antenna can be realized. Another leaky-wave antenna based on CRLH microstrip TL is proposed in [50]. The structure eliminates the open-stopband effects and has a constant radiation efficiency, obtained based on an accurate parametric design procedure and a full-wave numerical modal approach. In [51], an amplifier was added to the CRLH TL-based antenna design to regenerate the amplitude of a signal progressively leaked out in the radiation process. Therefore, high-gain active leaky-wave antenna was produced.

CRLH cells were realized in different types of transmission lines and technologies. For example, a coplanar waveguide CRLH TL was realized in [52]. Recently, substrate integrated waveguide (SIW) CRLH cells were proposed [53].

Other non-radiating devices which utilize the appealing properties of CRLH TLs are enormously found in the literature. This includes duplexers [54], directional couplers [55], power splitters [56], phase shifters [57], coupled-line couplers [58], power amplifiers [59], [60], and compressive receivers [61].

Hybrid approaches that combine the two metamaterial design approaches have been reported in [62]-[67]. In [62], CPW lines are loaded by complementary SRRs combined with series capacitive gaps in the conductor strip, located above the complementary SRRs, and grounded inductive stubs. This structure was used to obtain a compact UWB filter [62]. Gil *et al* proposed a comparable structure realized on a microstrip transmission line. The structure-based artificial lines were used to produce a compact power divider and a high selective bandpass filter [63]. In [64], a balanced CRLH line was realized by loading the host CPW TL with square-SRRs, located below the positions occupied by the short-circuited shunt-connected inductive stubs. A proper tuning of the resonators' dimensions and the stubs lengths allows wider transmission characteristics. In [65], capacitive open-ended stubs are connected to the SRR rings to modify the right-handed band's feature in a SRR-loaded CPW TL. The structure has a wide passband with high attenuation rates besides the passband due to its pair of transmission zeros at each side of the passband. These features make the structure very attractive for filter application. In [66], extra series and shunt capacitances were added to the prototype negative refractive index uniplanar transmission line proposed in [67]. The structure is balanced with wideband response due to the fine tuning between its advance and delay phase offset sections.

Other related structure, called dual CRLH, was proposed by Caloz [68]. The structure exhibits its RH band at low frequencies and its LH band at high frequencies. Several SRR-based balanced dual CRLH TLs with wideband bandpass response have been reported [69], [70].

References

[1] Pendry, J.B.; Holden, A.J.; Robbins, D.J.; Stewart, W.J.; "Magnetism from conductors and enhanced nonlinear phenomena," *Microwave Theory and Techniques, IEEE Transactions on*, vol.47, no.11, pp.2075-2084, Nov 1999.

[2] V. Veselago. "The electrodynamics of substances with simultaneously negative values of ε and μ," *Soviet Physics Uspekhi*, vol. 10, no. 4, pp. 509–514, Jan., Feb. 1968.

[3] Baena, J.D.; Bonache, J.; Martin, F.; Sillero, R.M.; Falcone, F.; Lopetegi, T.; Laso, M.A.G.; Garcia-Garcia, J.; Gil, I.; Portillo, M.F.; Sorolla, M.; , "Equivalent-circuit models for split-ring resonators and complementary split-ring resonators coupled to planar transmission lines," *Microwave Theory and Techniques, IEEE Transactions on* , vol.53, no.4, pp. 1451- 1461, April 2005.

[4] Crnojevic-Bengin, V.; Radonic, V.; Jokanovic, B.; "Fractal Geometries of Complementary Split-Ring Resonators," *Microwave Theory and Techniques, IEEE Transactions on* , vol.56, no.10, pp.2312-2321, Oct. 2008.

[5] Bilotti, F.; Toscano, A.; Vegni, L., "Design of Spiral and Multiple Split-Ring Resonators for the Realization of Miniaturized Metamaterial Samples," *Antennas and Propagation, IEEE Transactions on*, vol.55, no.8, pp.2258-2267, Aug. 2007.

[6] Saha, C.; Siddiqui, J.Y.; , "A comparative analysis for split ring resonators of different geometrical shapes," *Applied Electromagnetics Conference (AEMC), 2011 IEEE* , vol., no., pp.1-4, 18-22 Dec. 2011.

[7] Caloz, C.; Itoh, T.; "Transmission line approach of left-handed (LH) materials and microstrip implementation of an artificial LH transmission line," *Antennas and Propagation, IEEE Transactions on* , vol.52, no.5, pp. 1159- 1166, May 2004.

[8] I-Hsiang Lin; DeVincentis, M.; Caloz, C.; Itoh, T.;, "Arbitrary dual-band components using composite right/left-handed transmission lines," *Microwave Theory and Techniques, IEEE Transactions on* , vol.52, no.4, pp. 1142- 1149, April 2004.

[9] Zhang, J.; Cheung, S.W.; Yuk, T.I.; , "Compact composite right/left-handed transmission line unit cell for the design of true-time-delay lines," *Microwaves, Antennas & Propagation, IET*, vol.6, no.8, pp.893-898, June 7 2012.

[10] Shau-Gang Mao; Min-Sou Wu; Yu-Zhi Chueh; Chun Hsiung Chen; , "Modeling of symmetric composite right/left-handed coplanar waveguides with applications to compact bandpass filters," *Microwave Theory and Techniques, IEEE Transactions on* , vol.53, no.11, pp. 3460- 3466, Nov. 2005.

[11] Duran-Sindreu, M.; Velez, A.; Siso, G.; Velez, P.; Selga, J.; Bonache, J.; Martin, F.; , "Recent Advances in Metamaterial Transmission Lines Based on Split Rings," *Proceedings of the IEEE* , vol.99, no.10, pp.1701-1710, Oct. 2011.

[12] C. Caloz and T. Itoh, *Electromagnetic Metamaterials, Transmission Line Theory and Microwave Applications*, Wiley and IEEE Press, Hoboken, NJ, 2005.

[13] Hettak, K.; Dib, N.; Sheta, A.-F.; Toutain, S.; , "A class of novel uniplanar series resonators and their implementation in original applications," *Microwave Theory and Techniques, IEEE Transactions on* , vol.46, no.9, pp.1270-1276, Sep 1998.

[14] Zeland Software, Inc., "IE3D Simulator," Fremont, CA, 2002.

[15] Hettak, K.; Dib, N.; Omar, A.; Delisle, G.Y.; Stubbs, M.; Toutain, S.; , "A useful new class of miniature CPW shunt stubs and its impact on millimeter-wave integrated circuits," *Microwave Theory and Techniques, IEEE Transactions on* , vol.47, no.12, pp.2340-2349, Dec 1999.

[16] Hettak, K.; Laneve, T.; Stubbs, M.G.;, "Size-reduction techniques for CPW and ACPS structures," *Microwave Theory and Techniques, IEEE Transactions on* , vol.49, no.11, pp.2112-2116, Nov 2001.

[17] Dib, N.I.; Katehi, L.P.B.; Ponchak, G.E.; Simons, R.N.; , "Theoretical and experimental characterization of coplanar waveguide discontinuities for filter applications," *Microwave Theory and Techniques, IEEE Transactions on* , vol.39, no.5, pp.873-882, May 1991.

[18] Dib, N.I.; Katehi, L.P.B.; Ponchak, G.E.; Simons, R.N.; , "Theoretical and experimental characterization of coplanar waveguide discontinuities for filter applications," *Microwave Theory and Techniques, IEEE Transactions on* , vol.39, no.5, pp.873-882, May 1991.

[19] Pannier, P.; Kadri, L.; Seguinot, C.; Kennis, P.; Huret, F.; , "Accurate and efficient numerical method for the analysis of multimode waveguide discontinuities," *Microwave Theory and Techniques, IEEE Transactions on* , vol.48, no.2, pp.295-304, Feb 2000.

[20] Weller, T.M.; Henderson, R.M.; Herrick, K.J.; Robertson, S.V.; Kihm, R.T.; Katehi, L.P.B.; , "Three-dimensional high-frequency distribution networks. I. Optimization of CPW discontinuities," *Microwave Theory and Techniques, IEEE Transactions on* , vol.48, no.10, pp.1635-1642, Oct 2000.

[21] Chao-Hsiung Tseng; Tatsuo Itoh; , "Dual-Band Bandpass and Bandstop Filters Using Composite Right/Left-Handed Metamaterial Transmission Lines," *Microwave Symposium Digest, 2006. IEEE MTT-S International*, vol., no., pp.931-934, 11-16 June 2006.

[22] Kawai, T.; Nakamura, M.; Tanigawa, S.; Ohta, I.; Enokihara, A.; , "Band-broadening design technique of CRLH-TLs branch-line couplers operating at two arbitrary frequencies using CRLH-TLs matching networks," *Microwave Conference, 2009. EuMC 2009. European* , vol., no., pp.1295-1298, Sept. 29 2009-Oct. 1 2009.

[23] Elles, D.S.; Yong-Kyu Yoon; , "Compact dual band three way bagley polygon power divider using composite right/left handed (CRLH) transmission lines," *Microwave Symposium Digest, 2009. MTT '09. IEEE MTT-S International*, vol., no., pp.485-488, 7-12 June 2009.

[24] Hai Hoang Ta; Anh-Vu Pham; , "Compact Wilkinson power divider based on novel via-less composite right/left-handed (CRLH) transmission lines," *Communications and Electronics (ICCE), 2010 Third International Conference on* , vol., no., pp.313-317, 11-13 Aug. 2010.

[25] Chang-Jia Gao; Feng Wei; Xiao-Wei Shi; Yan-fu Bai; , "A novel tri-band power divider with coupled-line CRLH unit," *Microwave and Millimeter Wave Technology (ICMMT), 2012 International Conference on* , vol.4, no., pp.1-3, 5-8 May 2012.

[26] Hsin-Chia Lu; Yen-Liang Kuo; Po-Sheng Huang; Yi-Long Chang; , "Dual-band CRLH branch-line coupler in LTCC by lump elements with parasite control, "*Microwave Symposium Digest (MTT), 2010 IEEE MTT-S International* , vol., no., pp.393-396, 23-28 May 2010.

[27] I. Gil, J. Bonache, J. Garcia-Garcia, F. Falcone, and F. Martin "Metamaterials in microstrip technology for filter applications," *Proc. APS-URSI*, Washington, July 2005.

[28] C. Saha, J.Y. Siddiqui, and Y.M.M. Antar, "Square split ring resonator backed coplanar waveguide for filter applications," *General Assembly and Scientific Symposium, 2011 XXXth URSI* , vol., no., pp.1-4, 13-20 Aug. 2011.

[29] F. Martin, F. Falcone, J. Bonache, R. Marques and M. Sorolla, "Miniaturized coplanar waveguide stop band filters based on multiple tuned split ring resonators," *IEEE microwave and Wireless Component Letters,* vol. 13, no. 12, pp. 511-513, December 2003.

[30] J. D. Baena, R. Marques, F. Medina, and J. Martel, "Artificial magnetic metamaterial design by using spiral resonators," *Physical Review B (Condensed Matter and Materials Physics)*, 69(1):141-145, January 2004.

[31] R. Marques, F. Medina, and R. Rafii-El-Idrissi, " Role of bianisotropy in negative permeability and left-handed metamaterials," *Physical Review B (Condensed Matter and Materials Physics*), 65(144440/1):144440/6, April 2002.

[32] F. Falcone, T. Lopetegi, J. D. Baena, R. Marqués, F. Martín, and M.Sorolla, "Effective negative-ε stopband microstrip lines based on complementary split ring resonators," *IEEE Microw.Wireless Compon. Lett.*, vol. 14, no. 6, pp. 280–282, Jun. 2004.

[33] D.R. Smith and J.B. Pendry, "Homogenization of metamaterials by field averaging*," J. Opt. Soc. Am.*, vol. B 23, p. 391, 2006.

[34] Milosevic, V.; Jokanovic, B.; Bojanic, R., "Effective Electromagnetic Parameters of Metamaterial Transmission Line Loaded With Asymmetric Unit

Cells," *Microwave Theory and Techniques, IEEE Transactions on* , vol.61, no.8, pp.2761,2772, Aug. 2013.

[35]   Smith, D. R., S. Schultz, P. Markos, and C. M. Soukoulis, "Determination of effective permittivity and permeability of metamaterials from reflection and transmission coefficients," *Phys. Rev. B*, Vol. 65, 195104, 2002.

[36]   Schuhmann, R.; Weiland, T., "Efficient calculation of effective material parameters in metamaterials using FDTD and a modal approach," *Microwave Symposium Digest, 2002 IEEE MTT-S International* , vol.3, no., pp.2037,2040 vol.3, 2-7 June 2002.

[37]   Lubkowski, G.; Bandlow, B.; Schuhmann, R.; Weiland, T., "Effective Modeling of Double Negative Metamaterial Macrostructures," *Microwave Theory and Techniques, IEEE Transactions on* , vol.57, no.5, pp.1136,1146, May 2009.

[38]   *Vitaliy Zhurbenko, Thomas Jensen, Viktor Krozer, Peter Meincke, Analytical model for double split ring resonators with arbitrary ring width, Microwave and Optical Technology Letters, 2008, 50, 2.*

[39]   Shamonin, M.; Shamonina, E.; Kalinin, V.; Solymar, L., "Properties of a metamaterial element: Analytical solutions and numerical simulations for a singly split double ring," *Journal of Applied Physics* , vol.95, no.7, pp.3778,3784, Apr 2004.

[40]   Chen, Hongsheng; Ran, Lixin; Huangfu, Jiangtao; Grzegorczyk, Tomasz M.; Kong, Jin Au, "Equivalent circuit model for left-handed metamaterials," *Journal of Applied Physics* , vol.100, no.2, pp.024915,024915-6, Jul 2006.

[41]   Marques, R.; Mesa, F.; Martel, J.; Medina, F., "Comparative analysis of edge- and broadside- coupled split ring resonators for metamaterial design - theory and

experiments," *Antennas and Propagation, IEEE Transactions on* , vol.51, no.10, pp.2572,2581, Oct. 2003.

[42]   Lai, A.; Itoh, T.; Caloz, C., "Composite right/left-handed transmission line metamaterials," *Microwave Magazine, IEEE* , vol.5, no.3, pp.34,50, Sept. 2004.

[43]   Chao-Hsiung Tseng; Itoh, T., "Dual-Band Bandpass and Bandstop Filters Using Composite Right/Left-Handed Metamaterial Transmission Lines," *Microwave Symposium Digest, 2006. IEEE MTT-S International* , vol., no., pp.931,934, 11-16 June 2006.

[44]   Sanada, A.; Caloz, C.; Itoh, T., "Characteristics of the composite right/left-handed transmission lines," *Microwave and Wireless Components Letters, IEEE* , vol.14, no.2, pp.68,70, Feb. 2004.

[45]   Sanada, A.; Caloz, C.; Itoh, T., "Planar distributed structures with negative refractive index," *Microwave Theory and Techniques, IEEE Transactions on* , vol.52, no.4, pp.1252,1263, April 2004.

[46]   Lai, Anthony; Leong, K.M.K.H.; Itoh, T., "Infinite Wavelength Resonant Antennas With Monopolar Radiation Pattern Based on Periodic Structures," *Antennas and Propagation, IEEE Transactions on* , vol.55, no.3, pp.868,876, March 2007.

[47]   He-Xiu Xu; Guang-Ming Wang; Mei-qing Qi; Chen-Xin Zhang; Jian-Gang Liang; Jian-Qiang Gong; Yong-Chun Zhou, "Analysis and Design of Two-Dimensional Resonant-Type Composite Right/Left-Handed Transmission Lines With Compact Gain-Enhanced Resonant Antennas," *Antennas and Propagation, IEEE Transactions on* , vol.61, no.2, pp.735,747, Feb. 2013.

[48]   Lim, Sungjoon; Caloz, C.; Itoh, T., "Metamaterial-based electronically controlled transmission-line structure as a novel leaky-wave antenna with tunable

radiation angle and beamwidth," *Microwave Theory and Techniques, IEEE Transactions on* , vol.53, no.1, pp.161,173, Jan. 2005.

[49]   Cheng-Jung Lee; Leong, K.M.K.H.; Itoh, T., "Composite right/left-handed transmission line based compact resonant antennas for RF module integration," *Antennas and Propagation, IEEE Transactions on* , vol.54, no.8, pp.2283,2291, Aug. 2006.

[50]   Paulotto, S.; Baccarelli, P.; Frezza, F.; Jackson, D.R., "Full-Wave Modal Dispersion Analysis and Broadside Optimization for a Class of Microstrip CRLH Leaky-Wave Antennas," *Microwave Theory and Techniques, IEEE Transactions on* , vol.56, no.12, pp.2826,2837, Dec. 2008.

[51]   Casares-Miranda, F.P.; Camacho-Penalosa, C.; Caloz, C., "High-gain active composite right/left-handed leaky-wave antenna," *Antennas and Propagation, IEEE Transactions on* , vol.54, no.8, pp.2292,2300, Aug. 2006.

[52]   Shau-Gang Mao; Min-Sou Wu; Yu-Zhi Chueh; Chun Hsiung Chen, "Modeling of symmetric composite right/left-handed coplanar waveguides with applications to compact bandpass filters," *Microwave Theory and Techniques, IEEE Transactions on* , vol.53, no.11, pp.3460,3466, Nov. 2005.

[53]   Yuandan Dong; Itoh, T., "Composite Right/Left-Handed Substrate Integrated Waveguide and Half Mode Substrate Integrated Waveguide Leaky-Wave Structures," *Antennas and Propagation, IEEE Transactions on* , vol.59, no.3, pp.767,775, March 2011.

[54]   Horii, Y.; Caloz, C.; Itoh, T., "Super-compact multilayered left-handed transmission line and diplexer application," *Microwave Theory and Techniques, IEEE Transactions on* , vol.53, no.4, pp.1527,1534, April 2005.

[55]   Caloz, C.; Itoh, T., "A novel mixed conventional microstrip and composite right/left-handed backward-wave directional coupler with broadband and tight coupling characteristics," *Microwave and Wireless Components Letters, IEEE* , vol.14, no.1, pp.31,33, Jan. 2004.

[56]   Shau-Gang Mao; Yu-Zhi Chueh, "Broadband composite right/left-handed coplanar waveguide power splitters with arbitrary phase responses and balun and antenna applications," *Antennas and Propagation, IEEE Transactions on*, vol.54, no.1, pp.243,250, Jan. 2006.

[57]   Perruisseau-Carrier, J.; Skrivervik, A.K., "Composite right/left-handed transmission line metamaterial phase shifters (MPS) in MMIC technology," *Microwave Theory and Techniques, IEEE Transactions on* , vol.54, no.4, pp.1582,1589, June 2006.

[58]   Van Nguyen, H.; Caloz, C., "Generalized Coupled-Mode Approach of Metamaterial Coupled-Line Couplers: Coupling Theory, Phenomenological Explanation, and Experimental Demonstration," *Microwave Theory and Techniques, IEEE Transactions on* , vol.55, no.5, pp.1029,1039, May 2007.

[59]   Seung Hun Ji; Choon Sik Cho; Lee, J. -W; Jaeheung Kim, "Concurrent Dual-Band Class-E Power Amplifier Using Composite Right/Left-Handed Transmission Lines," *Microwave Theory and Techniques, IEEE Transactions on* , vol.55, no.6, pp.1341,1347, June 2007.

[60]   Yong-Sub Lee; Mun-Woo Lee; Yoon-Ha Jeong, "High-Efficiency Class-F GaN HEMT Amplifier With Simple Parasitic-Compensation Circuit," *Microwave and Wireless Components Letters, IEEE* , vol.18, no.1, pp.55,57, Jan. 2008.

[61]   Abielmona, S.; Gupta, S.; Caloz, C., "Compressive Receiver Using a CRLH-Based Dispersive Delay Line for Analog Signal Processing," *Microwave Theory and Techniques, IEEE Transactions on* , vol.57, no.11, pp.2617,2626, Nov. 2009.

[62] Gil, M.; Bonache, J.; Garcia-Garcia, J.; Martel, J.; Martin, F., "Composite Right/Left-Handed Metamaterial Transmission Lines Based on Complementary Split-Rings Resonators and Their Applications to Very Wideband and Compact Filter Design," *Microwave Theory and Techniques, IEEE Transactions on* , vol.55, no.6, pp.1296,1304, June 2007.

[63] Gil, M.; Bonache, J.; Martin, F., "Synthesis and applications of new left handed microstrip lines with complementary split-ring resonators etched on the signal strip," *Microwaves, Antennas & Propagation, IET*, vol.2, no.4, pp.324,330, June 2008.

[64] Niu, J. -X; Zhou, X. -L, "Resonant-type balanced composite right/ left-handed coplanar waveguide structure, "*Electronics Letters* , vol.44, no.10, pp.638,639, May 8 2008.

[65] Sanz, V.; Belenguer, A.; Martinez, L.; Boria, A.L.; Cascon, J.; Boria, V.E., "Balanced Right/Left-Handed Coplanar Waveguide With Stub-Loaded Split-Ring Resonators," *Antennas and Wireless Propagation Letters, IEEE*, vol.13, no., pp.193,196, 2014.

[66] Borja, A.L.; Belenguer, A.; Cascon, J.; Esteban, H.; Boria, V.E., "Wideband Passband Transmission Line Based on Metamaterial-Inspired CPW Balanced Cells," *Antennas and Wireless Propagation Letters, IEEE* , vol.10, no., pp.1421,1424, 2011.

[67] Eleftheriades, G.V.; Iyer, A.K.; Kremer, P.C., "Planar negative refractive index media using periodically L-C loaded transmission lines," *Microwave Theory and*

Techniques, IEEE Transactions on, vol.50, no.12, pp.2702, 2712, Dec 2002.

[68] Caloz, C., "Dual Composite Right/Left-Handed (D-CRLH) Transmission Line Metamaterial," *Microwave and Wireless Components Letters, IEEE* , vol.16, no.11, pp.585,587, Nov. 2006.

[69] Belenguer, A.; Cascon, J.; Borja, A.L.; Esteban, H.; Boria, V.E., "Dual Composite Right-/Left-Handed Coplanar Waveguide Transmission Line Using Inductively Connected Split-Ring Resonators," *Microwave Theory and Techniques, IEEE Transactions on*, vol.60, no.10, pp.3035,3042, Oct. 2012.

[70] Belenguer, A.; Borja, A.L.; Boria, V.E., "Balanced Dual Composite Right/Left-Handed Microstrip Line With Modified Complementary Split-Ring Resonators, "*Antennas and Wireless Propagation Letters, IEEE*, vol.12, no., pp.880, 883, 2013.

CHAPTER 3

Investigation of CPW CRLH TLs

This chapter introduces a review of the composite right/left-handed (CRLH) transmission lines approach. This approach will be later deployed into our TL-based inclusion in order to have a dual-resonant inclusion. Also, a new coplanar waveguide CRLH distributed cell is proposed. This cell utilizes a CPW series-connected resonator and two shunt-connected stubs. A very good agreement between simulated and theoretical results is found which validates the proposed cell. Finally, the dual-band property in CRLH TLs is investigated and verified by proposing two dual-band hybrid branch line couplers.

3.1 Introduction

The Russian physicist Victor Veselago investigated the feasibility of materials to have simultaneous negative permittivity and permeability [1]. He showed that according to Maxwell's equations there is no contradiction that electromagnetic waves can propagate in such medium. His work opens the doors to investigate the possibility to produce materials that allow propagation of electromagnetic waves having the electric field, the magnetic field, and the phase constant vectors build a left-handed triad.

Although left-handed (LH) materials have left-handed triad relationship, their pointing vector, which represents the group velocity, has a right-handed triad relationship. This means that the direction of the wave propagation in these materials, represented by the phase velocity, opposes the direction of the power flow, represented

by the group velocity. On other words, the phase and group velocities are anti-parallel. Hence, we can refer to this kind of materials as anti-parallel materials. The idea of anti-parallelism is the same as the idea of backward waves. Mediums that support this kind of propagation can be characterized using the dual configuration of the lumped element model of a conventional transmission line. i.e., a series-connected capacitor and a shut-connected inductor as shown in Figure 3.1
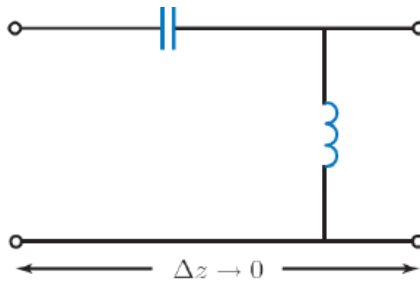
Figure 3.1 LH TL incremental circuit model [5]

3.2 Artificial (metamaterial-based) lines

Artificial (metamaterial-based) transmission lines have nonlinear dispersive relationship. This property makes these lines able to repeat their response on a nonlinear harmonic pattern. Hence, dual-band devices can be easily designed using these lines.

In the design of dual-band microwave devices at the microwave frequency range, microstriplines (MS) have mainly been used to guide electromagnetic waves. This is due to the appealing properties of MS such as their relatively low conductor loss, dielectric loss and radiation loss at microwave frequencies, and their easy adaptation to series connections with other circuit elements as well the availability of MS circuits which cover a wide range of applications [2].

However, in the millimeter-wave frequency range, serious drawbacks of MS based designs may appear due to the need for via holes for grounding purposes and shunt

connections. These via holes are rather costly to form, irreparable during fabrication, and may degrade the circuit performance, especially at higher frequencies, due to the parasitic inductance resulting from these holes.

Coplanar waveguides (CPW) have many advantages over microstrip lines as mentioned in the next section. Hence, producing new designs based on CPW artificial (left-handed) transmission lines would add extra appealing features to the new devices which utilize these lines. [3], [4].

Surface mount technology (SMT) is the dominant technology used to produce metamaterial based MW components because passive elements based on this technology have fixed lumped values for a proper range of frequencies [5]. Therefore, these elements are suitable for the design of dual-band circuits, in which the LE values at the two center band frequencies should be constant. However, there are several limitations related to the usage of SMT elements. Hence, distributed components (based on CPW TLs in our case) which have almost constant performance over a wide range of frequencies can be considered as better candidates for dual and wide band circuits.

3.3 Advantages of coplanar waveguide-based elements

The dominant mode in CPW transmission lines is an even quasi-TEM mode, called a CPW mode. The electric fields of this mode in the two adjacent CPW slots are opposite to each other. Hence, CPW operating in the CPW mode has low frequency dispersion and low radiation loss which makes CPW suitable for wide band circuit applications.

Most of metamaterial units and devices are based on microstrip transmission lines [6]-[10]. These lines may contain drilled via holes for grounding purposes. This will make shunt as well as series surface mounting of active and passive devices more difficult. In addition, the relatively high radiation loss and high frequency dispersion of

microstrip lines relative to CPW in both the microwave and millimeterwave frequency ranges makes CPW technology an excellent candidate for metamaterials based elements. These as well as several other advantages [3] make CPW more convenient for our proposed microwave devices.

3.4 Theory of composite right/lift handed transmission lines

The first practical metamaterial saw the light at the beginning of the 21 century, and more specifically in the year 2000 by Smith *et al* [11]. Their contribution was based on the work of Pendry *et al*. [12] who produced two types of materials. One having negative permittivity/positive permeability and the other one has positive permittivity/negative permeability. Both materials operate at the MW range. Smith combines the two aforementioned structures, namely: the thin wire (TW) and the split-ring resonator (SRR), respectively, to obtain a new artificial material with negative permittivity and permeability. Moreover, he introduces plasmonic expressions for the permittivity and the permeability of these structures. These expressions are related to the dimensions of the proposed materials and their operating frequencies [11].

In physics, backward waves (BWs) are well-know from the 1940s. They represent the antiparallel phase and group velocities phenomenon in some materials. The behavior of this kind of materials can be characterized by the following equivalent circuit model (Figure 3.2). However, these materials in general have a cell size dimension of $\lambda/2$ or $n \times \lambda/2$, which makes the diffraction/scattering phenomena the dominant propagation mechanism. Hence, we can't represent conventional BW materials using ε_r and μ_r. In contrary, refraction is the main propagation mechanism in metamaterials due to their smaller size. Hence, ε_r and μ_r can be used to represent these materials.

Furthermore, only higher modes are supported in BW materials unlike metamaterials which can be characterized using the circuit shown in Figure 3.2 on fundamental modes.
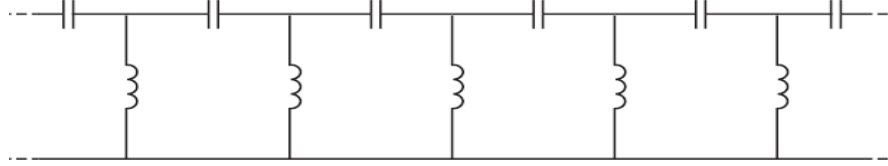
Figure 3.2 LE circuit model for a TL supporting backward waves [5]
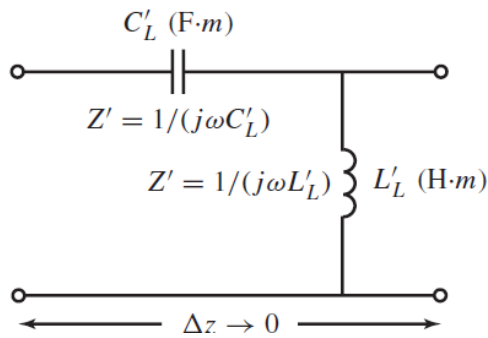
Figure 3.3 LE circuit model of an incremental LH TL [5]

The circuit model shown in Figure 3.3 represents a LH-metamaterial incremental transmission line. It can be shown that for this model the complex propagation constant γ, the propagation constant β, the characteristic impedance Z_c, the phase velocity v_p, and the group velocity v_g for the TL are given, respectively, by [5]:

$$\gamma = j\beta = \sqrt{Z'Y'} = \frac{1}{j\omega\sqrt{L'_L C'_L}} = -j\frac{1}{\omega\sqrt{L'_L C'_L}} \tag{3.1}$$

$$\beta = -\frac{1}{\omega\sqrt{L'_L C'_L}} < 0 \tag{3.2}$$

$$Z_C = \sqrt{\frac{Z'}{Y'}} = +\sqrt{\frac{L'_L}{C'_L}} > 0 \tag{3.3}$$

$$v_p = \frac{\omega}{\beta} = -\omega^2 \sqrt{L_L' C_L'} < 0 \qquad\qquad (3.4)$$

$$v_g = \left(\frac{\partial \beta}{\partial \omega}\right)^{-1} = \omega^2 \sqrt{L_L' C_L'} > 0 \qquad\qquad (3.5)$$

From (3.1)-(3.5), it can be concluded that using LH transmission lines we can eliminate the resonance behavior found on the resonant-type metamaterial, such as SRRs. Moreover, with a proper choice of the lumped elements values which built the LH TL, we can control the transmission losses (using a balance structures as shown later) and increase the bandwidth. However, and as a design condition, the dimensions of the metamaterial cells should be less than $\lambda_g/4$ [5].

In left-handed TLs, as the current flows along the series-connected capacitor, a magnetic flux is induced. This can be represented by a series-connected inductance. Moreover, a shunt capacitance is emerged due to the accumulation of charges between the center conductor and the ground. The four passive elements are shown in the incremental circuit model of a metamaterial TL in Figure 3.4 [5].
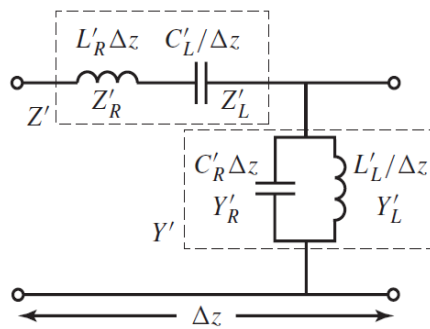
Figure 3.4 Incremental circuit model for a Composite Right/left handed TL [5].

The transmission line model in Figure 3.4 contains the passive elements used to model a right handed (conventional) TL and a LH artificial TL. Hence, it is called

- 32 -

composite right left handed TL. These artificial lines have many new properties which can be used to produce new microwave devices having new appealing properties [5].

3.5 Practical considerations

We discuss in Section 3.4 the backward waves and their lumped element model: a chain of series-connected capacitors and shunt-connected inductors. Choosing the specific values of these passive elements is very important to determine the response of many MW devices as described later in this chapter. Caloz *et al.* use the surface mount technology (SMT) to produce the left handed TL sections in their designs [4], [5]. However, there are some limitations related to this technology. For example, the lumped element values can be chosen from limited specific values depending on the manufacturers. For instant, if we want to implement a capacitor with a specific value we should choose the nearest value taken from the combination of many available capacitors, and hence, there could be a marginal error in that value compared to the designed one. Furthermore, the fabrication, installation, and integration of SMT elements in microwave circuits are more difficult than with distributed elements.

3.6 Implementing the series connected capacitance

An open ended TL can act as a capacitor with specific capacitance if the length, the characteristic impedance (Z_0) and the effective permittivity (ε_{eff}) of the line are known. The relationship between these four parameters can be presented as follow:

$$\omega C = \tan(\varphi)\,/Z_0 \qquad\qquad (3.6)$$

where,

$$\varphi = \beta l_{\text{open ended}}, \text{ and } \beta = \frac{\omega}{c}\sqrt{\varepsilon_{\text{eff}}} \ . \qquad\qquad (3.7)$$

l$_{\text{open ended}}$ is the length of the open ended line, ω is the angular frequency, and Z_0 is the characteristic impedance of the line. Figure 3.5 shows a series-connected distributed capacitor [13], in which the open-ended transmission line (horizontal stub) patterned in the center conductor of the CPW TL introduces its capacitance. The characteristic impedance and the effective permittivity of this inner stub equal 67 Ω and 5.67, respectively. For example, if we need to design a distributed capacitor having a capacitance of 7.9 pF at a specific operating frequency equaling 2 GHz, then, the only parameter that controls its capacitance, according to (3.6) is the length of the open-ended stub. By substituting the previous parameters values in (3.6) the length of the stub should equal 16.2 mm.
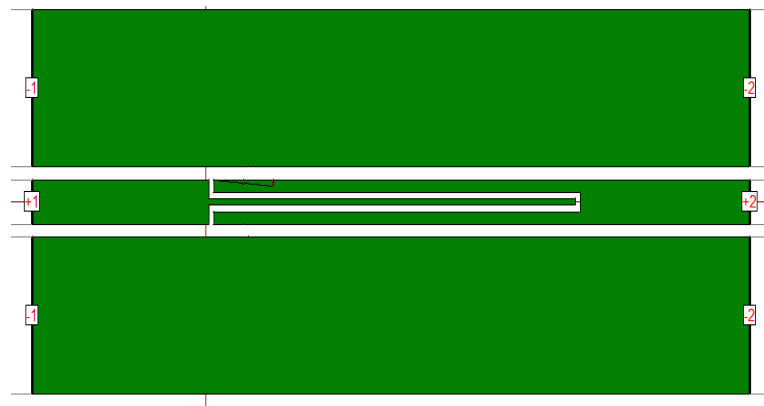
Figure 3.5 The distributed capacitor patterned in the center of a CPW TL

Figure 3.6 shows the response of the open-ended distributed stub patterned in the center of the CPW TL compared to the lumped element response. It can be shown that near the operating frequency, 2 GHz, the scattering parameters for the two capacitors have excellent match.
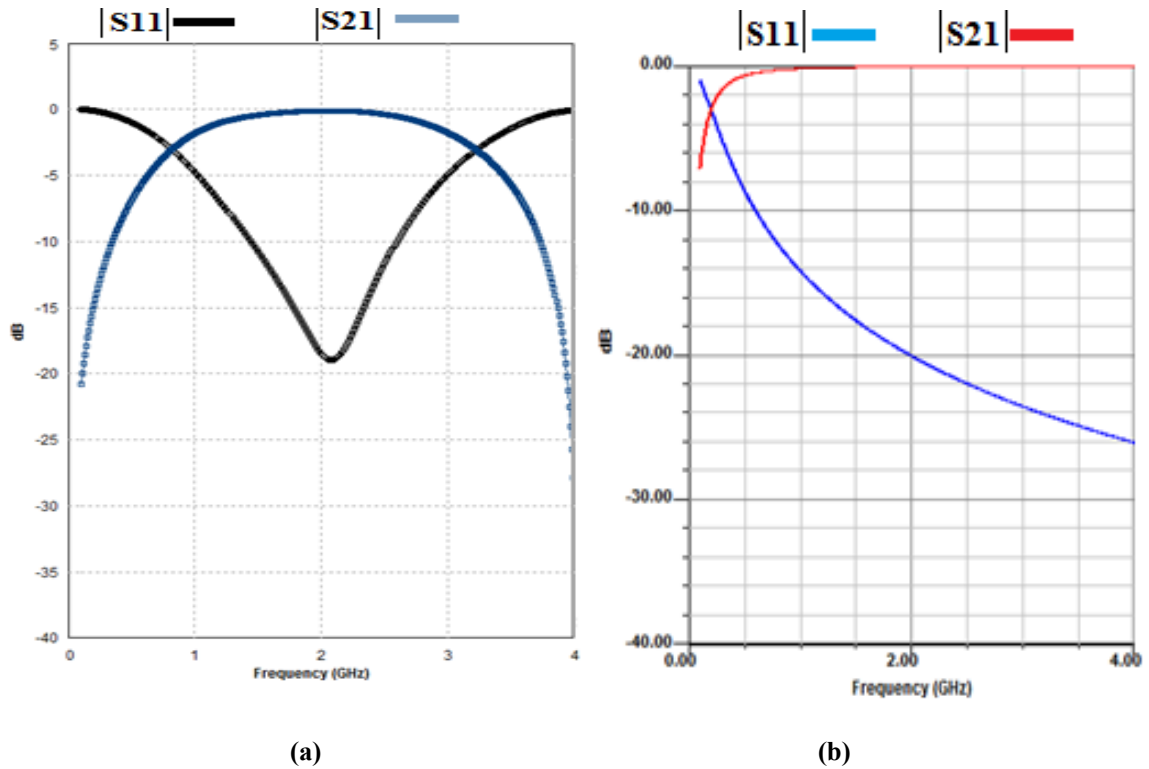
Figure 3.6 (a) The scattering parameters for the distributed capacitor, (b) The scattering parameters for the lumped element equivalent capacitor

It can be noticed that around 2 GHz, $|S_{21}|$ and $|S_{11}|$ for both the lumped and the distributed capacitors have close values. The same is applicable to their phases. Hence, the distributed capacitor can be used to substitute the series lumped capacitor needed to build the metamaterial TL cell.

Within the metamaterial cell, the length of the open-ended stub, which represents a capacitor, could exceed the metamaterial unit dimension condition ($\lambda_g/4$). For example, the length of the open-ended stub in the previous example equals 16.2, however, the effective homogenous condition ($\lambda g/4$) requests that this length should not exceed 15.7mm. Hence, we can use the series-connected parallel capacitor geometry proposed by Hettak *et al* [14] to decrease the capacitor's length as shown Figure 3.7. Using this configuration, the length of the distributed capacitor decreases from 16.5 mm to 14.35 mm. However, the new characteristic impedance and effective permittivity values of the

new topology become 62.9 Ω and 5.59, respectively. Figure 3.8 shows the scattering parameters of the new capacitor topology.
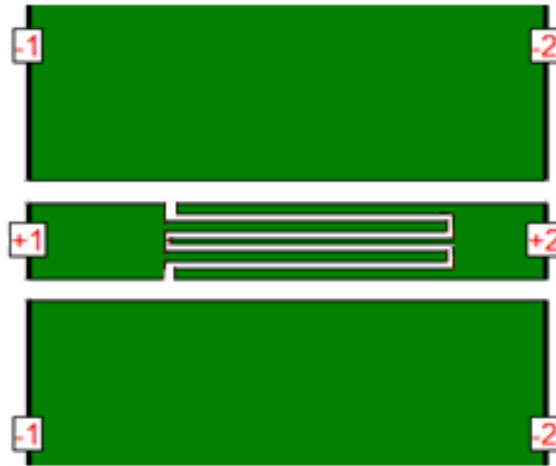
Figure 3.7 The configuration of the series connected parallel distributed capacitor
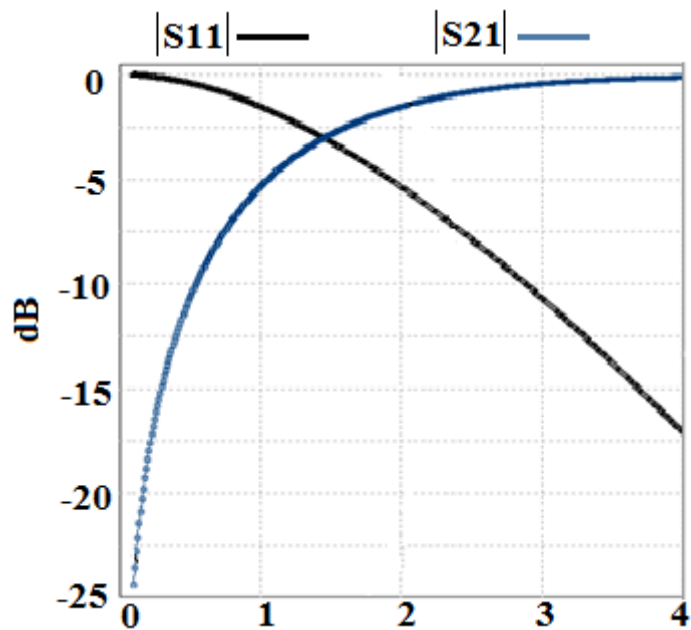
Figure 3.8 The scattering parameters |S11| and |S21| for the two-finger capacitor of Figure 3.7

3.7 Implementing the shunt inductor

A similar design procedure to the previous one can be applied to design a distributed inductor. However, the stub in the center of the CPW TL should be short-ended [13]. The ground plane at which the stub is short-ended is considered infinite for simplicity. The relationship between the operating frequency, the effective permittivity, the characteristic impedance, and the length of the short ended stub is determined by [15]:

$$L = \frac{Z_0 \tan(\beta l_{short\ ended})}{\omega} \qquad (3.8)$$

Figure 3.9 shows the shunt-connected short-ended stub which represents a shunt connected distributed inductor. All the dimensions are determined using the (3.8). Figure 3.10 shows the response of the distributed inductance.
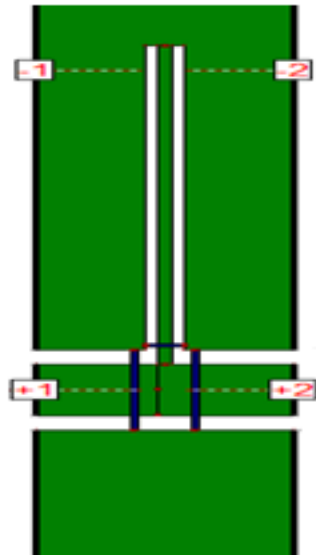
Figure 3.9 The distributed shunt-connected distributed inductor
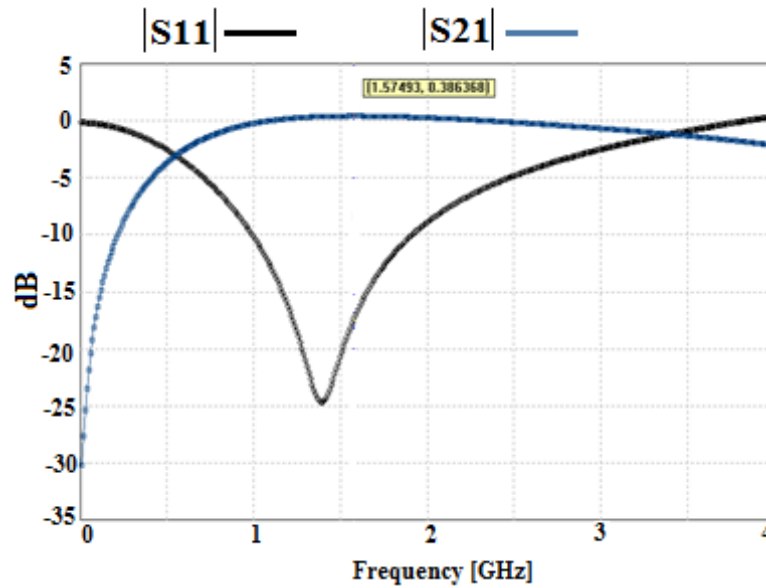
Figure 3.10 The scattering parameters response of the distributed inductor.

3.8 Distributed left-handed metamaterial unit

The left-handed metamaterial unit can be obtained by assembling the previous two distributed passive elements, namely, the series-connected distributed capacitor and the shunt-connect inductor. Figure 3.11 (a) shows the layout of the proposed unit. To have a symmetrical unit, another capacitor attached to the shunt-connected inductor. This T-shape unit layout has additional advantages over non-symmetric topology. Figures 3.11 (b), and (c) show the distributed and the lumped element model responses of the proposed unit, respectively. Very good matching between the two results can be noticed around the designed frequency (2 GHz).
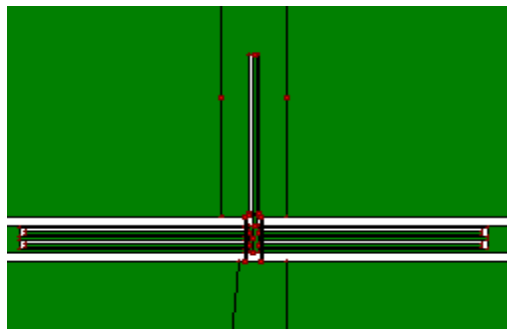
(a)
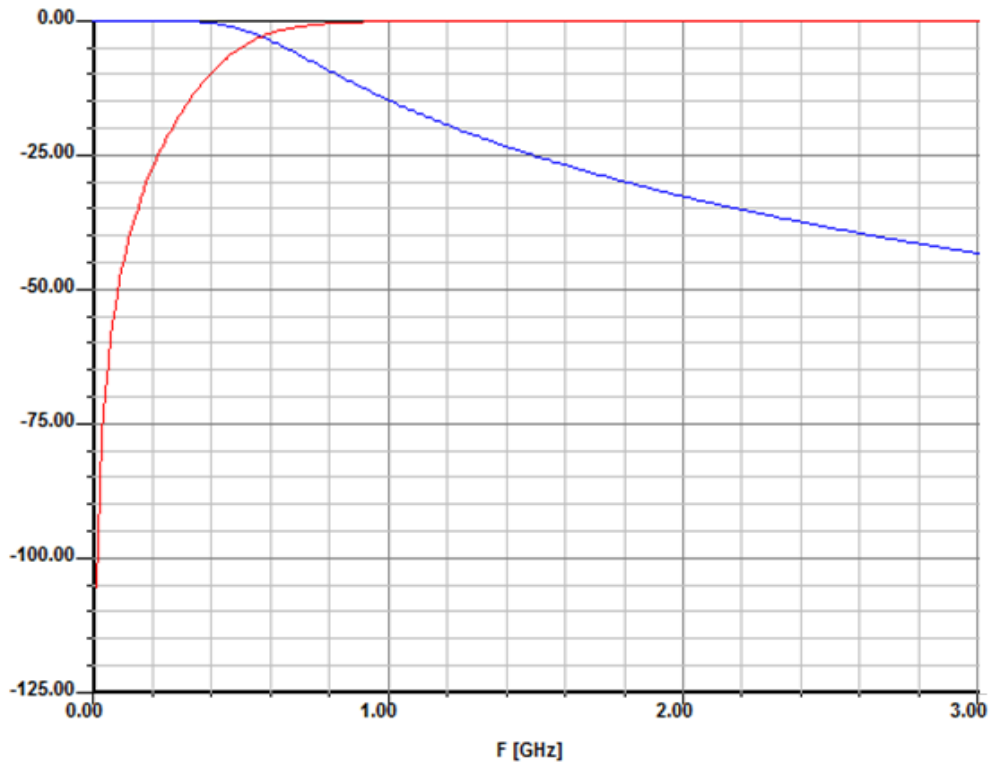
(b)
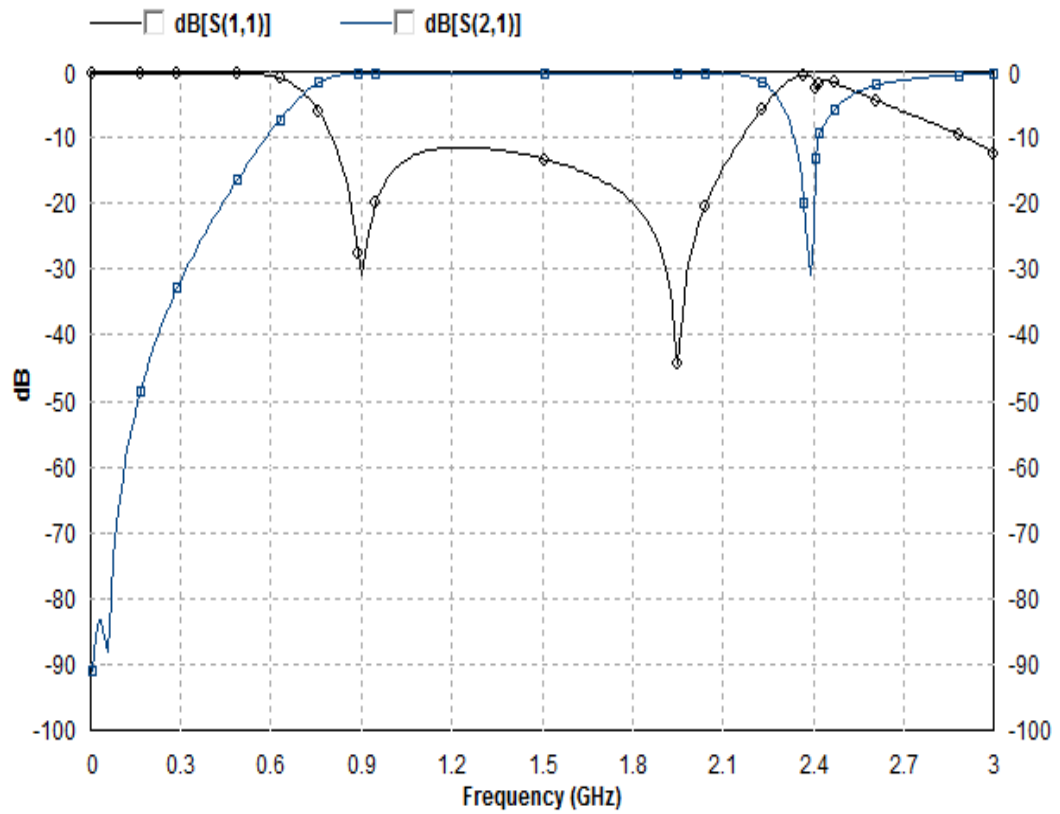
(c)

Figure 3.11 (a) LH MTM distributed symmetrical unit, (b) Equivalent lumped element circuit model response, (c) Distributed response.

3.9   Design of narrow band bandpass filter based on CRLH metamaterial unit

The CRLH cell used to build a metamaterial transmission line can be considered as a simple two-pole bandpass filter. Hence, the design procedure used to build a CRLH cell can be the same as the one used to design a two-pole BPF. In the next subsections, the procedure to design a BPF having the same LE model as in CRLH cells is introduced. Also, a distributed design example that uses this procedure with its related response is introduced.

3.9.1 Lumped element model of the cell

Figure 3.12 shows a two-pole lowpass filter which can be converted to a BPF by applying a standard frequency transformation [15]
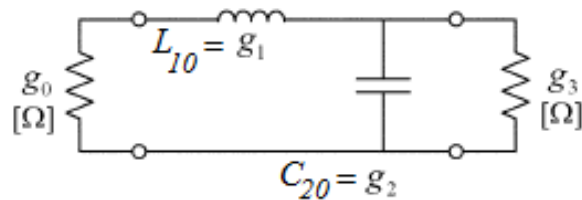
Figure 3.12 Two-pole prototype LPF

If ω_1 and ω_2 denote the edges of the passband of a general BPF, then a bandpass response can be obtained using the following frequency transformation [15].

$$\omega \leftarrow \frac{\omega_0}{\omega_2 - \omega_1}\left(\frac{\omega'}{\omega_0} - \frac{\omega_0}{\omega'}\right) = \frac{\Omega_C}{FBW_0}\left(\frac{\omega'}{\omega_0} - \frac{\omega_0}{\omega'}\right) \tag{3.9}$$

where ω and ω' are the angular frequencies of the LPF and the BPF, respectively. $\Omega_c =$ 1 rad /sec is the cutoff angular frequency of the prototype LPF. FBW_0, and ω_0, are the fractional bandwidth and the center frequency of the BPF, respectively. The resultant BPF is shown in Figure 3.13 and its elements are determined by substituting (3.9) in the expressions for the series reactance and shunt susceptance [15].
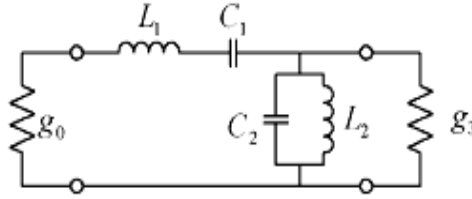
Figure 3.13 Two-pole BPF

$$jX_L = \frac{j}{\Delta}\left(\frac{\omega'}{\omega_0} - \frac{\omega_0}{\omega'}\right)L_K = \frac{j\omega' L_K}{\Delta\omega_0} - \frac{j\omega_0 L_K}{\Delta\omega'} \tag{3.10}$$

where, $\Delta = \dfrac{\omega_2 - \omega_1}{\omega_o} = FBW_o$

Therefore, the series inductor, L_k, is transformed into a series LC circuit with element values equals [15].

$$L'_K = \frac{L_K}{\Delta\omega_0} \quad , \quad C'_K = \frac{\Delta}{\omega_0 L_K} \tag{3.11}$$

We can define C'_K as a function of L'_K as follows,

$$C'_K = \frac{\Delta}{\omega_0 L_K} = \frac{1}{\omega_0^2 L'_K} \tag{3.12}$$

Similarly, it can be shown that a shunt capacitor C_k is transformed into a shunt LC circuit with element values equal [15]:

$$L'_K = \frac{\Delta}{\omega_0 C_K} \tag{3.13-a}$$

$$C_K^{'} = \frac{C_K}{\Delta \omega_0} \qquad \text{(3.13-b)}$$

From (3.5-a)

$$C_K = \frac{\Delta}{L_K^{'} \omega_0} \qquad \text{(3.13-c)}$$

Hence, (3.5-b) becomes

$$C_K^{'} = \frac{1}{L_K^{'} \omega_0^2} \qquad \text{(3.13-d)}$$

3.9.2 Design example of a bandpass filter using one CRLH unit

A bandpass Chebyshev filter (acting as a CRLH cell) centered at 5 GHz with a ripple in the passband of 0.01 dB is introduced in this section. From [16], the elements of the low pass prototype of Figure 3.12 are given by: $g_0=1$, $g_1=0.4488$, $g_2=0.4077$ and $g_3=1.1007$. The desired fractional bandwidth of the passband filter is 0.3, i.e., the equal-ripple bandwidths of the passband is 1.5 GHz. The values of the lumped elements of the BPF can be found using (3.10) and (3.13) as shown in Table 3.1

Table 3.1 The lumped elements values of the circuit configurations of the BPF shown in Figure 3.13

C_L = 0.425 pF	L_L=1.171 nH	C_R= 0.865 pF	L_R =2.381 nH

The series-connected series LC resonator is realized using the proposed resonator in [16] while the shunt-connected shunt resonator implemented using a short ended $\lambda/4$ stub.

Figure 3.3 shows the layout of the proposed filter (centered at 5 GHz) simulated on the commercial Duriod 6010 substrate with relative dielectric constant of 10.2, thickness of 0.635 mm, and a loss tangent of 0.0023. The metal is assumed copper of conductivity equals 5.8 x10^7 S/m. Table 3.2 shows the performance parameters of the filter.
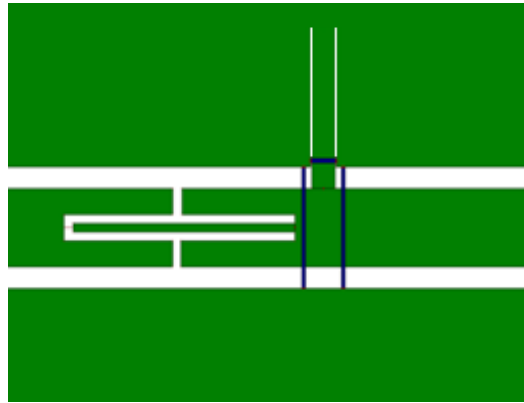
Figure 3.14 Layout of the proposed BPF (CRLH unit) Center at 5 GHz, FBW =0.3

Figure 3.15 shows the simulated results of the filter using IE3D [17]. The filter has excellent agreement between its lumped element model response and its distributed implementation response.
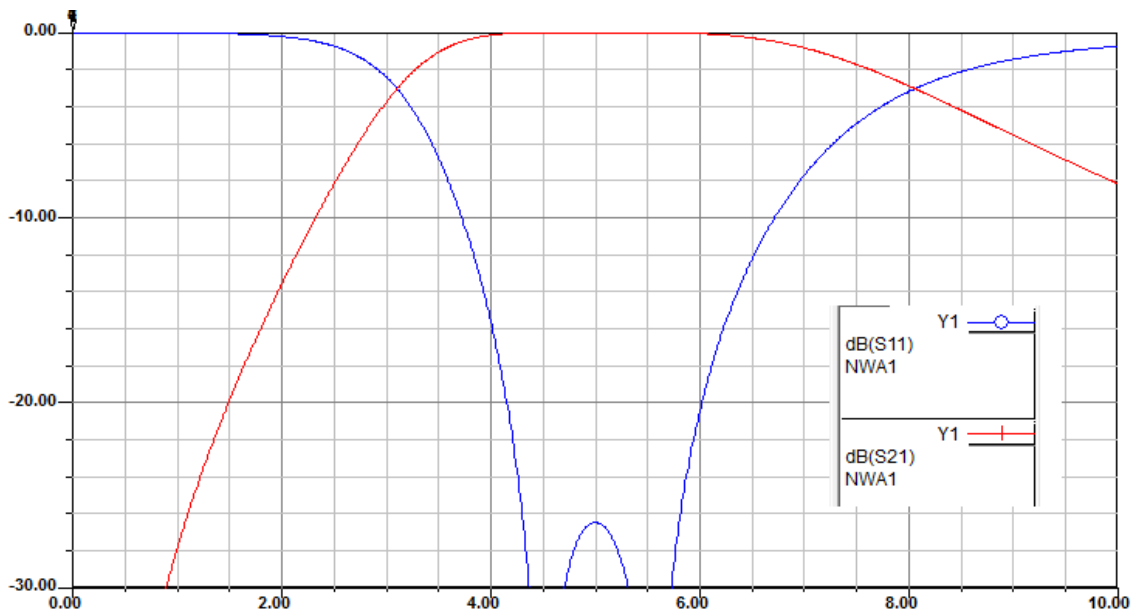
(a)
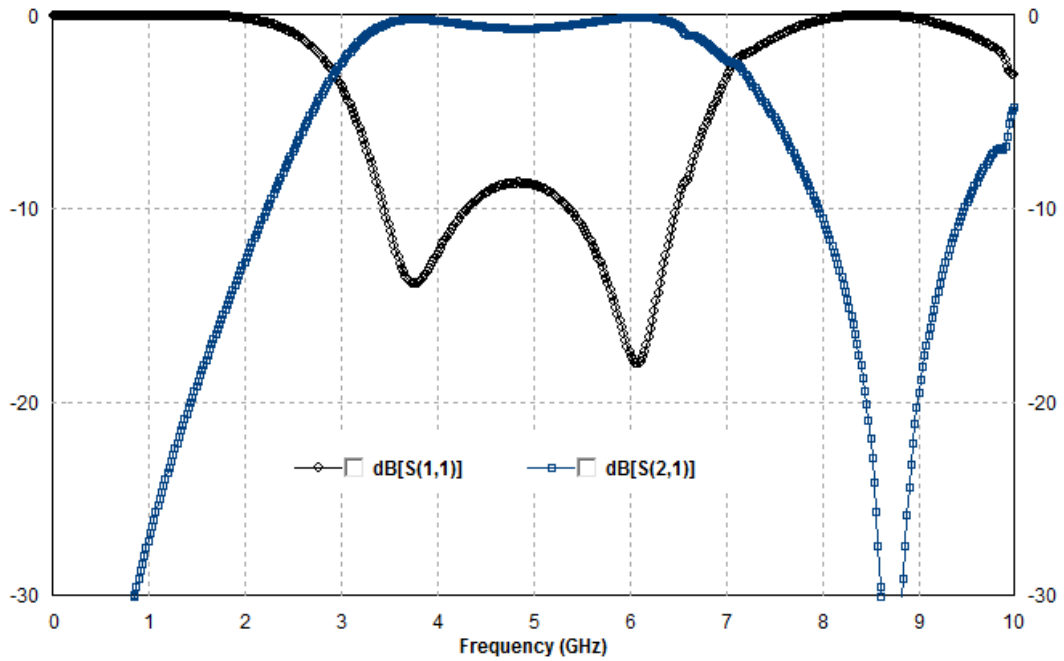
(b)

Figure 3.15 (a) The LE model response of the proposed unit (b) The distributed response

Table 3.2 The characteristics of the CRLH based bandpass filter centered at 5 GHz

criteria \ band	Lumped element model	Simulation
Return loss	27.2 dB	9.2 dB
Insertion loss	0.1 dB	0.3 dB
Q-factor	1.06	1.22
3-dB bandwidth	4.7 GHz	4.1 GHz

3.10 Dual-band property in CRLH TLs [5]

The propagation constant and the characteristic impedance for a pure right handed TL can be written as [5]:

$$\beta^{PRH} = \omega\sqrt{L_R' C_R'} \tag{3.14}$$

$$Z_C{}^{PRH} = \sqrt{\frac{L_R'}{C_R'}} \tag{3.15}$$

Therefore, the relationship between the operating frequency and the propagation constant is linear. On the other hand, in CRLH TL they have a nonlinear relationship as follow [5]:

$$\beta^{CRLH} = \omega\sqrt{L_R'C_R'} - \frac{1}{\omega\sqrt{L_L'C_L'}} \tag{3.16}$$

$$Z_C{}^{CRLH} = \sqrt{\frac{L_R'}{C_R'}} = \sqrt{\frac{L_L'}{C_L'}} \tag{3.17}$$

Hence, by choosing the appropriate values of L_R , C_R , L_L , C_L we can control the slope of the dispersive curve. This means that the two center band frequencies at which the transmission line repeats its response can be located at two non harmonic-related locations. As a result, dual-band devices can be produced using these artificial lines. Figure 3.16 shows an example of the dispersion diagram of a CRLH TL [5].
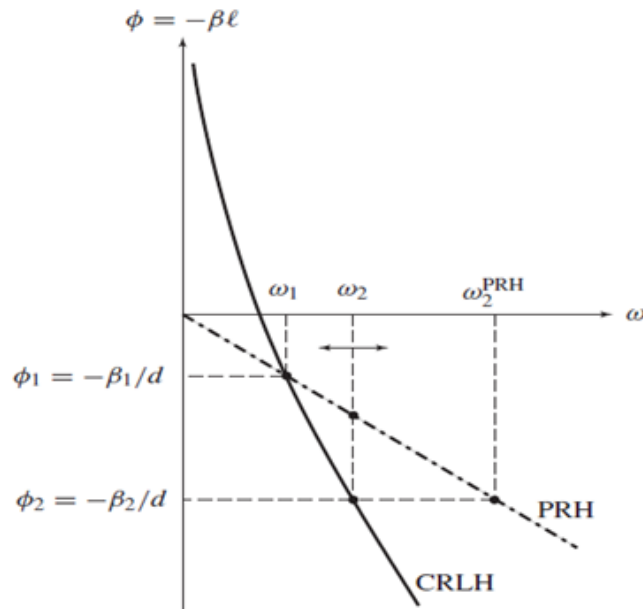
Figure 3.16 Dual-band property in a CRLH TL [5]

To find the values of the four passive elements needed to build a dual-band CRLH TL, we need to solve four equations which satisfy the dispersion diagram at the two

center band frequencies. Moreover, a specific characteristic impedance value of the transmission line has to be chosen (50 Ω in our case). Equations (3.16) and (3.17) have four unknowns in three equations. The fourth equation which meets the dispersion diagram at the second frequency band is [5]:

$$\beta_2^{CRLH} = \omega_2\sqrt{L_R'C_R'} - \frac{1}{\omega 2\sqrt{L_L'C_L'}} \tag{3.18}$$

Using a simple calculation approach, the values of the four passive elements used to build the CRLH cells can be found as [5]:

$$L_R' = \frac{Zt[\beta 2 - \beta 1(\omega_1/\omega_2)]}{\omega_2[1-(\omega 1/\omega 2)^2]} \tag{3.19-a}$$

$$C_R' = \frac{[\beta 2 - \beta 1(\omega_1/\omega_2)]}{\omega_2 Zt[1-(\omega 1/\omega 2)^2]} \tag{3.19-b}$$

$$L_L' = \frac{Zt[1-(\omega_1/\omega_2)^2]}{\omega_1[(\omega 1/\omega 2)\beta 2 - \beta 1]} \tag{3.19-c}$$

$$C_L' = \frac{1-(\omega_1/\omega_2)^2}{\omega_1 Zt[(\omega 1/\omega 2)\beta 2 - \beta 1]} \tag{3.19-d}$$

The inductors and capacitors values of a dual-band CRLH TL can be related to the required phase shifts of a specific dual-band operation. This is accomplished by substituting $\beta_i = -\varphi_i /(Np)$ (i = 1, 2) into equation (3.19) and yields the following LE circuit values [5]:

$$L_R = \frac{Zt[\varphi_1 1(\omega_1/\omega_2) - \varphi_2]}{N\omega_2[1-(\omega 1/\omega 2)^2]} \tag{3.20-a}$$

$$C_R = \frac{[\varphi_1(\omega_1/\omega_2) - \varphi_2]}{N\omega_2 Zt[1-(\omega 1/\omega 2)^2]} \tag{3.20-b}$$

$$L_L = \frac{NZt[1-(\omega_1/\omega_2)^2]}{\omega_1[\varphi_1 - (\omega 1/\omega 2)\varphi_2]} \tag{3.20-c}$$

$$C_L = \frac{N[1-(\omega_1/\omega_2)^2]}{\omega_1 Zt[\varphi_1 - (\omega 1/\omega 2)\varphi_2]} \tag{3.20-d}$$

3.11 Dual-band quarter wavelength TLs and stubs [5]

Many microwave devices consist of quarter-wavelength TL sections in the form of parallel stubs, impedance inverters, etc. For example, a conventional HBLC has four quarter-wavelength TLs. The input power for the HBLCs is split equally at the two output ports at the operating frequency. This response repeat itself each odd-multiple harmonic. i.e., the next center band frequency at which a conventional TL provides a similar response is located at one additional full turn in the Smith chart. On other words, the phase difference between f_1 and $f_2=3×f_1$ equals π.

On the other hand, CRLH TL can repeat its response at a frequency not necessarily the harmonic of the dominant operating frequency. This can be achieved by properly choosing the values of the passive elements of the CRLH cells.

For quarter wavelength application, we can choose any two values of φ_1 and φ_2 which make a π difference at ω_1 and ω_2, for example, let $\varphi_1= -\pi/2$ and $\varphi_2 =-3\pi/2$, hence, equation (3.20) becomes [5]:

$$L_R = \frac{Z_t\pi[1-3(\omega_1/\omega_2)]}{2N\omega_2[1-(\omega1/\omega2)^2]} \qquad (3.21\text{-a})$$

$$C_R = \frac{\pi[1-3(\omega_1/\omega_2)]}{2N\omega_2 Z_t[1-(\omega1/\omega2)^2]} \qquad (3.21\text{-b})$$

$$L_L = \frac{2NZt[1-(\omega_1/\omega_2)^2]}{\pi\omega_1[3(\omega1/\omega2)-1]} \qquad (3.21\text{-c})$$

$$C_L = \frac{2N[1-(\omega_1/\omega_2)^2]}{\pi\omega_1 Zt[3(\omega1/\omega2)-1]} \qquad (3.21\text{-d})$$

The balanced CRLH cell shown in Figure 3.4 can be presented as shown in the circuit model of Figure 3.17 [5].
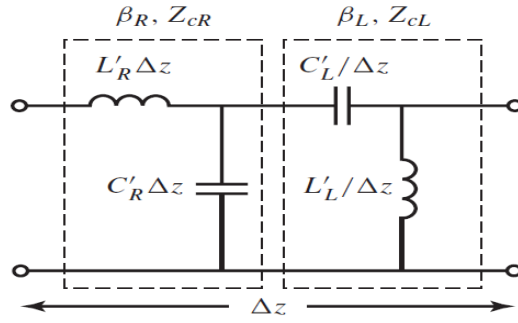
Figure 3.17 Simplified CRLH MTM unit cell (balanced cell) [5]

This means that we can decompose the CRLH TL circuit model into a pure right handed section and a pure left handed section, separated from each other. This separation enables designing the pure RH section using conventional TLs.

The total phase shift across a quarter-wave length CRLH TL can be represented as the sum of the contributions in phase shift from the pure left handed and right handed sections as follow [5]:

$$\varphi_1 = \varphi^{LH}(\omega_1) + \varphi^{RH}(\omega_1) = -\frac{\pi}{2} \tag{3.22}$$

$$\varphi_2 = \varphi^{LH}(\omega_2) + \varphi^{RH}(\omega_2) = -\frac{3\pi}{2} \tag{3.23}$$

The first terms in (3.22) and (3.23) represent the LH phase difference portion and the second terms represent the RH phase difference portion. The RH phase portion can be implemented using an appropriate length of a conventional transmission line, and the left handed section can be implemented using SMT elements or distributed passive elements; series-connected capacitors (C_L), and shunt-connected inductors (L_L).

3.12 A design example of a hybrid branch line coupler using CRLH TLs

A dual-band HBLC with center band frequencies at 0.9 GHz and 1.8 GHz is proposed in this section. These two bands are suitable for GSM/3G applications. Let

$\varphi_1 = -\pi/2$ and $\varphi_2 = -3\pi/2$ and the number of left-handed sections is two (N=2). In general, the composite right/left handed lumped element TL model is not necessarily symmetric, however, in this section a symmetrical model is used.

By substituting the values of ω_1, ω_2, φ_1, φ_2, and N in equations (3.21) we can find the values of the passive elements in the left-handed sections within the four branches. The RH sections have characteristic impedances of 50 Ω and 35.35 Ω [15]. Figure 3.18 shows one of the two artificial 35.35 Ω branches needed to build the dual band HBLC. The right hand section is divided into two equal-length sections located beside each extremity of the LH section.

The CRLH TL model is applicable to any kind of transmission lines (microstrip lines, coplanar waveguide, etc). Figure 3.18 shows the 35.35 Ω branch of the HBLC with a right handed section implemented using microstrip lines.
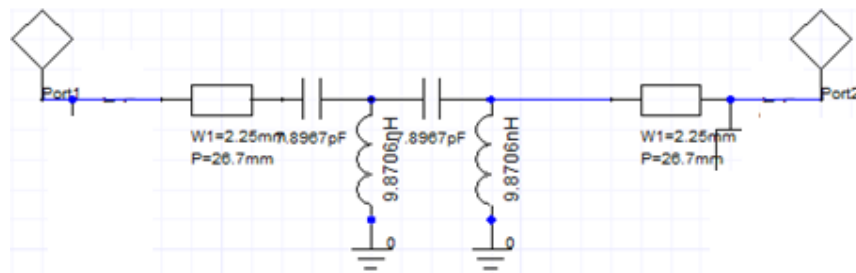
Figure 3.18 Semi-lumped circuit model of a 35.4 Ω branch of the HBLC

The LH section in Figure 3.18 is not symmetric, and hence, a symmetric version is designed as shown in Figure 3.19.
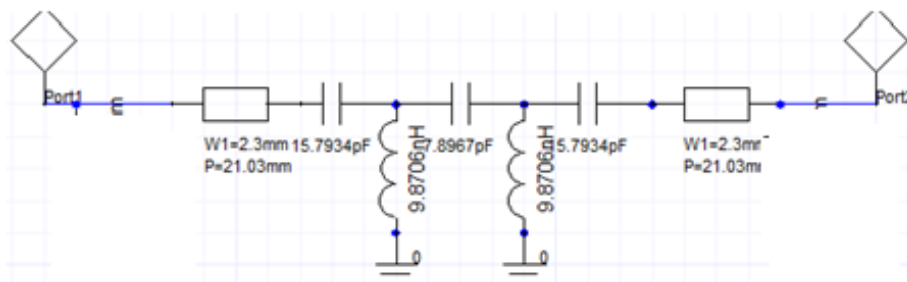
Figure 3.19 Semi-lumped symmetric lumped element model of the 35.4 Ω branch

The semi-lumped element model of the dual-band HBLC is shown in Figure 3.19. All branches are designed using the same procedure. The electrical length of the right handed section is a function of the two center band frequencies and the total phase shift at each band. In this example, the electrical length of the RH section equals 160.24^0 for both, the 35.35 Ω and 50 Ω branches. Hence, the electric length of each RH section located beside each of the extremities of the LH sections equals 80.12^0.

The magnitude and phase of the scattering parameters of the proposed HBLC are shown in Figure 3.20. The input power is equally split between the two output ports at the two center band frequencies. The phase imbalance between the two output ports almost equals 90^0 at the two center band frequencies. The results obtained in Figure 3.21 validate the proposed artificial lines for dual-band application.
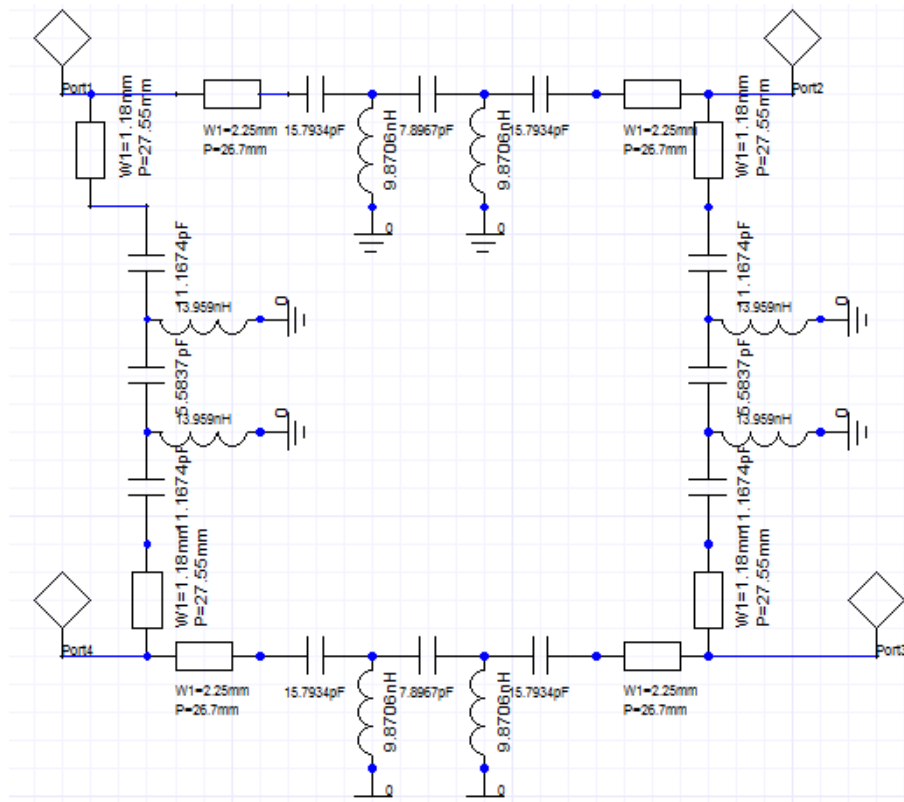
Figure 3.20 The semi LE model of the DB HBLC, N=2

The following comments are linked to the previous design. Firstly, the electrical length of each branch can be relatively high if the two center bands are close to each other. Therefore, the size of the HBLC can be electrically large compared to other dual-band HBLCs [18]-[20]. Secondly, the four T-junctions in the HBLC introduce parasitic discontinuities which affect the response; therefore, an optimization of the length of the RH sections might be needed to overcome this effect.
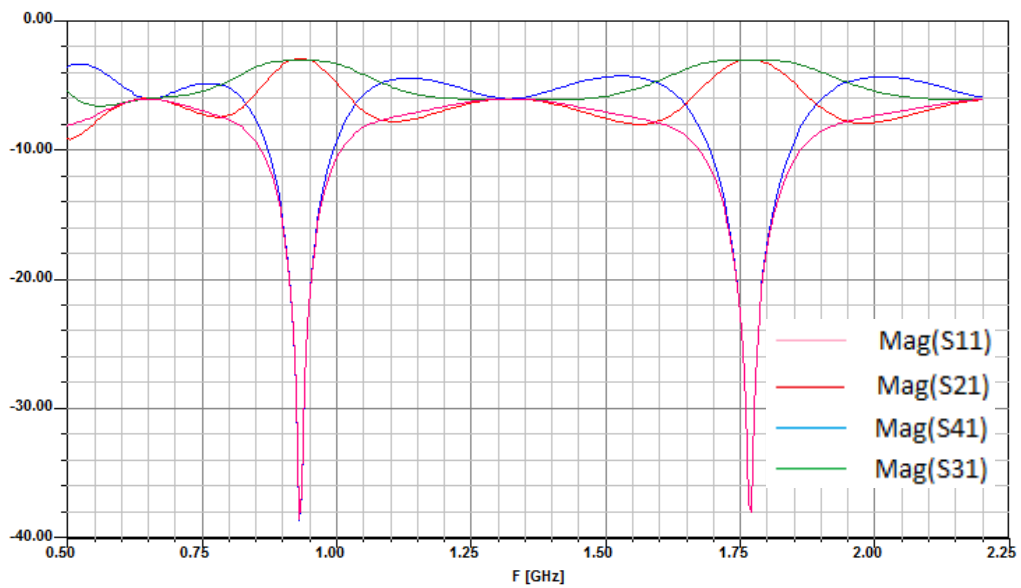
(a)
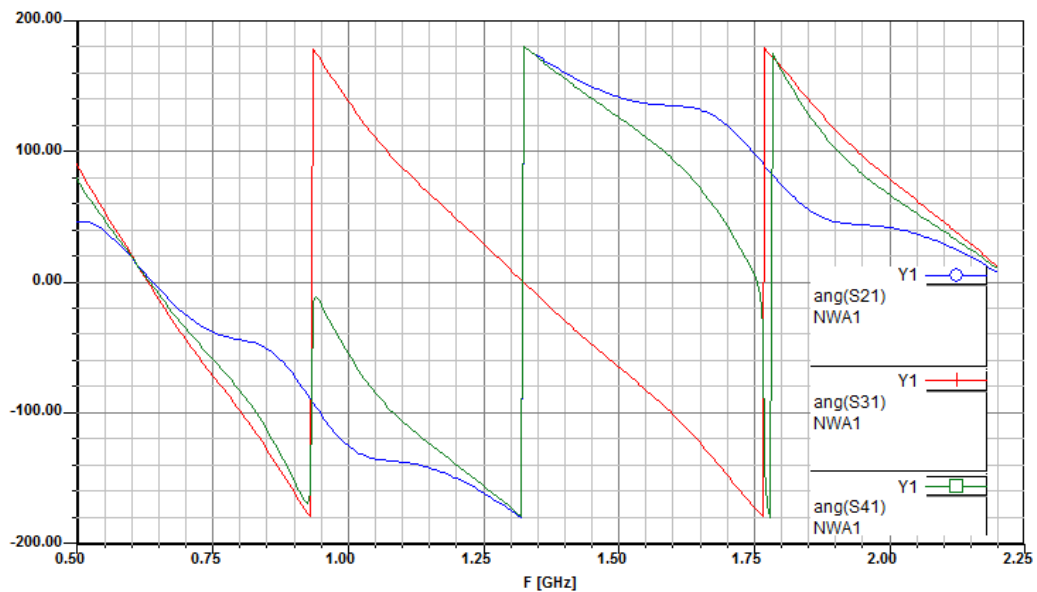
(b)

Figure 3.21 The scattering parameters of the proposed dual-band HBLC: (a) Magnitude, (b) Phase

For practical considerations, it is better to decrease the number of the LH passive elements to the minimum. However, this will degrade the performance of the artificial TL because infinite number of cells needed theoretically to represent any TL. In the following example, the same previous HBLC is designed using one symmetrical LH cell (N=1). The same procedure is implemented, and the new design is shown in Figure 3.22.
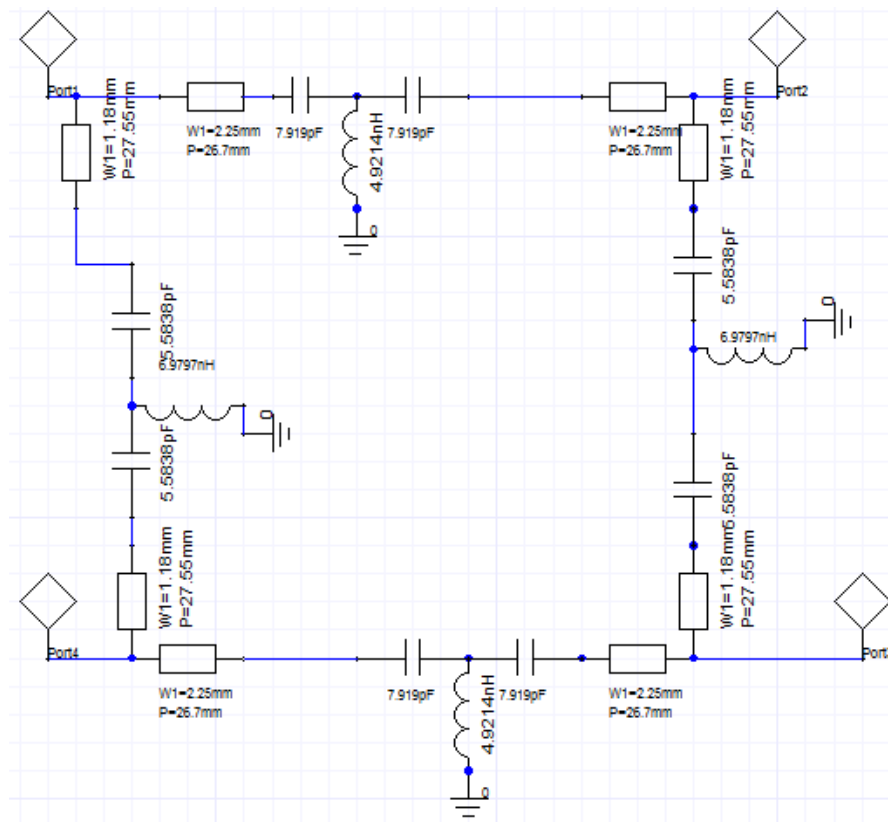
Figure 3.22 Semi-LE Model of a symmetric dual-band HBLC, $f_1 = 0.9\ GHz, f_2 = 1.8\ GHz$, N=1

The response of the HBLC is shown in Figure 3.23. Very good results in terms of the isolation levels, output ports power levels, and quadrature imbalance at the two center band frequencies are obtained. The response is very close to the response of the two-cell LH portion HBLC. Hence, we will use this lumped element model to design the distributed HBLC as introduced in the next section.
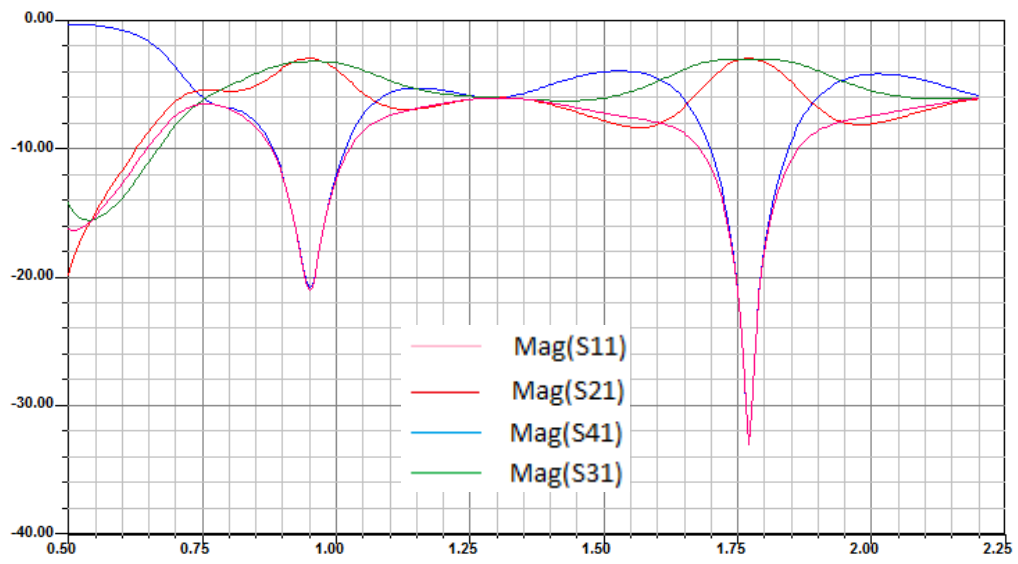
(a)
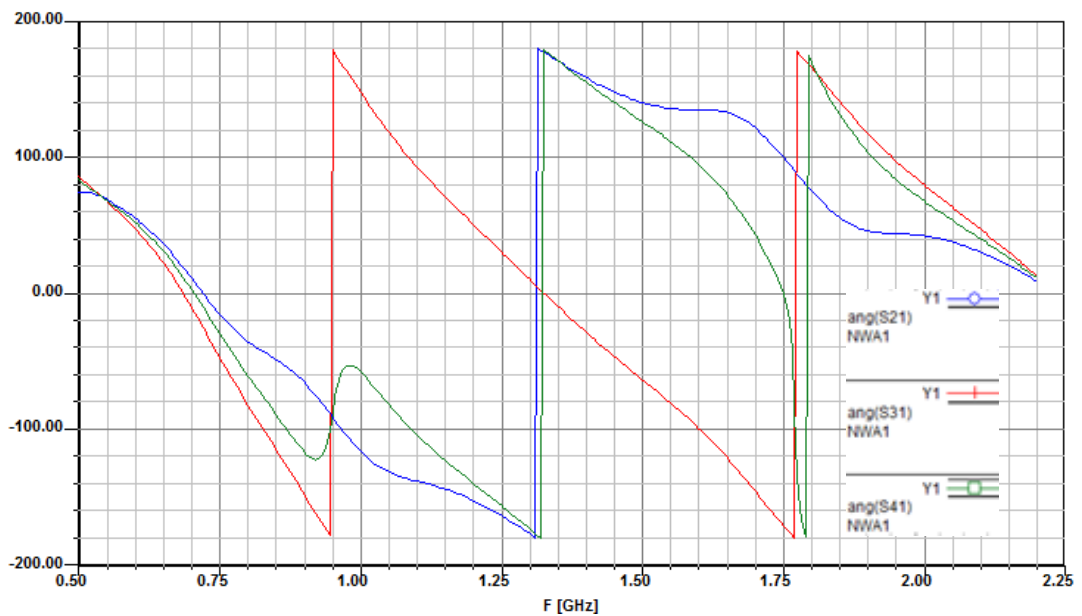
(b)

Figure 3.23 The scattering parameters of the proposed dual-band HBLC : (a) Magnitude, (b) Phase

3.13 Distributed implementation of the dual-band HBLC using CPW TL

The procedure to design the distributed dual-band HBLC can be summarized in the following points:

1) Determine the appropriate characteristic impedances of the four branches. 50 Ω and 35.35 Ω branches are usually used because the input ports of the measuring tools have input impedances equal 50 Ω.

2) Choose the center band frequencies at which the HBLC gives its response.

3) Choose the appropriate number of segments (N) for the left handed sections.

4) Find the values of C_L and L_L for each branch using (3.21), then, find the dimensions of the distributed capacitors (C_L) and the distributed inductors (L_L) using (3.6) - (3.8)

5) To find the dimensions of the distributed passive elements we need to know ε_{eff} and Z_0 for the open ended capacitive and short ended inductive stubs.

6) The distributed response for each branch has to be compared with its equivalent lumped element model response. Optimizations in the lengths of the open-ended stubs, short ended stubs, and the lengths of the right handed sections can be done in order to match the two responses.

7) Assemble all parts (superposition) to get the whole structure, and re-optimize all branches.

8) Because the dimensions of the distributed LH section: C_L and L_L are function of frequency. It will be difficult to reflect the same fixed lumped element values at ω_1 and ω_2 exactly. For this reason, the distributed element will be designed at the first frequency band in the next section, then, it will be designed at the average value of the two center band frequencies.

3.14 Design example of single-band distributed hybrid branch line coupler using CRLH TLs

A distributed single-band HBLC with center band frequency at 0.93 GHz is introduced in this section. Two similar 50 Ω, and 35.4 Ω branches are designed. The

number of the LH segments equals one (N=1) and the LH section is designed in a symmetrical T shape. φ1 and φ2 equals –π/2 and -3π/2, respectively. Using (3.21) we can find that: C_L=2.79 pF , C_R=9.57 pF, L_L = 6.97 nH, L_R =23 .93 nH for each of the two 50 Ω branches and C_L =3.98 pF , C_R= 13.67 pF, L_L =4.88 nH , L_R = 16.75 nH for each of the two 35.4 Ω branches. The characteristic impedances for the open ended capacitive fingers and the short-ended shunt connected inductive stub in the distributed LH part are 63 Ω and 80.5Ω, respectively. Their effective permittivity (ε_{eff}) equal 5.6 and 5.4, respectively. The lengths of these stubs equal 16.9 mm and 10.5 mm for the 50 Ω branches, respectively, and 20.5 mm and 7.8 mm for the 35.4 Ω branches, respectively. Figure 3.24 shows the layout of the distributed CPW HBLC with center band frequencies at 0.9 GHz. The coupler was designed on a Duriod 6010 substrate having a relative dielectric constant of 10.2, a tangent loss of 0.002, a conductivity of 5.8 x10 S/m of copper, and a dielectric substrate thickness of 0.635 mm. Figure 3.25 shows the simulated response of the proposed CPW HBLC using IE3D [17]
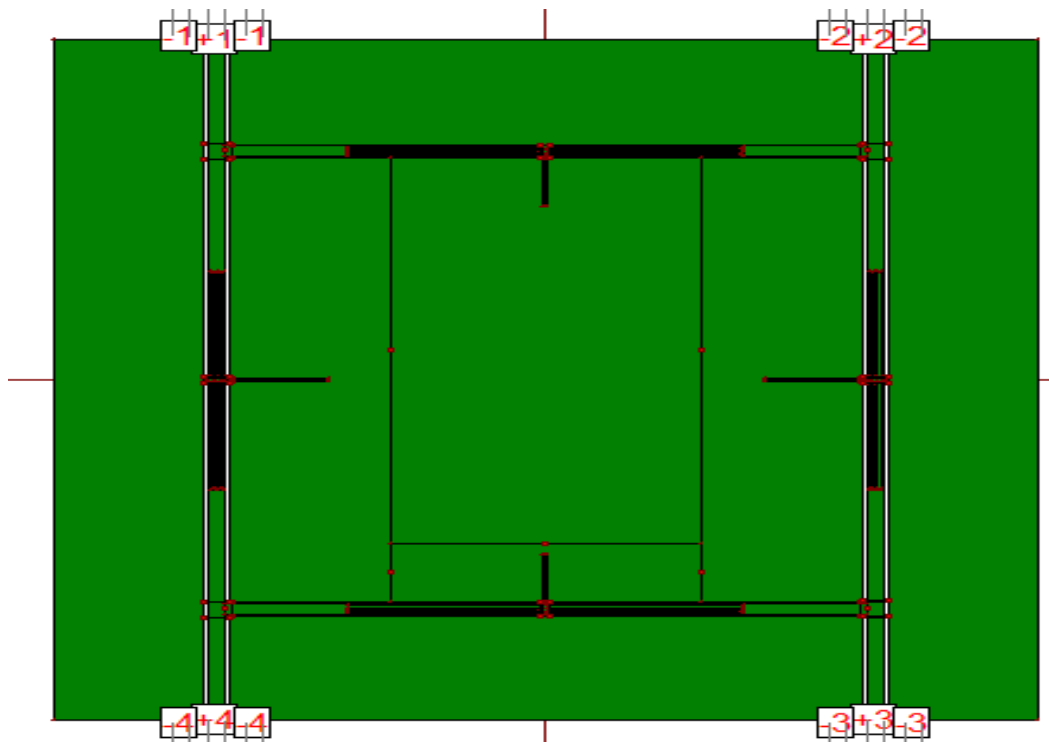
Figure 3.24 The layout of the single-band HBLC using the CRLH TLs.
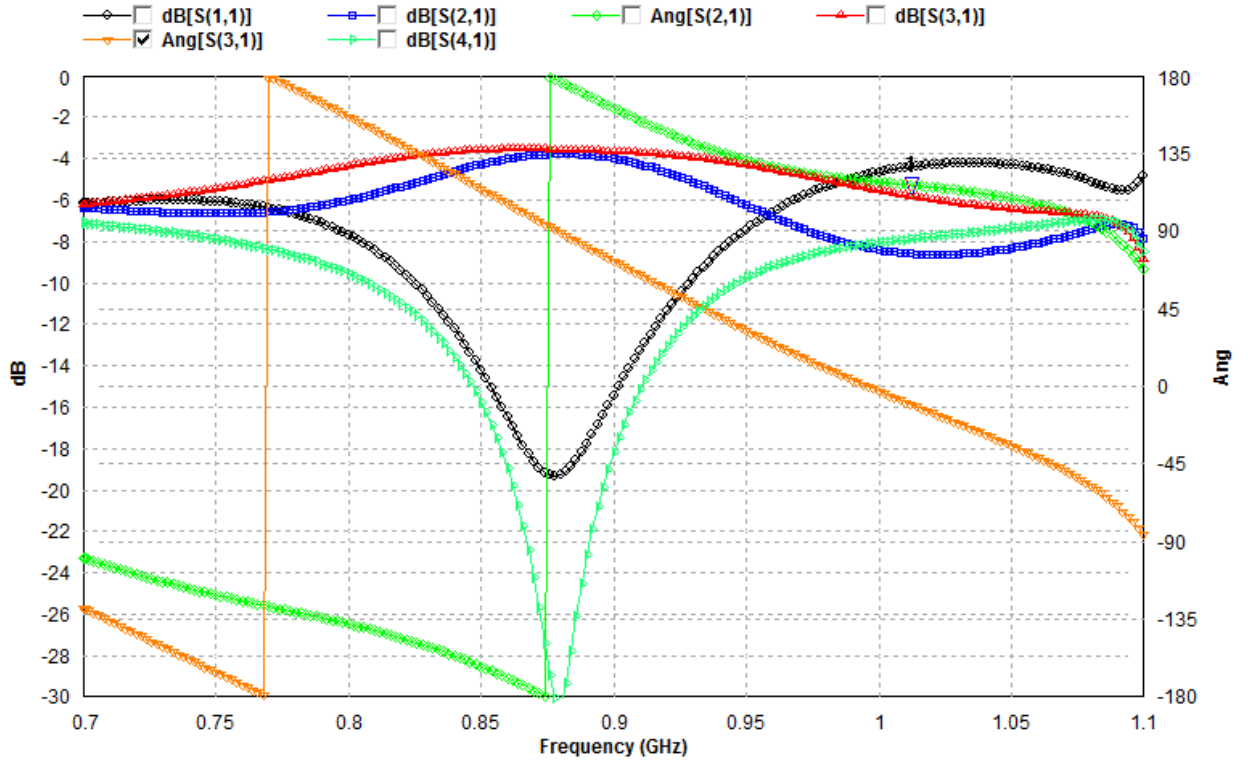
Figure 3.25 The simulated responses of the Single-band HBLC at 0.93 GHz of Figure 3.24

Table 3.3 Performance parameters of the single-band HBLC designed at 0.9 GHz

Operating frequency	0.88 GHz
Return loss (dB)	19.24 dB
Output 1 (S_{21})	3.87 dB
Output 2 (S_{31})	3.72 dB
Amplitude imbalance	0.2 dB
Phase imbalance	86.96^0

The center band frequency of the HBLC is shifted slightly to the left by 0.02 GHz.

The characteristics parameters of the single-band HBLC is shown in Table 3.3

In this section, we investigate producing a single band HBLC using CRLH TLs though

the CRLH TL theory has the advantage of producing dual-band devices. In the next

section, the distributed passive elements are designed at a frequency value equals the average of the two center bands.

3.15 A Design example of dual-band hybrid branch line coupler (distributed)

In this section a dual-band distributed CPW HBLC with center band frequencies at 0.9 GHz and 1.8 GHz is introduced. The distributed passive elements were designs to operate at average value of the two center band frequencies. Figure 3.26 shows the layout of the dual-band CPW HBLC designed using CPW TLs having a substrate with a relative dielectric constant of 10.2, a tangent loss of 0.002, a conductivity of 5.8 x10 S/m of copper, and a dielectric substrate thickness of 0.635 mm.
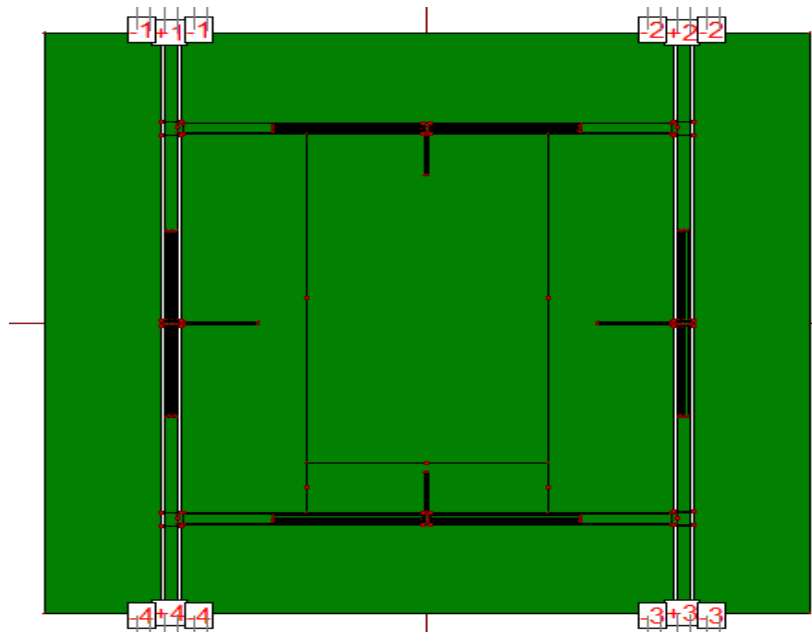
Figure 3.26 Layout of the dual-band HBLC using the CRLH TLs, designed at the average value of the two center band frequencies.

Figure 3.27 shows the simulated characteristics of our dual-band CPW HBLC using IE3D [17].

(a)

(b)
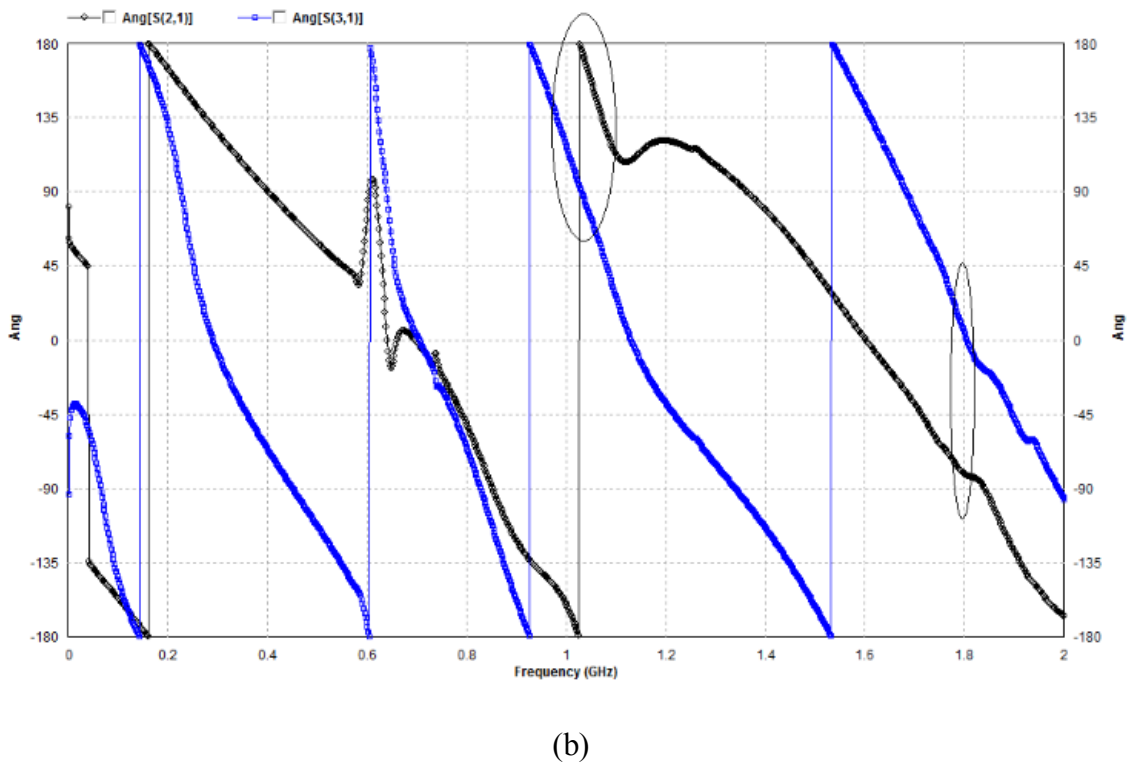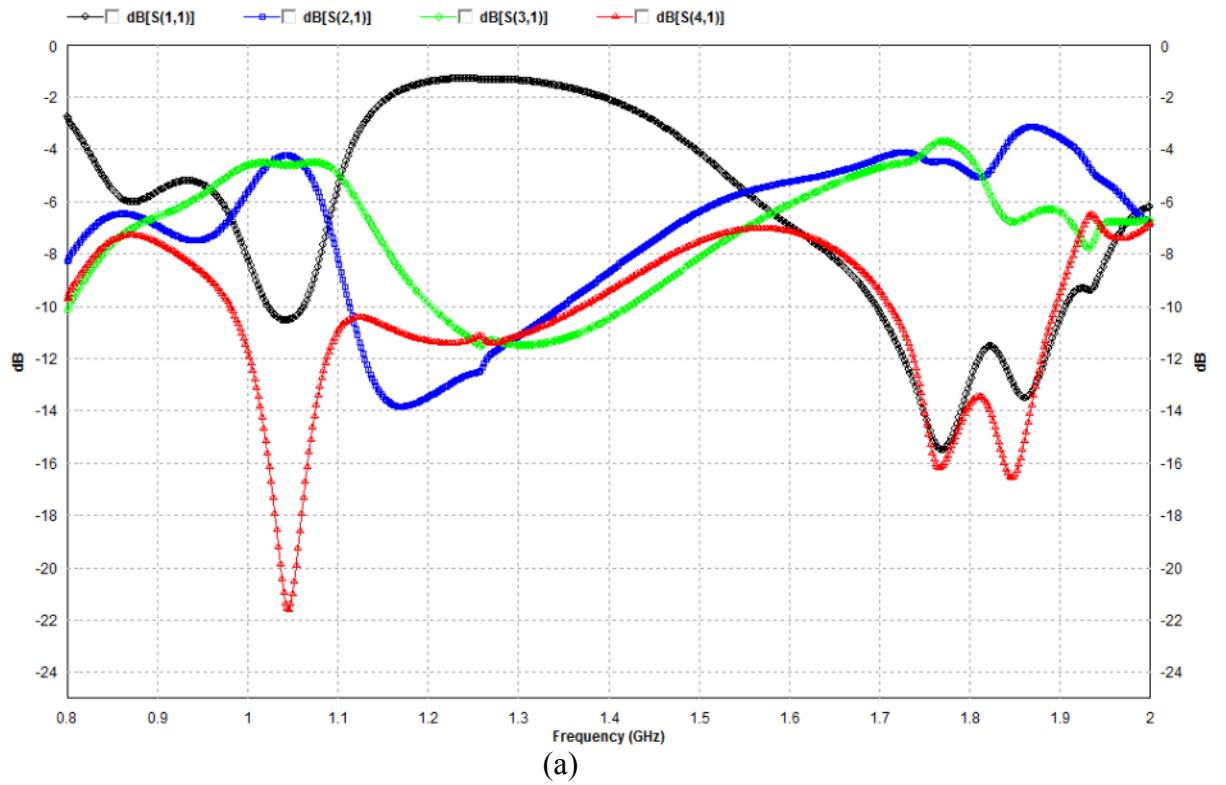
Figure 3.27 The simulated responses of the dual-band HBLC at 0.93 and 1.78 GHz of Figure 3.26

It can be shown from Figure 3.27 that the center band frequencies of our dual-band HBLC is shifted slightly to the right by 0.094 GHz for the first band and to the right by 0.01GHz for the second band. The performance parameters of the dual-band HBLC at 1.024 GHz and 1.79 GHz is shown in Table 3.4.

Table 3.4 Characteristics of the dual-band HBLC at 0.93 GHz and 1.78 GHz

Operating frequency	1.024 GHz	1.79 GHz
Return loss (dB)	10.20 dB	11.60 dB
Output 1 (S_{21})	4.55 dB	4.68 dB
Output 2 (S_{31})	4.53 dB GHz	3.97 dB
Amplitude imbalance	0.02 dB	0.71 dB
Phase imbalance	86.99^0	90.24^0

3.16 Conclusion

This chapter reviews the design procedure to produce balanced CRLH TLs. Also, the dual-band property found in these lines is investigated thoroughly. Distributed implementations for a CPW CRLH cell and two HBLCs are introduced. These artificial lines will later be used to replace conventional TLs in a prototype TL-based inclusion to obtain a dual-resonant inclusion.

References

[1] V. Veselago. "The electrodynamics of substances with simultaneously negative values of ε and μ," *Soviet Physics Uspekhi*, vol. 10, no. 4, pp. 509–514, Jan., Feb. 1968

[2] R.W. Jackson, "Consideration in the use of coplanar waveguide for millimeter wave integrated circuits," *IEEE Trans. On Microwave Theory and Techniques*, Vol.MTT-34, pp. 1450-1456, Dec.1986.

[3] C.P. Wen, "Coplanar Waveguide: A Surface Strip Transmission Line Suitable for Nonreciprocal Gyromagnetic Device Applications," *IEEE Trans. Microwave theory tech.*, Vol.17, No.12, pp.1087-1090, Dec .1969.

[4] J. Browne," Broadband Amps Sport Coplanar Waveguide," *Microwave RF*, Vol.26, No.2, pp.131-134, Feb. 1987.

[5] C. Caloz and T. Itoh, *Electromagnetic Metamaterials, Transmission Line Theory and Microwave Applications*, Wiley and IEEE Press, Hoboken, NJ, 2005.

[6] Ming-Chun Tang; Shaoqiu Xiao; Bingzhong Wang; Jian Guan; Tianwei Deng, "Improved Performance of a Microstrip Phased Array Using Broadband and Ultra-Low-Loss Metamaterial Slabs," *Antennas and Propagation Magazine, IEEE* , vol.53, no.6, pp.31,41, Dec. 2011

[7] Wiwatcharagoses, N.; Chahal, P., "A novel reconfigurable metamaterial unit cell based Composite Right/Left Handed microstrip design*," Antennas and Propagation (APSURSI), 2011 IEEE International Symposium on* , vol., no., pp.2954,2957, 3-8 July 2011

[8] Le-Wei Li; Ya-Nan Li; Tat Soon Yeo; Mosig, J.R.; Martin, O. J F, "A broadband and high-gain metamaterial microstrip antenna," *Applied Physics Letters* , vol.96, no.16, pp.164101,164101-3, Apr 2010

[9] Eccleston, K.W.; Junyao Zong, "Implementation of a Microstrip Square Planar N -Way Metamaterial Power Divider," *Microwave Theory and Techniques, IEEE Transactions on*, vol.57, no.1, pp.189,195, Jan. 2009.

[10] Gil, I.; Bonache, J.; Garcia-Garcia, J.; Martin, F., "Tunable metamaterial transmission lines based on varactor-loaded split-ring resonators," *Microwave Theory and Techniques, IEEE Transactions on* , vol.54, no.6, pp.2665,2674, June 2006.

[11] D. R. Smith, W. J. Padilla, D. C. Vier, S. C. Nemat-Nasser, and S. Schultz. "Composite medium with simultaneously negative permeability and permittivity," *Phys. Rev. Lett.*, vol. 84, no. 18, pp. 4184–4187, May 2000.

[12] Pendry, J.B.; Holden, A.J.; Robbins, D.J.; Stewart, W.J.; , "Magnetism from conductors and enhanced nonlinear phenomena," *Microwave Theory and Techniques, IEEE Transactions on* , vol.47, no.11, pp.2075-2084, Nov 1999.

[13] N. Dib, L. Katehi, G. Ponchak, and R. Simons, "Theoretical and experimental characterization of coplanar waveguide discontinuities for filter applications," *IEEE Trans. Microwave Theory Tech.*, vol. 39, pp. 873–882, May 1991.

[14] D. M. Pozar, *Microwave Engineering*, 2nd ed. New York: Wiley, 1998.

[15] G. Matthaei, L. Young, and E. M. T. Jones, *Microwave Filter, Impedance-Matching Networks, and Coupling Structures*. Norwood, MA: Artech House, 1980.

[16] K. Hettak, N.I Dib, A.-F.Sheta, and S.Toutain," A class of Novel Uniplanar Series Resonators and Their Implementation in Original Applications," *IEEE Trans. Microwave Theory Tech.*, Vol.46, No.9, pp.1270-1276, Sept.1998.

[17] Zeland Software, Inc., "IE3D Simulator," Fremont, CA, 2009.

[18] Hyunchul Kim; Byungje Lee; Myun-Joo Park, "Dual-Band Branch-Line Coupler With Port Extensions," *Microwave Theory and Techniques, IEEE Transactions on* ,vol.58, no.3, pp.651, 655, March 2010.

[19] Myun-Joo Park; Byungje Lee, "Dual-band, cross coupled branch line coupler," *Microwave and* Wireless Components *Letters, IEEE* , vol.15, no.10, pp.655,657, Oct. 2005.

[20] Sinchangreed, V.; Uthansakul, M.; Uthansakul, P., "Design of tri-Band quadrature hybrid coupler for WiMAX applications," *Intelligent Signal Processing and Communications Systems (ISPACS), 2011 International Symposium on* , vol., no., pp.1,4, 7-9 Dec. 2011.

CHAPTER 4

A New Type of Transmission Line-Based Metamaterial Inclusions

In this chapter, a new type of transmission line-based metamaterial resonator is proposed. The new structure is based on a modified uniplanar series resonator bent to form a close square loop inclusion which contains a distributed capacitance and inductance. Many advantages of the proposed structures over conventional split ring resonators are discussed. Based on simple transmission line theory, the resonant frequency at which a deep rejection frequency band occurs with sharp cutoff rates beside the stopband, due to the presence of negative effective permeability in the dielectric slab of the host transmission line in the vicinity of resonance is calculated and compared with simulated and measured results.

Moreover, this chapter introduces another two AMM inclusions that utilize other CPW TLs' discontinuities (gap in the center conductor, and high impedance TL segments). The two designs are simulated, fabricated and tested. Their simulated and measured responses are also in excellent match which validate the two design inclusions.

4.1 Theory and design of the new TL-based inclusion

Many techniques are used to find the distributed capacitance and inductance within SRRs [1]-[3]. For example, Marqués *et al.* find an expression for the distributed capacitance based on the per unit length (p.u.l) capacitance between two coupled

metallic strips printed on a dielectric substrate and having the same dimensions and separation distance as in the two mutually coupled rings in conventional SRRs [3] using the well-known expression $C_{p.u.l} = \beta/\omega Z_0$ [4], where β is the propagation constant and Z_0 is the characteristic impedance of the two coupled metallic strips.

On the other hand, calculating the distributed inductance is much more complex. Hence, in order to simplify finding a closed form mathematical expression, Marqués *et al*. assume that the inductance in SRRs can be approximated as the inductance of one ring having a radius equals to the average radii of the two rings [3].

For all the proposed geometries which are driven from conventional SRRs there are some advantages and disadvantages. Our goal is to design a new AMM with the following advantages. Firstly, the distributed capacitance and inductance within the resonators can be calculated accurately using simple TL theory. This means that we will not use complex expressions or approximations. Secondly, the proposed geometry should offer the possibility to tune its distributed elements separately, unlike other structures in the literature in which the capacitance and inductance are linked together by many common dimensions. This will allow us to control the Q-factor in the proposed resonators. Thirdly, the AMM has only one controlling dimension to tune the resonant frequency. Finally, the proposed AMM is more compact as compared to conventional AMMs.

In order to find an accurate and simple expression for the resonant frequency in AMMs, both the distributed capacitance and inductance should have this property. Hettak *et al*. proposed a class of series-connected resonators in [5], and solved their uniplanar resonators based on space-domain integrated equations (SDIE) technique using the method of moments in conjunction with simple TL theory.
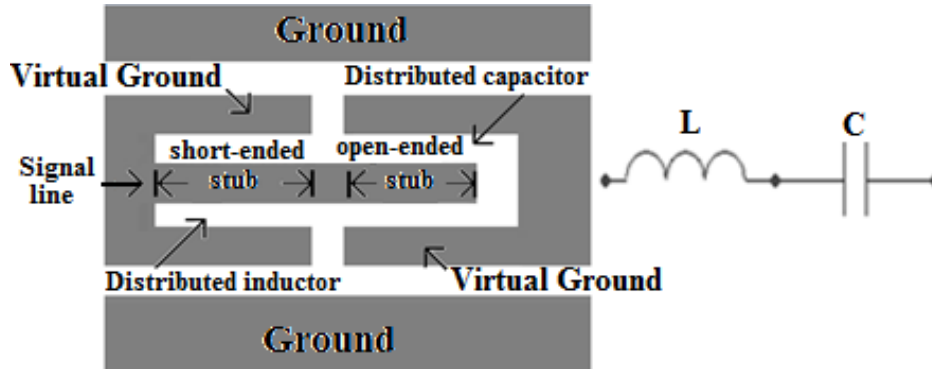
Figure 4.1 Top view of the series connected resonator realized on CPW and its equivalent lumped element model [5].

Figure 4.1 shows one of the proposed resonators in [5] realized using CPW TLs and its equivalent circuit elements. This structure consists of an open-ended stub in series with a short-ended stub in the center conductor (signal line as shown in Figure 4.1). According to [5], the two metallic strips on each side of the open- and short- ended stubs in the center strip behave as virtual finite grounds (see Figure 4.1). If the length of each inner stub is less than or equal to $\lambda_g/8$, then they can represent a distributed capacitance and inductance, respectively. Equations (4.1) and (4.2) express the equivalent lumped element values for the open-ended and short-ended stubs within the center conductor of the CPW related to their lengths as:

$$C = \frac{\tan(\beta l_{open\ ended})}{\omega Z_0} \tag{4.1}$$

$$L = \frac{Z_0 \tan(\beta l_{short\ ended})}{\omega} \tag{4.2}$$

where $l_{open\ ended}$ and $l_{short\ ended}$ are the lengths of the open ended and short ended stubs, respectively, ω is the angular frequency, and Z_0 is the characteristic impedance of the stubs patterned in the center conductor.
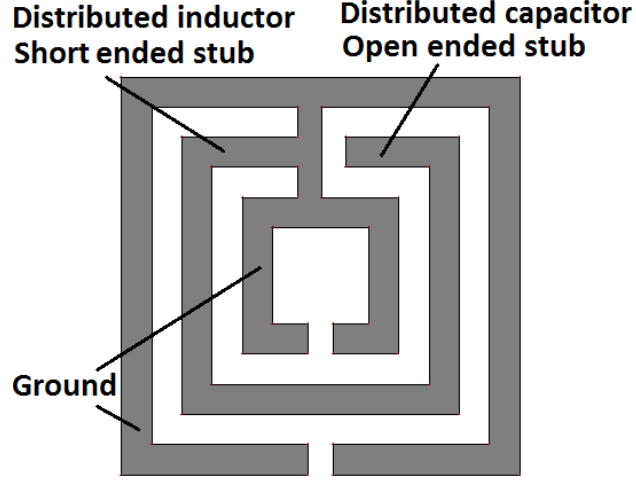
Figure 4.2 Layout of the proposed AMM.

By tuning the previous geometry into a closed loop inclusion, we can end up with a new AMM geometry as shown in Figure 4.2. The resonant frequency of the proposed geometry can be defined as:

$$\omega_0 = \frac{1}{\sqrt{LC}} = \frac{\omega}{\sqrt{\tan(\beta l_{short\ ended})\tan(\beta l_{open\ ended})}} \tag{4.3}$$

where,

$$\beta = \frac{\omega}{c}\sqrt{\varepsilon_{eff}} \tag{4.4}$$

For simplicity, let $l_{open\ ended} = l_{short\ ended} = l$. Therefore,

$$\frac{f_0}{f} = \frac{1}{\tan\left(\frac{\omega}{c}\sqrt{\varepsilon_{eff}}\ l\right)} = \frac{1}{\tan\left(\frac{2\pi}{\lambda_g}l\right)} = 1 \tag{4.5}$$

where λ_g is the guided wavelength and ε_{eff} is the effective permittivity of the open and short-ended center stubs. In order to properly use (4.5) the resonant frequency should equal the operating frequency at which the distributed capacitance and inductance are designed to have their fixed calculated lumped values. This means that the right hand side of (4.5) should equal to unity. Hence, the obtained length of the open-ended and short ended stubs is given by:

$$l = \frac{\pi c}{4\omega\sqrt{\varepsilon_{eff}}} = \frac{c}{8f\sqrt{\varepsilon_{eff}}} = \frac{\lambda_g}{8} \tag{4.6}$$

4.2 Advantages of the proposed design over conventional SRRs

The following can be concluded from the previous equations. Firstly, the resonant frequency depends only on one dimension (i.e. the stubs' lengths), unlike SRR or other AMMs derived from conventional SRRs.

Secondly, one can independently tune the values of the distributed passive elements by changing the length of the inner stubs. This property gives an advantage over SRRs, whose distributed capacitance and inductance are linked together by many common geometrical dimensions. Hence, using the proposed AMM, the quality factors in AMM-based microwave circuits can be simply controlled by independently changing the stubs' length. This property can significantly enhance and control the passbands, stopbands, and the fractional bandwidths in AMM-based filters.

Thirdly, the resonant frequency does not depend on the characteristic impedance of the open and short-ended stubs. This property gives us more design flexibility in choosing the width of the center stubs and the spacing between the finite grounds and the stubs. Therefore, these dimensions can be decreased to provide additional compactness, as long as they meet the fabrication limits.

Fourthly, the resonant frequency of the proposed AMM is lower than the resonant frequency of a similar-size conventional square split resonator. Hence, a significant reduction in the size of the proposed AMM is achieved as compared to a conventional square SRR having the same resonant frequency .

Fifthly, since the proposed resonator depends on TL theory, it is possible to scale the lengths of the center stubs (one dimensional scaling) in order to linearly shift the resonant frequency .

Finally, the expression in (4.6) is simple, straightforward, and accurate, as long as the lengths of the inner stubs equal to $\lambda_g/8$.

4.3 A design example (simulations, and measurements)

To demonstrate the performance of the proposed structure, a one-period square resonator backed CPW has been designed and fabricated as shown in Figure 4.3. The substrate used is RT/Duroid 6010LM which has a dielectric constant of 10.2, loss tangent of 0.0023, and a thickness of 0.635 mm. The designed resonant frequency of the proposed AMM is 3.4 GHz. Hence, using (4.6) the open- and short-ended stubs within the resonators are 4.20 mm, given that ε_{eff} =6.89, which is the same as ε_{eff} for a finite-ground CPW TL having the same dimensions as the inner stubs [6].

Figure 4.4 shows the simulated and measured scattering parameters of the proposed metamaterial-based resonator. We used the full-wave electromagnetic simulator IE3D which is based on the method of moments to design the AMM [7]. The simulated resonant frequency appears at 3.35 GHz, which is very close to the theoretical value (3.4 GHz). The small difference between the simulated and the theoretical values can be attributed to the parasitic discontinuities in CPW TLs. However, these discontinuities have a negligible effect on the performance of the AMM. A shift of 0.02 GHz in the resonant frequency between the measured and simulated responses is observed as shown in Figure 4.4. This shift maybe due to fabrication tolerance.

Table 4.1 summarizes the simulated and measured characteristics of the proposed AMM. The 3-dB bandwidth and the Q-factor can be easily controlled since they are directly linked to the tunable distributed capacitance and inductance within the AMM. Besides its accurate estimated resonant frequency, the proposed AMM shows very good

values of insertion loss (>10 dB), return loss (< 2.5 dB) and Q-factor (>20). Hence, it can be an excellent candidate for resonance-based microwave circuits.

According to [2], the resonant frequency of a conventional square SRR having the same dimensions as our proposed AMM, and loaded into the same CPW TL, is 4.36 GHz. Hence, the proposed AMM has a size reduction factor of 23.62% as compared to conventional S-SRRs.
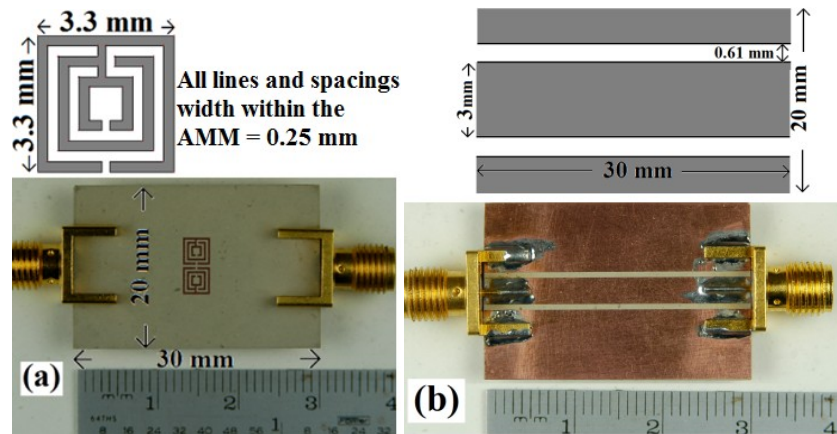
Figure 4.3 Layout and photograph of the fabricated CPW TL loaded by the proposed AMM. (a) Bottom view. (b) Top view.
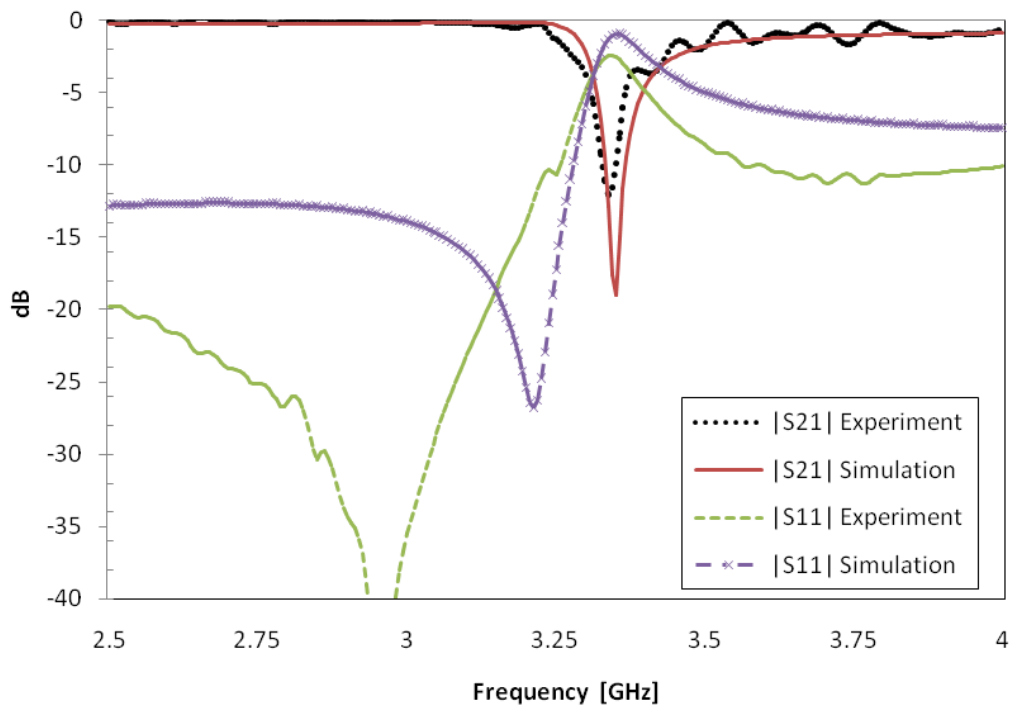
Figure 4.4 The scattering parameters of the proposed AMM in Figure 4.3 loaded into CPW TL.

Table 4.1 Performance of the proposed AMM (Designed f_c = 3.4 GHz)

	Simulation	Measurement
Resonant frequency	3.35 GHz	3.33 GHz
Return loss	0.9691 dB	2.49 dB
Insertion loss	18.99 dB	12.08 dB
Q-factor	26.80	24.27

4.4 A modified AMM structure

In this section, a similar geometry to the previous AMM is proposed. The new structure is shown in Figure 4.5. The capacitive open-ended stub and the inductive short-ended stubs are marked in blue and brown circles, respectively.
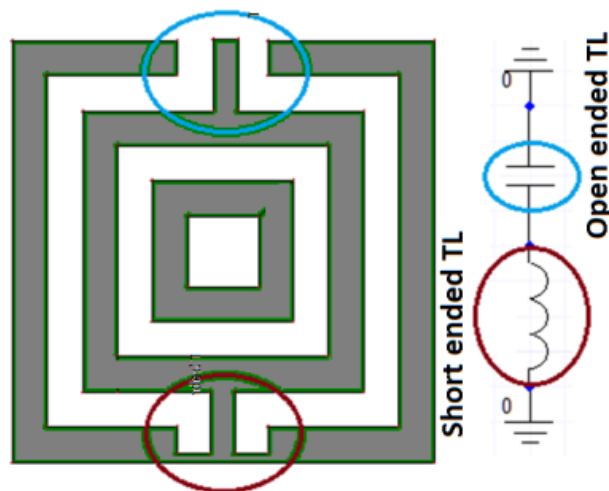
Figure 4.5 Layout of the modified proposed AMM

The two stubs are shorter than those in the previous prototype structure. Hence, this inclusion resonates at higher frequency for same size layout. Figure 4.6 shows the simulated scattering parameters of the AMM loaded into the same dimension CPW TL, and Table 4.2 summarizes its performance.
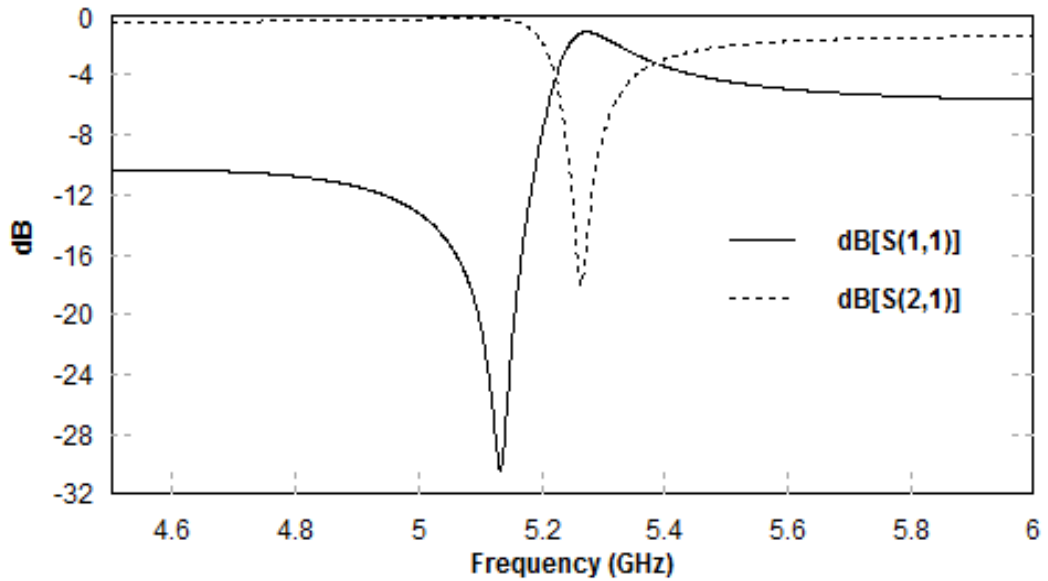
Figure 4.6 The scattering parameters of the AMM loaded into CPW TL.

Table 4.2 Performance of the AMM shown in Figure 4.5

	Simulation
Resonant frequency	5.26 GHz
Return loss	1.17 dB
Insertion loss	17.89 dB
Q-factor	26.31

4.5 Other metamaterial inclusions based on CPW discontinuities

This section introduces a new inclusion based on other coplanar waveguide (CPW) discontinuities. Figure 4.7 (a) shows the layout of the inclusion. The structure can be separated into two parts; a distributed capacitance across the gap on the center strip of the CPW TL, and a distributed inductive high-impedance TL. The two passive distributed elements are connected in series and bent into a closed-loop square shape in order to permit the flow of the resonant currents.

The coupling capacitance value across the gap is given by $C_g = -\text{Im}(Y_{12})/\omega$, where ω is the angular frequency, and Y_{12} is the transmission admittance across the gap. It is shown that C_g has almost a fixed value of 0.24 pF between 3 GHz and 5.2 GHz.
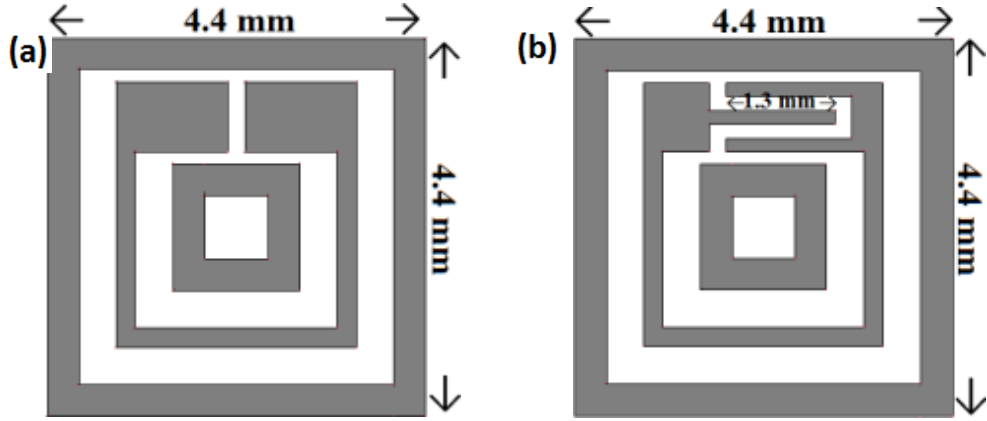
Figure 4.7 Layout of the CPW TL-based discontinuities inclusions. (a) with a capacitive gap. (b) with an interdigited finger.

The inductance of the distributed high-impedance TL is related to its length (l_h), characteristic impedance (Z_h), and the effective permittivity (ε_{eff}) of the TL as [4] :

$$L = \frac{\sqrt{\varepsilon_{eff}}\ l_h\ Z_h}{v_0} \tag{4.7}$$

where v_0 is the speed of light in free space. The resonant frequency (f_r) is given by:

$$f_r = \frac{1}{2\pi\sqrt{LC}} = \frac{1}{2\pi\sqrt{\dfrac{\sqrt{\varepsilon_{eff}}\ l_h\ Z_h\ C}{v_0}}}. \tag{4.8}$$

In order to decrease the size of the proposed inclusion, the geometry of the distributed capacitor in Figure 4.7 (a) is modified. The new capacitive element which is shown in Figure 4.7 (b) increases the capacitance within the inclusion. Hence, the resonant frequency for the modified inclusion is shifted to the left compared to the resonant frequency of the first inclusion. This modification provides additional compactness when compensating this shift. According to the TL theory, the open-ended

stub in the center strip of a CPW TL demonstrates a capacitive response [8]. Its capacitance is given as:

$$C_s = \frac{tan(\frac{\omega}{v_0}\sqrt{\varepsilon_{eff}}\; l_{open\,ended})}{\omega Z_0} \qquad (4.9)$$

where $l_{open\,ended}$ and Z_0 are the length and the characteristic impedance of the open-ended stub, respectively. Therefore, the resonant frequency can be determined by

$$f_r = \frac{1}{2\pi\sqrt{LC_s}} = \frac{1}{2\pi\sqrt{\dfrac{\sqrt{\varepsilon_{eff}}\; l_h\, Z_h\, tan(\frac{\omega}{c}\sqrt{\varepsilon_{eff}}\; l_{open\,ended})}{v_0\,\omega\, Z_0}}}. \qquad (4.10)$$

According to (4.9) the capacitive element can be controlled by changing the length of the open-ended stub. On the other hand, the capacitance in the first inclusion can be tuned by changing the gap width in the center strip (g). In general, the coupling capacitance is proportional to g^{-1}.

4.5.1 Design examples, simulations and measurements

The two inclusions are printed on a host CPW TL. The substrate used to hold the inclusions is a RT/Duroid 6010 substrate with a dielectric constant of 10.2 and a thickness of 0.635 mm. The parameters needed in (4.7) and (4.9) are chosen as: $Z_h = 84\ \Omega, l_h = 7.6$ mm, $\varepsilon_{eff} = 6$, g=0.2 mm, $Z_0 = 34\ \Omega$, and $l_{open\,ended} = 1.3$ mm to provide resonant frequencies at 4.5 GHz and 3.9 GHz for the two inclusions, respectively. The capacitive and inductive elements in the two inclusions are tuned independently.

Figure 4.8 and Figure 4.9 show the simulated and measured results for the first and second designs, respectively. Very good agreements between the responses are

achieved. Narrow bandstop regions are obtained at the resonance. The insertion losses and the attenuation rates values obtained near the resonance prove their high performance. Table 4.3 summarizes the simulated and measured parameters for the two inclusions.

Table 4.3 Performance of the two inclusions of Figure 4.7

Parameter	1st design (Simulated)	1nd design (Measured)	2st design (Simulated)	2nd design (Measured)
f_r	4.50 GHz	4.51 GHz	3.87 GHz	3.89 GHz
Return loss	1.42 dB	2.61 dB	2.15 dB	2.90 dB
Insertion loss	14.73 dB	10.19 dB	9.79 dB	8.47 dB
Q-factor	26.47	32.21	35.18	43.22
3-dB BW	0.17 GHz	0.14 GHz	0.11 GHz	0.09 GHz
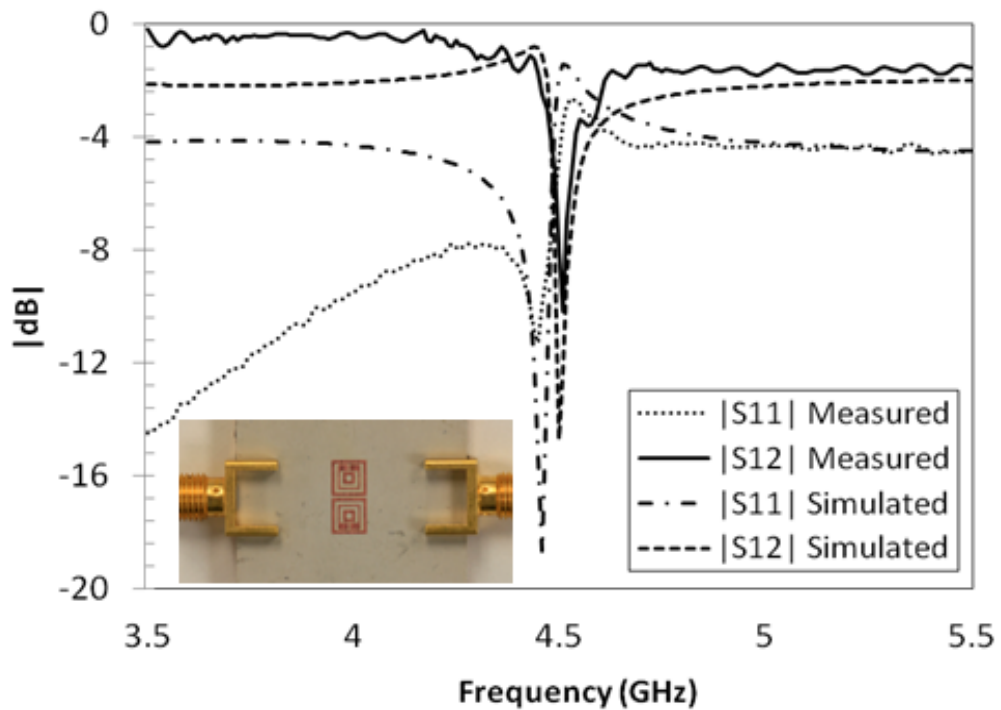
Figure 4.8 Simulated and measured S-parameters of the first inclusion.
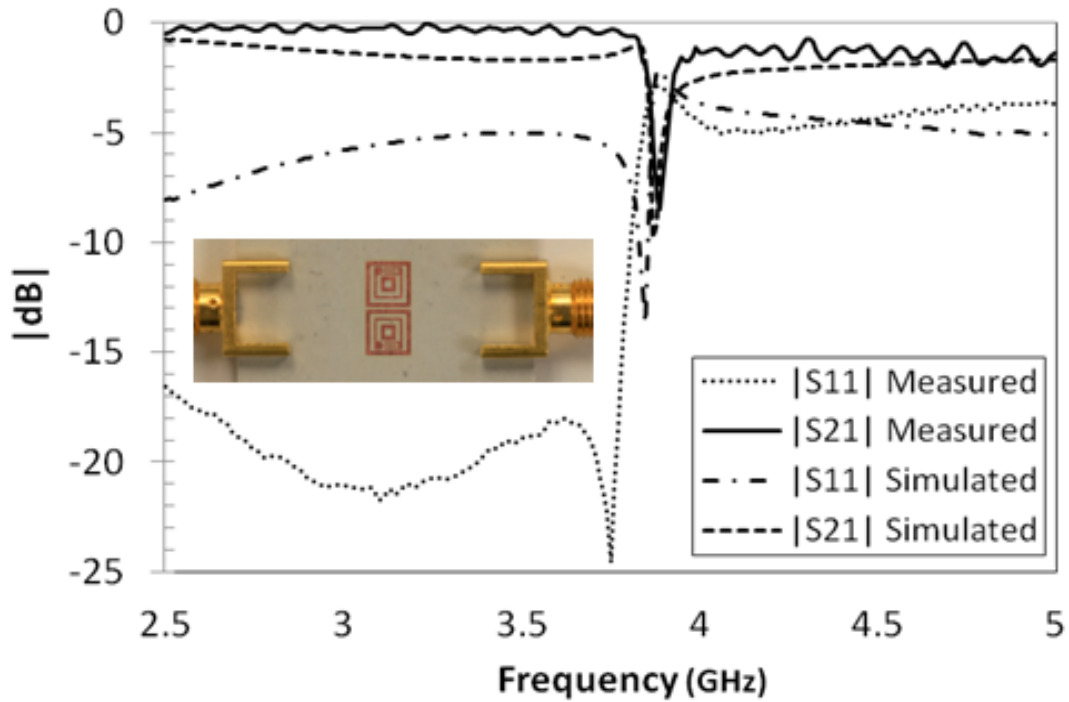
Figure 4.9 Simulated and measured S-parameters of the second inclusion.

4.6 Conclusion

In this chapter a new type of TL-based metamaterial resonators was introduced. The distributed capacitors and inductors within the proposed resonators were controlled in a simple and straightforward way. Hence, many advantages of the new designs over the conventional implementation were achieved. In addition, two other CPW discontinuities-based metamaterial inclusions were proposed. The inclusions contain distributed capacitors and inductors connected along a folded coplanar waveguide transmission line. Despite they share the same high-impedance inductive element; the capacitive part was represented by a gap in the center strip in the first inclusion and an open-ended stub in the center strip in the second inclusion. Numerical and experimental results for all proposed inclusion were in excellent agreement. The demonstrated high performance recommends the proposed structures as perfect candidates in the design of resonant-based microwave circuits.

References

[1] J. B. Pendry, A. J. Holden, D. J. Ribbins, and W. J. Stewart, "Magnetism from conductors and enhanced nonlinear phenomena," *IEEE Trans. Microwave Theory Tech.*, vol. 47, pp. 2075–2084, Nov. 1999.

[2] C. Saha, J.Y. Siddiqui, and Y.M.M. Antar, "Square split ring resonator backed coplanar waveguide for filter applications," *General Assembly and Scientific Symposium, 2011 XXXth URSI* , vol., no., pp.1-4, 13-20 Aug. 2011.

[3] R. Marqués, F. Mesa, J. Martel, and F. Medina, "Comparative analysis of edge- and broadside-coupled split ring resonators for metamaterial design—Theory and experiment," *IEEE Trans. Antennas Propag.*, vol. 51, no. 10, pp. 2572–2581, Oct. 2003.

[4] D. M. Pozar, Microwave Engineering. New York: Wiley, 2005.

[5] K. Hettak, N. Dib, A.-F.Sheta,and S.Toutain, "A class of Novel Uniplanar Series Resonators and Their Implementation in Original Applications," *IEEE Trans. Microwave Theory Tech.*, vol. 46, No. 9, pp.1270-1276, Sept.1998.

[6] R. N. Simons, Coplanar waveguide circuits, components, and systems, New York: John Wiley & Sons, 2001.

[7] Zeland Software, Inc., "IE3D Simulator," Fremont, CA, 1997.

[8] N. Dib, L. Katehi, G. Ponchak, and R. Simons, "Theoretical and experimental characterization of coplanar waveguide discontinuities for filter applications," IEEE Trans. Microwave Theory Tech., vol. 39, pp. 873–882, May. 1991.

CHAPTER 5

Applications of the Proposed TL-Based Inclusions

To examine the inherent capacity of the proposed TL-based inclusions, two design examples that utilize the new inclusions are proposed in this chapter, a dual-band bandstop filter and two hybrid branch line couplers. The inclusions provide a narrow bandstop response in the first design, and a miniaturization effect in the second design. Simulation results for the inclusions and the related applications show very good agreement with measurements. The DBBSF shows a good bandpass response with sharp attenuation near the passband. The HBLC with two resonators per branch had a 16.95% size reduction factor as compared to a conventional HBLC. These results validate the utilization of the proposed resonators in realizing microwave circuits.

5.1 Dual-band bandstop filter example

In this section we present a new DBBS filter with a designed center band frequencies at 1.6 GHz and 2.2 GHz, based on the technique developed in [1] in which a lumped element model of four series-connected parallel LC resonators is derived from a prototype Chebyshev low pass filter after two successive frequency transformations.

Abu Safia *et al*. used the same technique to implement their DBBSF using the compact series-connected parallel LC resonators proposed in [2] to implement the four resonators in [3]. In [4], Marqués *et al*. proposed a lumped element equivalent circuit

model for the basic cell of a SRR loaded into CPW wherein the SRR was modeled as a series-connected parallel LC resonators attached to the host CPW TL. Thus, we replace each series-connected parallel LC resonator in the DBBSF by our proposed AMMs patterned in the backside of the CPW dielectric substrate. Using the expressions developed in [1] in conjugation with the design's center band frequencies and specifications, the values of the lumped elements of the series-connected parallel resonators of the DBBSF can be found. Two resonators have their resonant frequency at 1.6 GHz, and the other two resonate at 2.2 GHz.

Figure 5.1 shows a layout of the DBBS filter with the four resonators on its substrate. This circuit is fabricated on RT/Duroid 6010 substrate with a dielectric constant of 10.2 and a thickness of 0.635 mm. Figure 5.2 shows the simulated and measured scattering parameters of the filter. Very good agreement is obtained between simulated and measured results which is also indicated in Table 5.1 and Table 5.2.
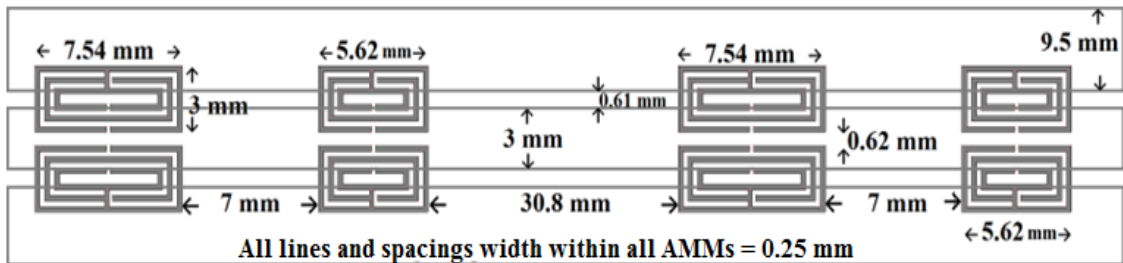
Figure 5.1 Layout of the proposed CPW DBBS filter.

Table 5.1 Performance of the proposed DBBSF at the first and

	Simulation	Measurement
Operating Frequency	1.63 GHz	1.64 GHz
Return loss	1.04 dB	1.88 dB
Insertion loss	42.98 dB	25.55 dB
Q-factor	8.41	11.45

Table 5.2 Performance of the proposed DBBSF at the second band

	Simulation	Measurement
Operating Frequency	2.18 GHz	2.18 GHz
Return loss	0.81 dB	1.68 dB
Insertion loss	45.73 dB	25.52 dB
Q-factor	14.54	13.41

There are two transmission zeroes around 1.6 GHz and 2.2 GHz, each with a shift of less than 0.05 GHz as compared to simulation. Other characteristics such as the insertion losses (>25 dB), return losses (< 2 dB), attenuation rates near the resonance (>200 dB/GHz), and Q-factors (>10) for each band demonstrate the high performance of the proposed filter.
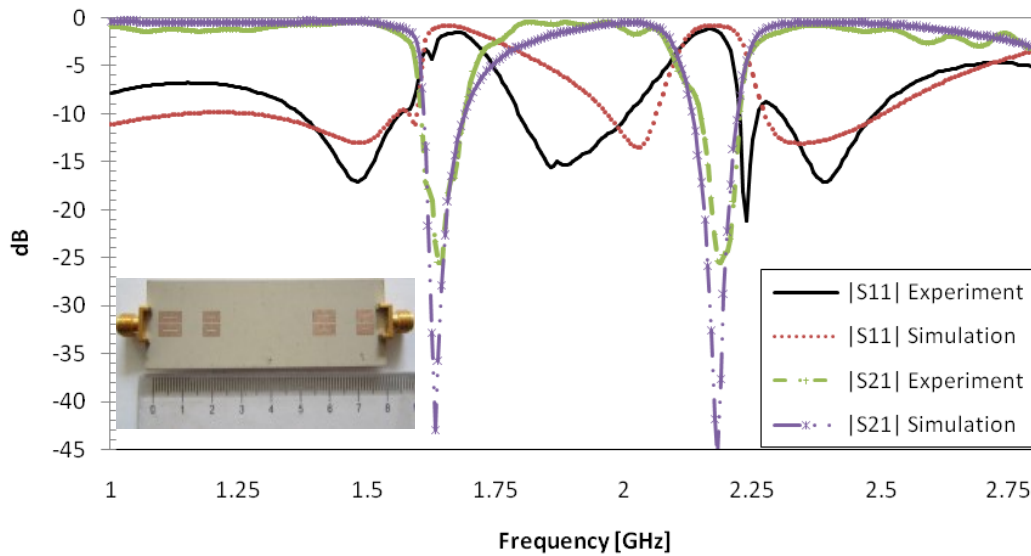
Figure 5.2 Measured and simulated scattering parameters of the Dual BSF shown in Figure 5.1.

The modified inclusion proposed Section 4.4 is also used to produce a dual-band bandstop filter. The first and third resonators (from the left side of Figure 5.1) are designed to resonate at 1.8 GHz and the second and fourth resonators are designed to

resonate at 2.4 GHz. Hence, the new DBBSF can be used to block GSM/Wi-Fi signals. Figure 5.3 shows the layout of the dual-band bandstop filter and Figure 5.4 shows its simulated response. Tables 5.3 and Table 5.4 summarize the filter's performance at the first and second bandstops, respectively.
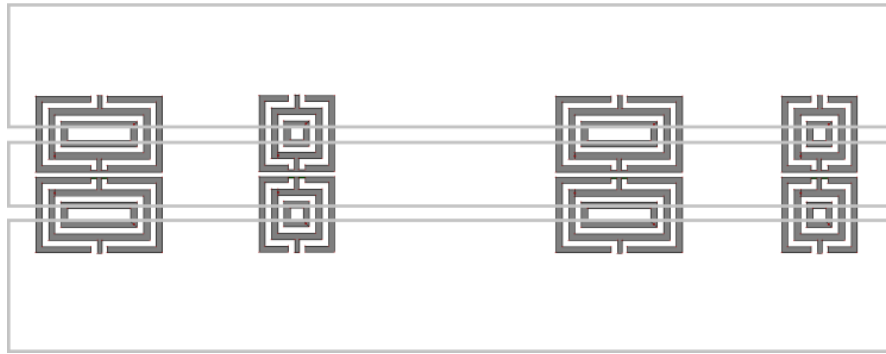
Figure 5.3 Layout of the proposed CPW DBBS filter.
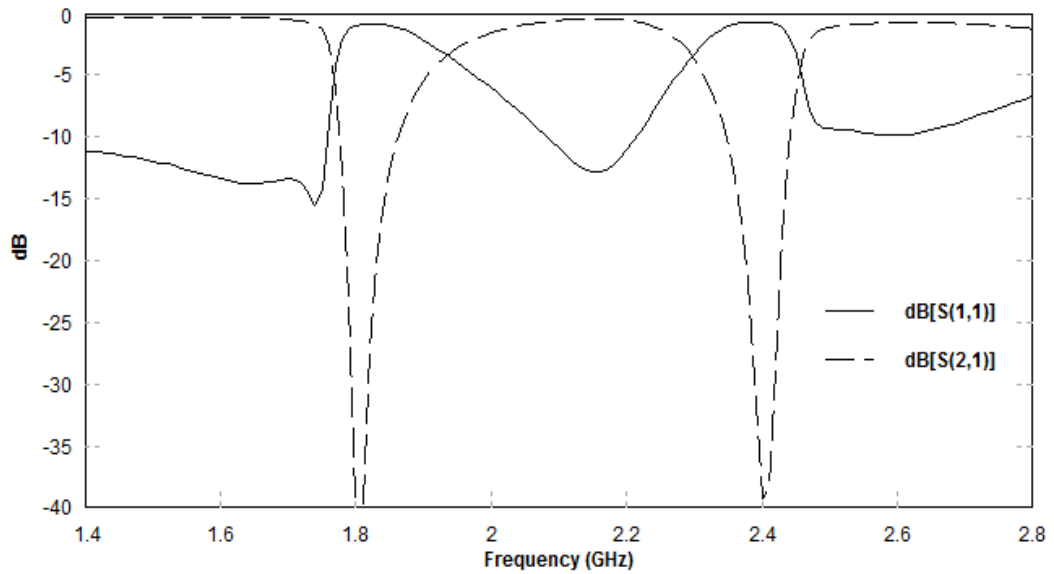
Figure 5.4   Simulated scattering parameters of the Dual BSF.

Table 5.3 Performance of the proposed DBBSF at the first band

	Simulation
Operating Frequency	1.80 GHz
Return loss	0.87 dB
Insertion loss	39.54 dB
Q-factor	15.66

Table 5.4 Performance of the proposed DBBSF at the second band

	Simulation
Operating Frequency	2.40 GHz
Return loss	0.69 dB
Insertion loss	39.05 dB
Q-factor	17.82

5.2   Theory of slow wave propagation in AMM-loaded TLs

TL-loaded AMMs can be modeled using a series-connected shunt LC resonator mutually coupled with the host TL as shown in Figure 5.5 [5]. The inductor and capacitor come from the short-ended and open ended TLs within the inclusion, respectively. The conductor and dielectric losses are assumed to be negligible for simplicity. Hence, the total power loss (characterized by the resistant R in Figure 5.6) is attributed to radiation effects [6].
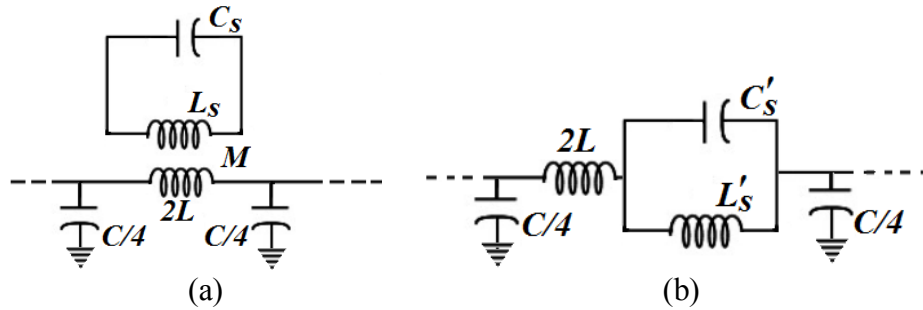
Figure 5.5 (a) Lumped-element equivalent circuit for the basic cell of the SRR loaded transmission line. (b) Simplified circuit with the series branch replaced by its equivalent impedance [5].

The S-parameters for a TL segment loaded with one AMM cell with an electrical length of kd (k: wave number and also propagation constant along the line without the inclusion) can be derived using either the ABCD matrices analysis or using a simple TL theory. The TL analysis approach proposed in [6] is followed here to find the S-parameters and compactness factor of the new structure. As described in Figure 6.5, Let V^+ denotes the incident voltage, V_1 denotes the total voltage at the left reference plane t_1, V denotes the voltage across the resonator, V_2 denotes the transmitted voltage at the

right reference plane t_2, Z is the impedance of the resonant circuit and Z_0 is the characteristic impedance of the line. Q is the quality factor of the parallel resonant circuit given by $\omega C/G$ (G= 1/R) [6].
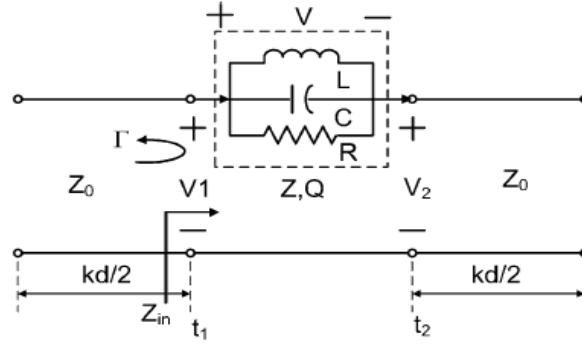
Figure 5.6 The simplified model of the host TL loaded by AMM [6]

Due to the additional capacitance and/or inductance added to the host TL, the propagation constant (β) of the host line becomes different than the propagation constant (k) of a conventional TL having the same physical length [6]. Based on the operating frequency, the host line can present a slow-wave or a fast-wave TL medium [6].

The slow-wave phenomenon appears at frequencies below the resonant frequency of the AMM [6]. It has been utilized to reduce the size of several conventional MW circuits but not with quantitative reasoning [6]. In this section, we introduce closed-form expressions for the slow-wave factor (compactness factor) using the simple TL theory approach proposed in [6]. The slow-wave factor is important since its inverse directly gives the reduction rate of the line [6].

The radiation rate becomes very small at low frequencies. This means that R becomes very large as the frequency goes to zero [6]. Hence, we may assume that $R \rightarrow \infty$ in the low-frequency range [6]. Also, we can approximate the series-connected LC

resonator to be an inductor (we can neglect the capacitor in Figure 5.6 at low frequencies) [6].

Using the expression of the reflection coefficient $\Gamma = j\omega L/(2Z_0 + j\omega L)$ in Figure 5.6, the voltage can be expressed as [6]:

$$V_2 = V^+(1 + \Gamma)\frac{Z_0}{Z_0 + j\omega L} = \frac{2Z_0 V^+}{2Z_0 + j\omega L} \tag{5.1}$$

and S_{21} is given by [6]:

$$S_{21} = \frac{V_2}{V^+} = \frac{2Z_0}{2Z_0 + j\omega L} \tag{5.2}$$

at low-frequencies, the phase of S_{21} can be approximated as [6]:

$$\angle S_{21} = -\tan^{-1}\left(\frac{\omega L}{2Z_0}\right) \tag{5.3}$$

therefore, the electrical length of the loaded TL is given by [6]:

$$\beta L = kd + \tan^{-1}\left(\frac{\omega L}{2Z_0}\right) \tag{5.4}$$

The dispersion factor for a transmission line loaded with the proposed inclusion equals [6]:

$$\frac{\beta}{k} = \frac{kd + \tan^{-1}\left(\frac{\omega L}{2Z_0}\right)}{kd} \tag{5.5}$$

The inductor, in the previous analysis, is considered a frequency-independent lumped element. A more accurate model can be derived if the inductor considered as a frequency-dependent distributed element. Figure 5.5 shows the inclusion mutually coupled (inductive coupling) with the host line. The extra series-connected inductance into the loaded line can be expressed as $L' = CM^2\omega^2$, where C is the capacitance of the open-ended line within the inclusion [5]. M is the mutual coupling between the inclusion and the line [5]. The value of the capacitance after considering the mutual coupling with the host line is $C' = L/M^2\omega^2$, where L is the inductance of the short-ended line within the inclusion [5].

Now, the reflection coefficient becomes $\Gamma = j\omega L'/(2Z_0 + j\omega L')$, and S_{21} is given by

$$S_{21} = \frac{V_2}{V^+} = \frac{2Z_0}{2Z_0 + j\omega L'} = \frac{2Z_0^2}{2Z_0^2 + j\tan(\beta l_{o.c})M^2\omega^2} \tag{5.6}$$

The phase of S_{21} can be approximated as:

$$\angle S_{21} = -\tan^{-1}\left(\frac{\tan(\beta l_{o.c})M^2\omega^2}{2Z_0^2}\right) \cong -\tan^{-1}\left(\frac{\beta l_{o.c}\, M^2\omega^2}{2Z_0^2}\right) \tag{5.7}$$

Therefore, the electrical length of the loaded TL is given by

$$\beta L = kd + \tan^{-1}\left(\frac{\beta l_{o.c}\, M^2\omega^2}{2Z_0^2}\right) \tag{5.8}$$

The dispersion factor for a transmission line loaded with the inclusion equals:

$$\frac{\beta}{k} = \frac{kd + \tan^{-1}\left(\frac{\beta l_{o.c}\, M^2\omega^2}{2Z_0^2}\right)}{kd} \tag{5.9-a}$$

or,

$$l_{o.c} = \frac{2Z_0^2}{\beta M^2\omega^2}\tan\left(\frac{kd(1-RPF)}{RPF}\right) \tag{5.9-b}$$

where RPF is the reduction percentage factor, defined as the inverse of (β/k), and can be found theoretically using (5.9-b) or from simulations. To verify our approach, a microstrip line having a characteristic impedance of 50 Ω and an electrical length of 90^0 (operating frequency equals 1 GHz) was used as a host transmission line. Several inclusions with different $l_{o.c}$ values were etched on the ground plane of the host line in order to reduce the host line's length. Figure 5.7 shows the simulated results versus the theoretical results for the reduction percentage factor. The difference between the two curves can be referred to the capacitive effect within the inclusion which can be neglected at frequencies below the resonant frequency.
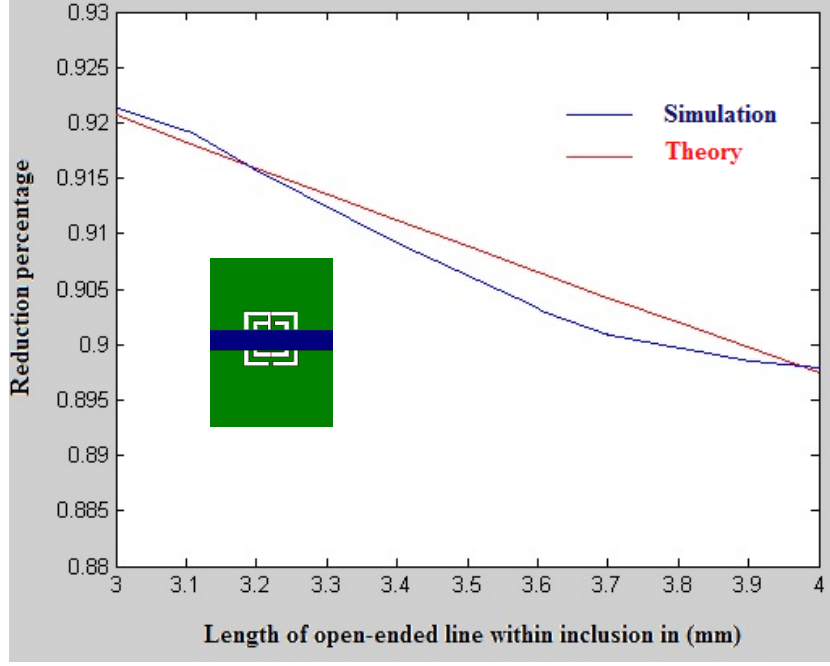
Figure 5.7 **Reduction percentage factor in the length of a host microstrip line etched with different** $l_{o.c}$ **values' inclusions. (f=1 GHz, Z$_0$=50 Ω , $\varepsilon_{eff} = 6.67$. M=1.02×10^{-8})**

The second approach to extract the S-parameters is the ABCD matrices equivalence of the line. The ABCD matrix of the inclusion can be expressed as:

$\begin{bmatrix} 1 & Z \\ 0 & 1 \end{bmatrix}$, where $Z = \dfrac{1}{j\omega C' + \frac{1}{j\omega L'}}$. Considering only the inductance as explained before, the

ABCD matrix of the line is given by:

$$\begin{bmatrix} \cos\dfrac{kd}{2} & jZ_0\sin\dfrac{kd}{2} \\ jY_0\sin\dfrac{kd}{2} & \cos\dfrac{kd}{2} \end{bmatrix} \times \begin{bmatrix} 1 & \dfrac{j\tan(\beta l_{o.c})M^2\omega^2}{Z_0} \\ 0 & 1 \end{bmatrix} \times \begin{bmatrix} \cos\dfrac{kd}{2} & jZ_0\sin\dfrac{kd}{2} \\ jY_0\sin\dfrac{kd}{2} & \cos\dfrac{kd}{2} \end{bmatrix} =$$

$$\begin{bmatrix} \cos kd - \dfrac{\tan(\beta l_{o.c})M^2\omega^2\sin kd}{2Z_0} & \dfrac{j\tan(\beta l_{o.c})M^2\omega^2}{2}(\cos kd + 1) + jZ_0\sin kd \\ \dfrac{j\tan(\beta l_{o.c})M^2\omega^2}{2Z_0^2}(\cos kd - 1) + \dfrac{j\sin kd}{Z_0} & \cos kd - \dfrac{\tan(\beta l_{o.c})M^2\omega^2\sin kd}{2Z_0} \end{bmatrix} \qquad (5.10)$$

Therefore, the S-parameters of the line can be easily extracted. For example, S$_{21}$ equals

$$S_{21} = 2/(A+B/Z_0+CZ_0+D) = \dfrac{2Z_0^2}{2Z_0^2 + j\tan(\beta l_{o.c})M^2\omega^2} + e^{-jkd} \qquad (5.11)$$

which is the same result obtained using the TL theory analysis. Figure 5.8 shows the theoretical using (5.11) versus the simulated results of $\angle S_{21}$ for the TL-loaded inclusion of Section 4.3. A very good agreement between the two lines is obtained. The miniaturization factor equals 83.3 %, and it is approximately linear in the range of frequencies below the resonance. From (5.11) it can be shown that $l_{o.c}$ and the miniaturization factor have a direct proportional relationship.
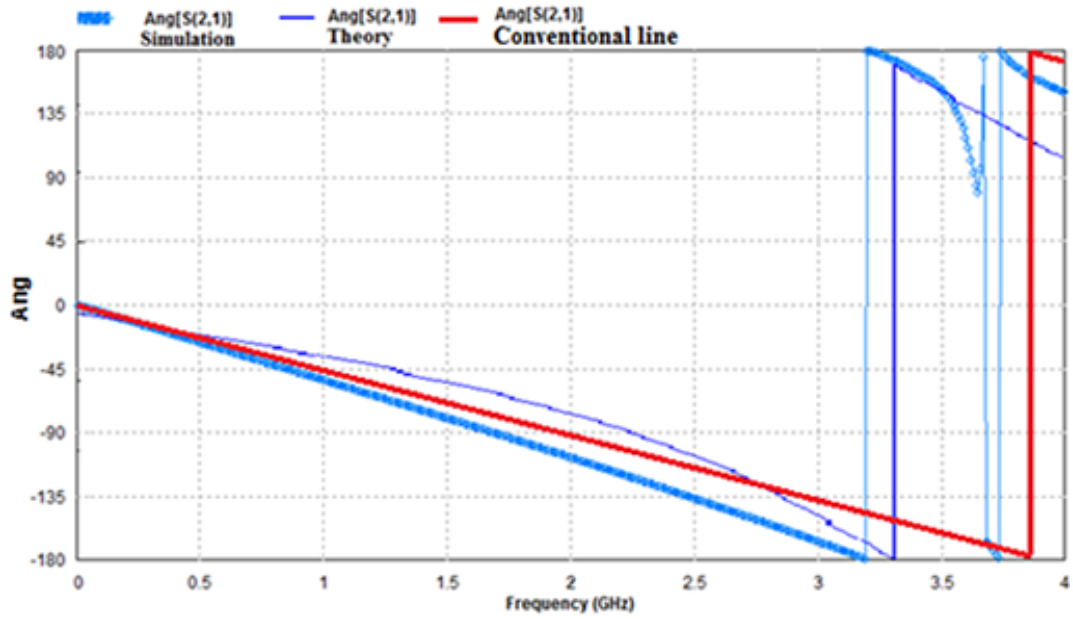
Figure 5.8 Simulated and theoretical results of $\angle S_{21}$ for SRR loaded TL and unloaded TL

The ABCD matrix of the loaded TL considering the series-connected LC (with the capacitor) resonator is:

$$\begin{bmatrix} \cos\theta_1 & jZ_0\sin\theta_1 \\ jY_0\sin\theta_1 & \cos\theta_1 \end{bmatrix} \times \begin{bmatrix} 1 & Z \\ 0 & 1 \end{bmatrix} \times \begin{bmatrix} \cos\theta_2 & jZ_0\sin\theta_2 \\ jY_0\sin\theta_2 & \cos\theta_2 \end{bmatrix} \qquad (5.12)$$

where $\theta = \beta l$ is the electrical length of the TLs on each side of the inclusion, and

$$Z = \frac{1}{j\omega C' + \frac{1}{j\omega L'}} = \frac{j\tan(\beta l_{o.c})M^2\omega^2}{Z_0(1-\tan(\beta l_{o.c})\tan(\beta l_{s.c}))}. \qquad (5.13)$$

Using the ABCD matrix to S-parameters conversion relationship, the magnitude and phase of S_{21} can be expressed as

$$|S_{21}| = \frac{2Z_0\left|\left(1-\tan(\beta l_{o.c})\tan(\beta l_{s.c})\right)\right|}{\sqrt{\left[2Z_0\left(1-\tan(\beta l_{o.c})\tan(\beta l_{s.c})\right)\right]^2+\left(\frac{\tan(\beta l_{o.c})M^2\omega^2}{Z_R}\right)^2}} \qquad (5.14)$$

and,

$$\angle S_{21} = -\tan^{-1}\left[\frac{\tan(\beta l_{o.c})M^2\omega^2}{2Z_RZ_0\left(1-\tan(\beta l_{o.c})\tan(\beta l_{s.c})\right)}\right] \qquad (5.15)$$

Figure 5.9 shows the resonance behavior of several inclusions having different values of open-ended and short ended inner lines. A very good match between the simulated and theoretical results is obtained which validates our modeling approach.
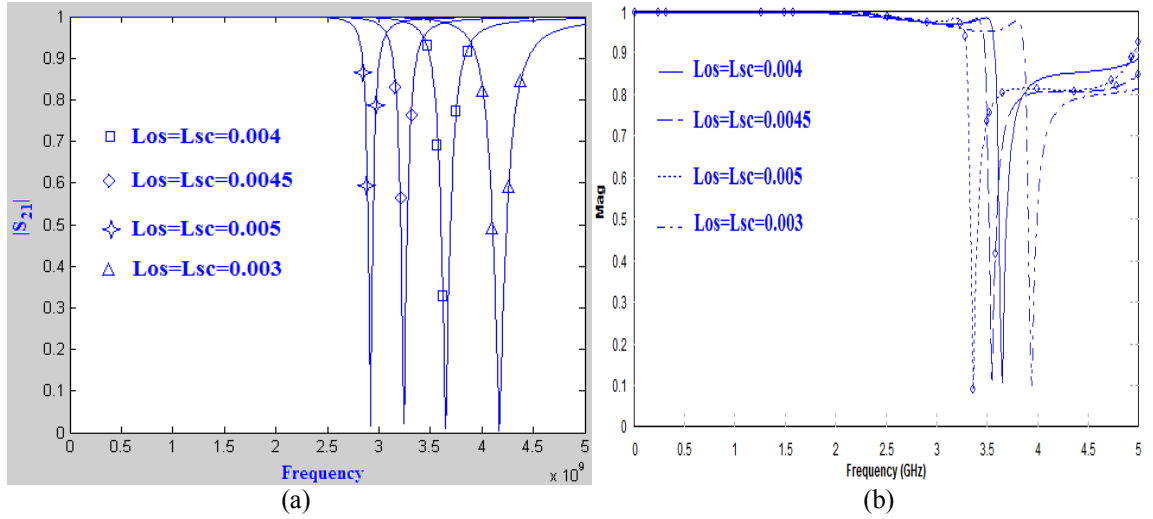
Figure 5.9 (a) Theoretical results of |S$_{21}$| (b) Simulated results of |S$_{21}$|

The power dissipated due to AMM-etching into a host transmission line can be characterized by the power dissipated in *R,* the resistance shown in Figure 5.6. This power represents the total power loss due to the lossy conductor, lossy dielectric material, and radiation loss [6]. The RT/Duroid 6010 substrate used in all proposed designs has a negligible conductor and dielectric losses. Hence, the power dissipated in *R* is mainly a radiation power loss [6]. The radiation efficiency (η) is give by $\eta = P_r/P_{in}$ where P_r is the radiation power, and P_{in} is the input power. To simplify the calculations η is calculated at the resonant frequency of the inclusion at which the

inclusion's impedance becomes purely resistive [6]. The radiation power and input

power are given by [6]:

$$P_r = \frac{|V|^2}{2R} = \frac{|V_1 - V_2|^2}{2R} = \frac{2|V^+|^2 \left|\frac{R}{R + 2Z_0}\right|}{R} \tag{5.16}$$

$$P_{in} = \frac{|V^+|^2}{2Z_0}, \tag{5.17}$$

and,

$$\eta = \frac{4RZ_0}{R^2 + 4RZ_0 + Z_0^2} = 1 - |S_{11}|^2 - |S_{21}|^2 \tag{5.18}$$

η can be found from the simulated or measured scattering parameters using the formula

$(1 - |S_{11}|^2 - |S_{21}|^2)$. Then, from (5.18) we can find R or using the following

expression [6]:

$$R = \frac{2Z_0}{\eta}\left(1 - \eta + \sqrt{1 - 2\eta}\right) \tag{5.19}$$

For example, using the scattering parameters values in Table 4.1 in conjunction with

(5.18) and (5.19), η and $R,$ for our proposed prototype TL-based inclusion, are

determined as 0.367 and 313 Ω, respectively. Moreover, at resonance, C_s'=3.7 pF,

L_s'=0.617 nH, L=2.89 nH, C=0.745 pF, and $M = 1.37 \times 10^{-9}$.

5.3 Miniature hybrid branch line coupler (HBLC)

A dual counterpart of the SRR, called complementary SRR (CSRR), exhibits

negative permittivity and was first introduced in [7]. A TL loaded by this resonator

synthesizes a delay line, i.e., the electrical length of a fixed-length TL effectively

increases by etching the CSRRs on its ground plane. Hence, it is useful to use this kind

of TL in microwave circuits to achieve size reduction. In this section we propose two

new HBLCs, where each of their branches is loaded by one or two complimentary

AMMs. Their resonant frequency was chosen to be far enough from the passband of

the HBLCs in order to avoid being in the bandstop region of the loaded complimentary resonators. The electric length of each branch can be tuned by changing the number of the loaded resonators and the separation between them in case there are more than two per branch. This separation determines the magnetic and electric coupling between the adjacent cells which gives us more design flexibility in controlling the miniaturization factor. It can be shown that the more resonators loaded in each branch, a larger increment in the electric length will be obtained, and hence, greater size reduction can be achieved.
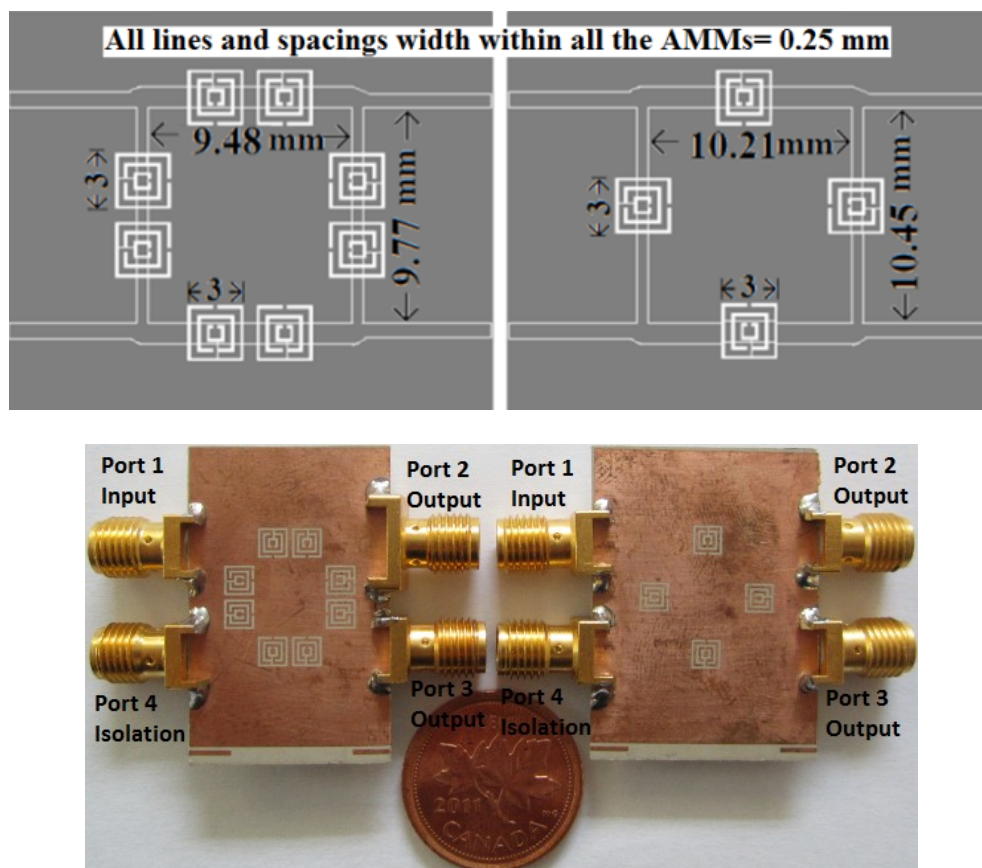
Figure 5.10 Layout and photograph of the fabricated HBLCs loaded by one resonator in each branch (Right) and two resonators in each branch (Left).

The layout and photograph of the implemented HBLCs loaded by one resonator per branch and two resonators per branch are shown in Figure 5.10, including port labels. The operating frequency is chosen as 2.4 GHz which is suitable for Wi-Fi applications.

Both circuits are fabricated on RT/Duroid 6010 substrates with a dielectric constant of 10.2 and a thickness of 0.635 mm. For both circuits the measured scattering parameters are shown in Figure 5.11, and their measured performances parameters are summarized in Table 5.5. In the two circuits, the phase differences between S_{21} and S_{31} are close to 90^0 at 2.4 GHz with, with quadrature phase difference errors less than 1^0. The amplitude imbalance between S_{21} and S_{31} is less than 0.2 dB in both circuits, which means that the incident power is evenly divided between ports 2 and 3 with insertion losses less than 3.7 dB. The isolation/return losses are larger than 15 dB in the two circuits, and the size reduction factors for the new HBLCs compared to the conventional HBLC for one and two resonators loaded per branch are 10.58% and 16.95%, respectively. Hence, this loading technique minimizes the size of HBLCs without affecting their high performance.

Table 5.5 Performance of the HBLCs (Measured Response)

Loading per branch	One resonator	Two resonators
Operating Frequency	2.41 GHz	2.39 GHz
Return loss	15.25 dB	19.54 dB
Isolation	16.61 dB	17.33 dB
Output 1	-3.65 dB	-3.44 dB
Output 2	-3.50 dB	-3.27 dB
Amplitude Imbalance	0.15 dB	0.17 dB
Outputs phase Difference	0.08	0.04
Miniaturization factor	10.58 %	16.95%
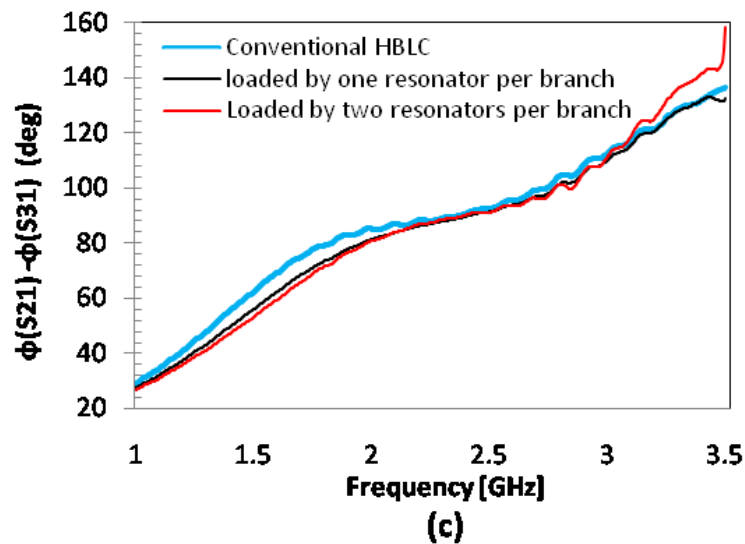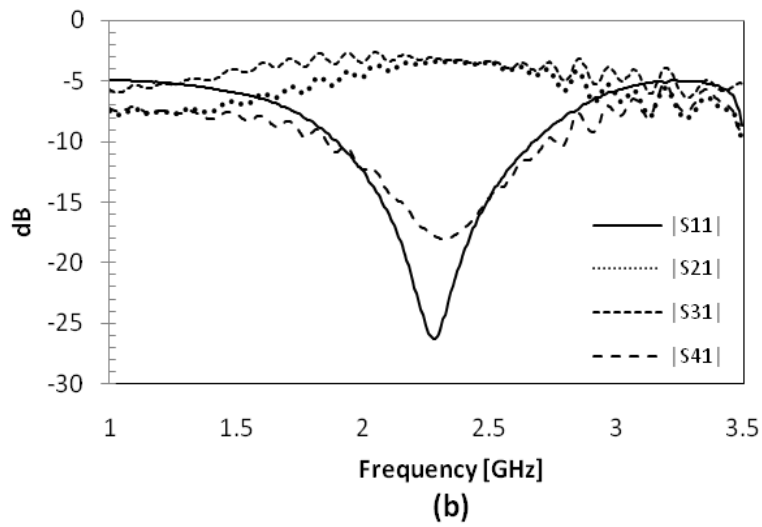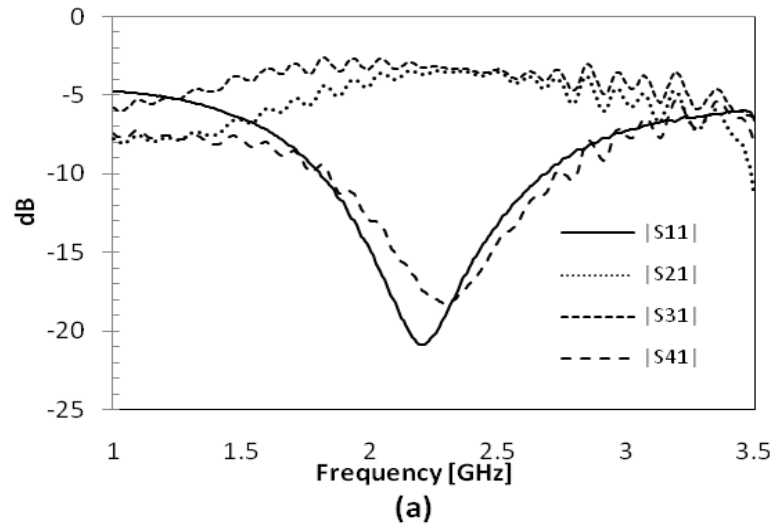
Figure 5.11 **Measured responses for the proposed HBLCs shown in Figure 5.10.** **(a) Measured S-parameters of the HBLC loaded by one resonator per branch. (b) Measured S-parameters of the HBLC loaded by two resonators per branch. (c) Measured output phase differences in the loaded HBLCs as compared to a conventional HBLC.**

Now, the complimantay shape of the modified inclusion proposed in Section 4.4 is loaded in the ground plane of two HBLCs. Figure 5.12 shows the layout of the ground plane of the two compact HBLCs. The first coupler is loaded by two resonator per branch and the second one is loaded by one resonators per branch.
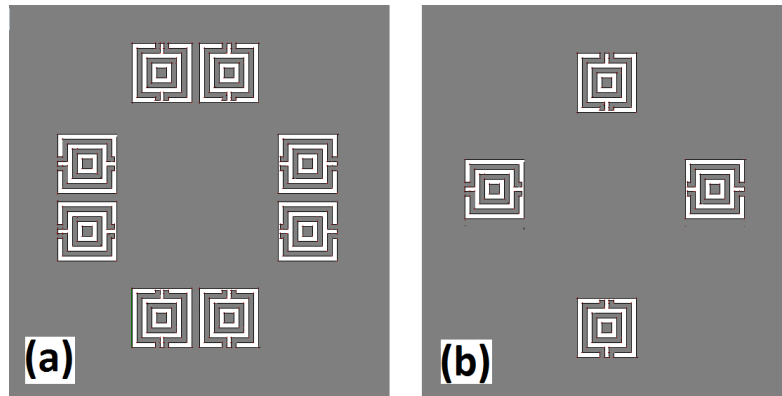
Figure 5.12 Layout of the ground planes of the proposed HBLCs loaded by (a) two resonators in each branch and (b) one resonator in each branch.

The simulated responses of the two couplers are shown in Figure 5.13, and their performance parameters are shown it Table 5.6.

(b)

(c)
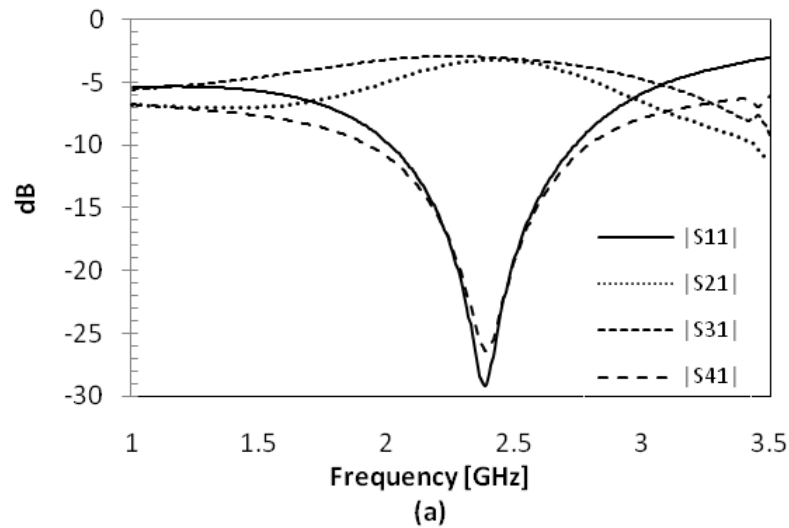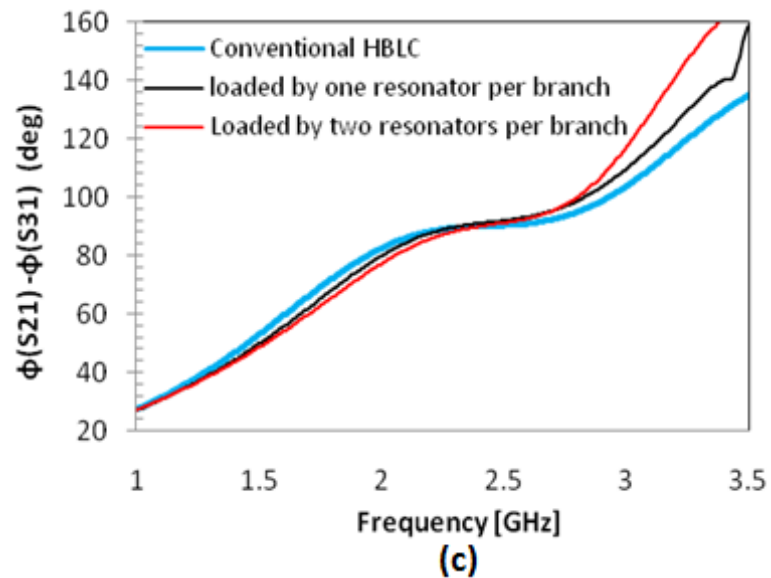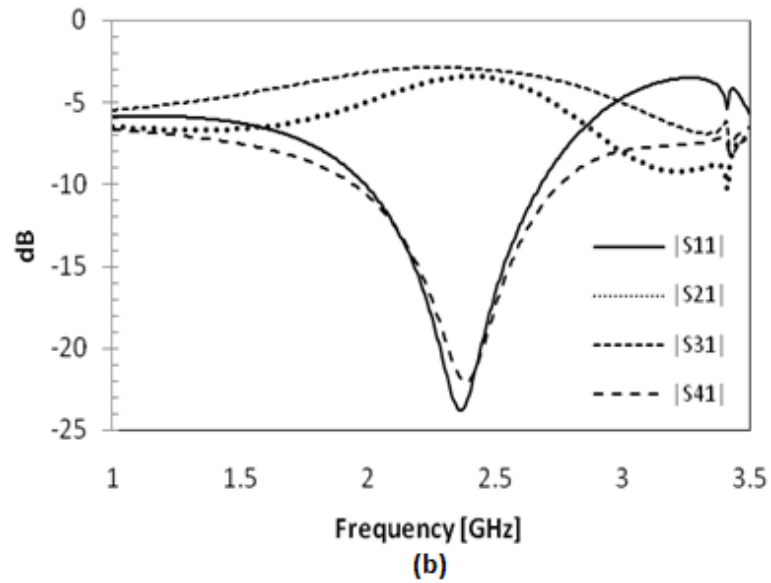
Figure 5.13 Simulated responses for the proposed HBLCs shown in Figure 5.12. (a) Simulated S-parameters of the HBLC loaded by one resonator per branch. (b) Simulated S-parameters of the HBLC loaded by two resonators per branch. (c) Simulated outputs phase difference in the loaded HBLCs compared with convention HBLC.

Table 5.6 Performances of the HBLCs (simulated response)

Loading per branch	One resonator	Two resonators
Operating Frequency	2.41 GHz	2.40 GHz
Return loss	29.18 dB	23.78 dB
Isolation	26.33 dB	22.07 dB
Output 1	-3.23 dB	-3.41 dB
Output 2	-3.03 dB	-2.94 dB
Amplitude Imbalance	0.2 dB	0.47 dB
Outputs phase Difference	0.09	0.06
Miniaturization factor	14.78 %	18.41%

5.4 Conclusions

Verifying our new TL-based AMMs was achieved using two design examples: a DBBSF loaded by four of the proposed resonators and two HBLCs loaded by one and two resonators per branch. A complete design procedure was presented, and the simulation results showed very good agreement with measurements. The DBBSF showed a good bandpass response with sharp attenuation near the passband. The HBLC with two resonators per branch had around 20 % size reduction factor compared to a conventional HBLC, which validated the utilization of the proposed resonators in realizing microwave circuits.

References

[1] H. Uchida, H. Kamino, K. Totani, N. Yoneda, M. Miyazaki, Y. Konishi,S. Makino,J. hirokawa, and M. Ando, "Dual-band-rejection filter for distortion reduction in RF transmitters," *IEEE Trans. Microwave. Theory Tech.,* vol.52, no. 11, pp. 2550–2556, Nov. 2004.

[2] K. Hettak, N. Dib, A.-F.Sheta, and S.Toutain, "A class of Novel Uniplanar Series Resonators and Their Implementation in Original Applications," *IEEE Trans. Microwave Theory Tech*., vol.46, no.9, pp.1270-1276, Sept.1998.

[3] O. H. A. Safia, A. A. Omar, and M. C. Scardelletti, "Design of dual-band bandstop coplanar waveguide filter using uniplanar series-connected resonators," *Progress In Electromagnetics Research Letters*, vol. 27, pp. 93-99, 2011.

[4] J. Bonache, F. Martín, F. Falcone, J. García, I. Gil, T. Lopetegi, M. A. G. Laso, R. Marqués, F. Medina, and M. Sorolla, "Super compact split ring resonators CPW

bandpass filters," in *IEEE-MTT Int. Microw. Symp. Dig.*, Fort Worth, TX, Jun. 2004, pp. 1483–1486.

[5] Baena, J.D.; Bonache, J.; Martin, F.; Sillero, R.M.; Falcone, F.; Lopetegi, T.; Laso, M.A.G.; Garcia-Garcia, J.; Gil, I.; Portillo, M.F.; Sorolla, M.; , "Equivalent-circuit models for split-ring resonators and complementary split-ring resonators coupled to planar transmission lines," *Microwave Theory and Techniques, IEEE Transactions on* , vol.53, no.4, pp. 1451- 1461, April 2005.

[6] Hyung-Mi Kim; Lee, B., "Bandgap and slow/fast-wave characteristics of defected ground structures (DGSs) including left-handed features," *Microwave Theory and Techniques, IEEE Transactions on* , vol.54, no.7, pp.3113,3120, July 2006.

[7] F. Falcone, T. Lopetegi, J. D. Baena, R. Marqués, F. Martín, and M.Sorolla, "Effective negative-ε stopband microstrip lines based on complementary split ring resonators," *IEEE Microw.Wireless Compon. Lett.*, vol. 14, no. 6, pp. 280–282, Jun. 2004.

CHAPTER 6

Dual-Resonant Metamaterial Inclusion Using Composite Right/left-handed Transmission Line Elements

This chapter introduces a dual-resonant inclusion based on a geometrical modification of the TL-based inclusion proposed in Section 4.3. Because of the TL-based property of that inclusion, it is possible to replace its conventional open-ended and short-ended lines with CRLH TLs in order to have the dual-resonant-response inclusion. The new inclusion can be used as a simple dual-band bandstop filter and deployed into several antenna designs as shown later in this chapter.

This chapter is organized as follows: Section 6.1 discusses thoroughly the harmonic resonant behavior of the prototype TL-based inclusion used to attain our proposed dual-resonant inclusion. In Section 6.2, we introduce the idea of using CRLH TL-based distributed elements in order to have a dual-resonant inclusion. A design procedure for the proposed inclusion is introduced in Section 6.3. In Section 6.4, a design example of the proposed inclusion having resonant frequencies at 3.5 GHz and 5.5 GHz is introduced. Simulated and measured results are also shown and discussed in this section. In Section 6.5, the inclusion is utilized to produce two antenna designs: a dual-band CPW-fed single folded slot antenna and an UWB dual-notched antenna. As will be seen, a very good performance for each proposed structure is obtained.

6.1 Higher harmonic resonance in the TL-based inclusion

In general, the capacitive and inductive elements values within a conventional SRR are functions of its geometry. For simplicity purposes, both values are considered frequency independent. Hence, one resonant frequency is estimated. On the other hand, our TL-based inclusion has higher order resonant frequencies at odd harmonics due to the TL-based nature of its distributed passive elements.

For simplicity, let the length of the open-ended line ($l_{o.e}$) in the prototype inclusion equal the length of the short-ended line ($l_{s.e}$) and is denoted by (l). Therefore, the resonant frequencies (first and higher-order resonant frequency) can be expressed as:

$$f_n = (2n - 1)\frac{c}{8\sqrt{\varepsilon_{eff}}\, l.}$$

(6.1)

where n =1, 2, 3, …., ε_{eff} is the effective permittivity of the open-ended and short-ended lines, and c is the speed of light in free space. Using (6.1), it can be shown that the inclusion's first and second resonant frequencies occur at frequencies having guided wavelengths equals eight times and 8/3 times l, respectively. In the next section, the prototype inclusion is modified to produce a dual-resonant inclusion resonates at two non-harmonic frequencies.

6.2 Theory of the dual-resonant inclusion

The phase-response curve of a CRLH TL can intercept a desired pair of phases at any arbitrary pair of frequencies (f_1, f_2). Hence, it supports dual-band operation. Replacing the open-ended and short ended lines in the previous inclusion by proper CRLH TLs can allow non-harmonic resonance behavior. Hence, the second resonant frequency can be higher or lower than $3 \times f_r$. However, in our designed inclusion, the second resonant frequency is chosen to be less than $3 \times f_r$. i.e., the phase slope-response curve is

nonlinearly increased between the two successive resonant frequencies. The green dashed line in Figure 6.1 describes our case.
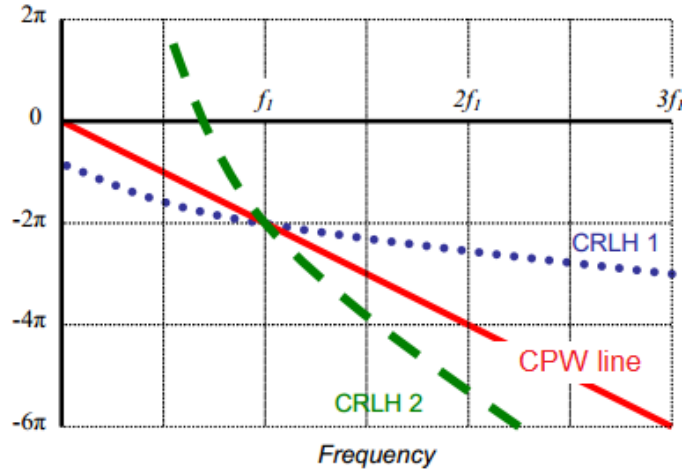
Figure 6.1 Phase response of conventional CPW transmission line and CRLH transmission lines.
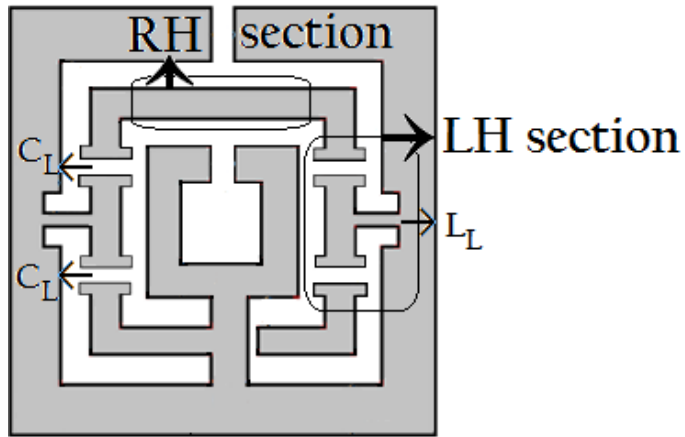
Figure 6.2 Layout of the proposed dual-resonant inclusion.

Figure 6.2 shows the layout of the proposed inclusion. The LH part in each CRLH TL-based element consists of two series-connected capacitors (C_L) separated by a shunt-connected inductor (L_L). On the other hand, the RH part is realized using a conventional TL. The inclusion resonates consequently at two guided waves, making phase shifts (in degrees) along the open-ended and short-ended lines of 45^0 and 135^0, respectively. The non-harmonic pair of phases at the first and second resonant frequencies can be expressed as:

$$\phi_{CRLH}(f_1 = f_R) = -(2m_R - 1)\frac{\pi}{4} \tag{6.2}$$

$$\phi_{CRLH}(f_2 < 3f_R) = -(2m_R + 1)\frac{\pi}{4} \tag{6.3}$$

where,

$$\phi_{CRLH} = \phi_{R,CPW} + \phi_{L,CPW} = -2\pi f \frac{\sqrt{\varepsilon_{eff}}}{c} \ell_{R,CPW} + \frac{N}{2\pi f \sqrt{L_L C_L}} \tag{6.4}$$

and m_R= 1, 2, 3, ... f_1, f_2 are the first and second resonant frequencies, $\ell_{R,CPW}$ is the

length of the RH CPW part in each passive element, and N is the number of LH cells.

The Q-factor and bandwidth at each resonant frequency can be determined using the

determinant of the phase relation in (6.4):

$$\frac{\partial \phi_{CRLH}}{\partial f} = -2\pi \frac{\sqrt{\varepsilon_{eff}}}{c} \ell_{CPW} - \frac{N}{2\pi f^2 \sqrt{L_L C_L}} \tag{6.5}$$

6.3 Design procedure for the dual-resonant inclusion

The design procedure for the new inclusion can be summarized in the following

points:

1) We initially determine the values of the inclusion's first and second resonant

frequencies, the characteristic impedance of its CRLH TL-based elements, and the LH

cells' number.

2) The electrical lengths (in degrees) of the open-ended and short-ended CRLH TLs

equal 45^0 at the first resonance and 135^0 at the second resonance. Solving (6.4) using

the two conditions in (6.2) and (6.3), in conjunction with the characteristic impedance

balance condition ($\boldsymbol{Z_{c,CRLH} = Z_{c,R} = \sqrt{L_L/C_L}}$) [1]. The values of C_L, L_L, and the RH

phase delay (in radians) for each CRLH TL-based element are expressed as:

$$L_L = \frac{4NZ[1-(\omega_1/\omega_2)^2]}{\pi\omega_1[5(\omega_1/\omega_2)-1]} \tag{6.6}$$

$$C_L = \frac{4N[1-(\omega_1/\omega_2)^2]}{\pi\omega_1 Z[5(\omega_1/\omega_2)-1]} \tag{6.7}$$

$$\phi_{RH} = \frac{-\omega_1 \pi [5-(\omega_1/\omega_2)]}{4\omega_2 [1-(\omega_1/\omega_2)^2]} \tag{6.8}$$

It can be noticed that ϕ_{RH} is only a function of f_1 and f_1.

3)   The coupling capacitor (C_L) across the gap is given by $C_L = -Im(Y_{12})/\omega$, where ω is the angular frequency, and Y_{12} is the transmission admittance. The gap's width is adjusted to fit the designed equivalent LE capacitor's response [2]. Moreover, the dimensions of the shunt-connected inductive line are chosen to fit the designed LE inductor's response.

4) The two CRLH TLs are connected in series and folded to form a square-looped layout. Then, the inclusion is loaded on a proper host transmission line (CPW TL in our case).
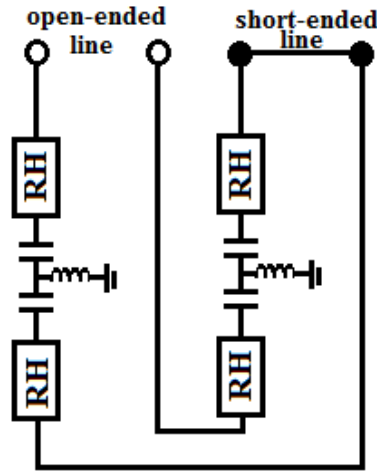
Figure 6.3 Semi-distributed model of the proposed inclusion.

Figure 6.3 shows the semi-distributed model of the inclusion. The ABCD matrix for each CRLH TL-based element can be expressed as:

$$\begin{bmatrix} \cos\phi_{RH} & jZ_0\sin\phi_{RH} \\ jY_0\sin\phi_{RH} & \cos\phi_{RH} \end{bmatrix} \times \begin{bmatrix} 1-\dfrac{1}{\omega^2 L_L C_L} & \dfrac{2}{j\omega C_L}-\dfrac{1}{j\omega^3 C_L^2 L_L} \\ \dfrac{1}{j\omega L_L} & 1-\dfrac{1}{\omega^2 C_L L_L} \end{bmatrix}$$

$$\times \begin{bmatrix} \cos\phi_{RH} & jZ_0\sin\phi_{RH} \\ jY_0\sin\phi_{RH} & \cos\phi_{RH} \end{bmatrix} \tag{6.9}$$

Based on (6.9) and (6.4), the capacitance and inductance of the new CRLH TL-based elements within the new inclusion can be given as:

$$C = \frac{\tan(\beta l_{RH} - \frac{N}{2\pi f \sqrt{L_L C_L}})}{\omega Z_0} \tag{6.10}$$

$$L = \frac{Z_0 \tan(\beta l_{RH} - \frac{N}{2\pi f \sqrt{L_L C_L}})}{\omega} \tag{6.11}$$

where, $l_{RH} = -\frac{c.\phi_{RH}}{2\pi f \sqrt{\varepsilon_{eff}}}$, and the ABCD matrix of a TL loaded with our proposed inclusion is given by

$$\begin{bmatrix} \cos\theta & jZ_0\sin\theta \\ jY_0\sin\theta & \cos\theta \end{bmatrix} \begin{bmatrix} 1 & Z \\ 0 & 1 \end{bmatrix} \begin{bmatrix} \cos\theta & jZ_0\sin\theta \\ jY_0\sin\theta & \cos\theta \end{bmatrix} \tag{6.12}$$

where,

$$Z = \frac{1}{j\omega C\prime + \frac{1}{j\omega L\prime}} = \frac{j\tan(\beta l_{RH} - \frac{N}{2\pi f^2 \sqrt{L_L C_L}})M^2\omega^2}{Z_0\left(1 - \tan\left(\beta l_{RH} - \frac{N}{2\pi f^2 \sqrt{L_L C_L}}\right)\tan\left(\beta l_{RH} - \frac{N}{2\pi f^2 \sqrt{L_L C_L}}\right)\right)} \tag{6.13}$$

θ is the electrical length of the TL sections at each side of the inclusion (assumed equal for simplicity), $L' = CM^2\omega^2$, $C' = L/M^2\omega^2$, where M is the mutual coupling between the inclusion and the host line.

6.4 Design example, simulated and measured results

To demonstrate the performance of the proposed structure, a dual-resonant inclusion resonates at 3.5 GHz and 5.5 GHz is designed. Figure 6.4 shows the layout of the inclusion loaded on a host CPW TL. The inclusion is fabricated on a RT/Duroid 6010LM substrate with a dielectric constant of 10.2 and a thickness of 0.635 mm. The LH section in each CRLH TL consists of one symmetrical T-shape cell (N=1) whereas the RH section (finite ground CPW TL), used to build the inclusion has a characteristic impedance (Z_{cR}) of 73.64 Ω and an effective permittivity equals 6.89. Following the

aforementioned design procedure, the values of C_L and L_L equal 1.02 pF and 2.8 nH, respectively. ϕ_{RH} equals 113.7^0 From Z_{cR} and ϕ_{RH}, the design parameters of the RH CPW TL section can be straightforwardly obtained [3].
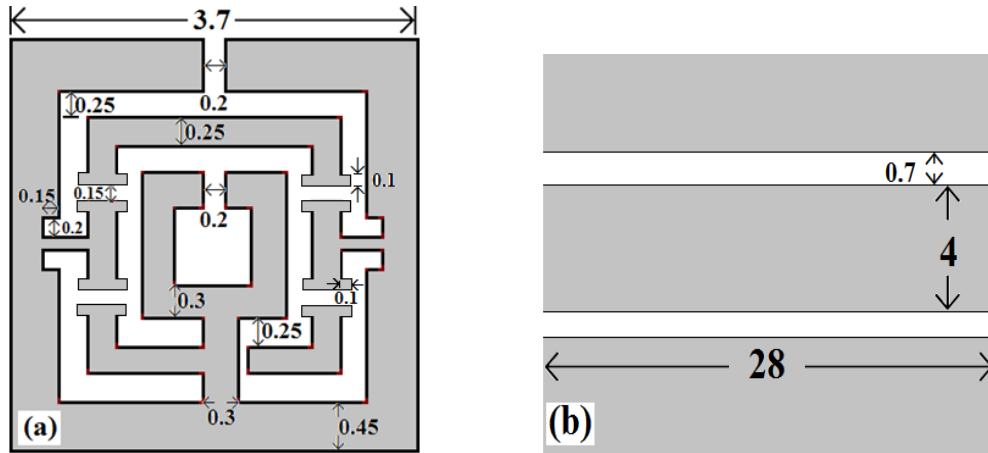
Figure 6.4 Layout of the dual-band design example inclusion (resonates at 3.5GHz and 5.5 GHz) loaded on a host CPW TL (a) Bottom view. (b) Top view.

Figure 6.5 shows the simulated and the measured scattering parameters of the inclusion, and Table 6.1 shows its performance parameters.
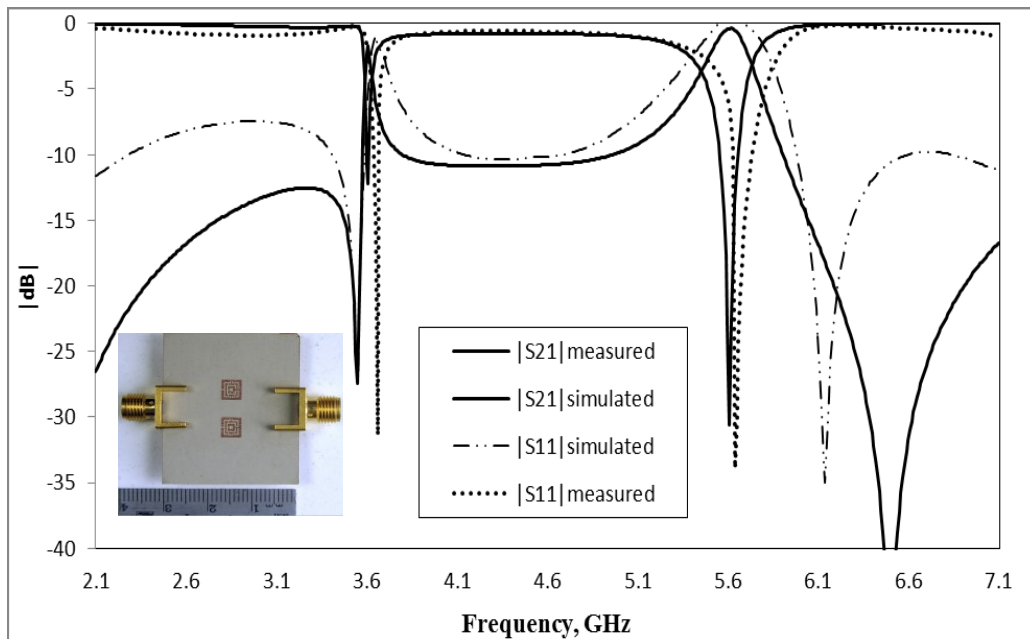
Figure 6.5 Simulated and measured responses of the dual-band SRR loaded into a CPW TL.

Table 6.1 Characteristic parameters of the dual-band inclusion of Fig 6.5.

Parameter	1st resonance (Simulated)	1nd resonance (Measured)	2st resonance (Simulated)	2nd resonance (Measured)
f_r	3.65 GHz	3.61 GHz	5.64 GHz	5.61 GHz
Return loss	0.94 dB	1.67 dB	0.11 dB	0.33 dB
Insertion loss	31.33 dB	12.25 dB	33.94 dB	30.58 dB
Q-factor	230.4	2016.51	201.61	205.23

The inclusion has two resonant frequencies at 3.5 GHz and 5.5 GHz. A small shift of less than 0.2 GHz from the designed resonant frequency values is noticed. This shift can be explained as a reason of the undesirable TL discontinuities within the inclusion. The insertion losses (>10 dB), return losses (<1.5 dB), and Q-factors (>200) values at each resonant frequency demonstrate the high performance of the inclusion.

6.5 Applications to antenna designs

To validate the potentiality of the proposed inclusion, two antenna designs that utilize the new inclusion are introduced. In the first antenna, we replace the open-ended stub in a conventional CPW-fed single folded slot antenna [4] by a folded open-ended CRLH TL to get the dual-band radiation response. In the second antenna, the complementary geometry of the inclusion is loaded on the Y-shape patch of an UWB antenna [5]; this kind of etching blocks the antenna radiation at the inclusion's resonant frequencies.

The two antennas are self-matched to their feeding lines. Hence, no external matching circuits are needed. Hence, the two antennas have compact sizes and simple topologies.

6.5.1 Dual-band CPW-fed single folded slot Antenna

Conventional single folded slot antenna radiates when the open-ended stub's length,

L_s, equals λ_g /2 at the desired radiation frequency. A second harmonic resonant frequency occurs at a center band frequency having a guided wavelength equivalent to the stub's length (λ_g=L_s) [6].

To obtain the dual-band radiation operation at two resonant frequencies having various f_1 /f_2 rations, a suitable CRLH TL can be designed according to the aforementioned design procedure. Then, it is used to replace the conventional stub.

Based on [4], and [6], the pair of phases needed to calculate the LH and RH sections' elements at the two designed operating frequencies (3.5 GHz and 6.5 GHz) is (ϕ_1, ϕ_2) = ($-\pi$, -2π). Using the aforementioned design procedure (Z_c = 50 Ω, $N = 1$), the values of L_L=6.68 nH, C_L= 5.34 pF, ϕ_{RH} = 199.5^0, and $\ell_{R,CPW}$ = 28.01 mm (Length). Fine-tuning the RH section's length and the slot width using IE3D for optimal performance at the two resonant frequencies is performed. After a few repeated simulations, it is found that increasing the RH length to 28.33 mm, results in more accurate resonant frequencies locations and matching.

CPW is used to feed the proposed antenna because of their uniplanar structure, and the ease of making shunt and series connections. The substrate chosen is RT/Duroid 6010LM with a thickness of 0.635 mm and ε_r =10.2. Figure 6.6 shows the layout and photograph of the proposed antenna.

The experimental and simulated return losses of the antenna are shown in Figure 6.7. Very good agreement is obtained which validates the antenna design. A small shift of less than 0.1 GHz from to the designed value is noticed.
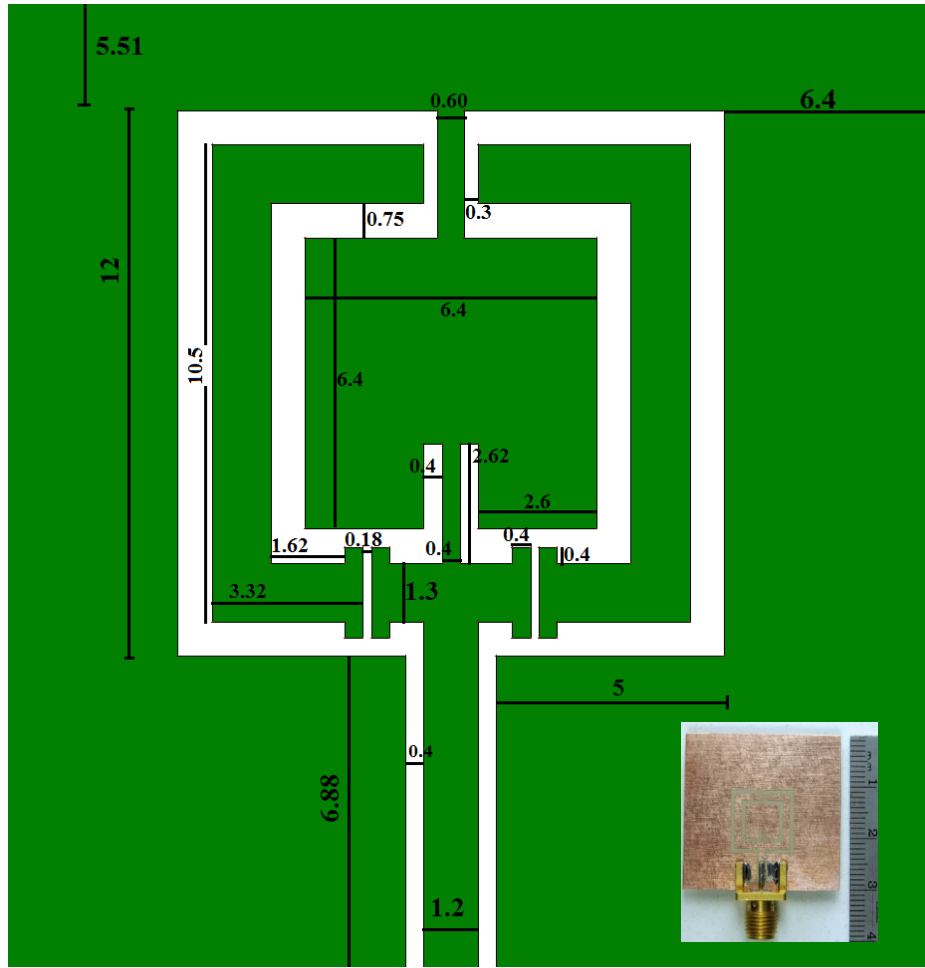
Figure 6.6 Layout and photograph of the dual-band antenna (resonates at 3.5 GHz and 6.5 GHz) loaded on a host CPW TL (all dimensions in mm)
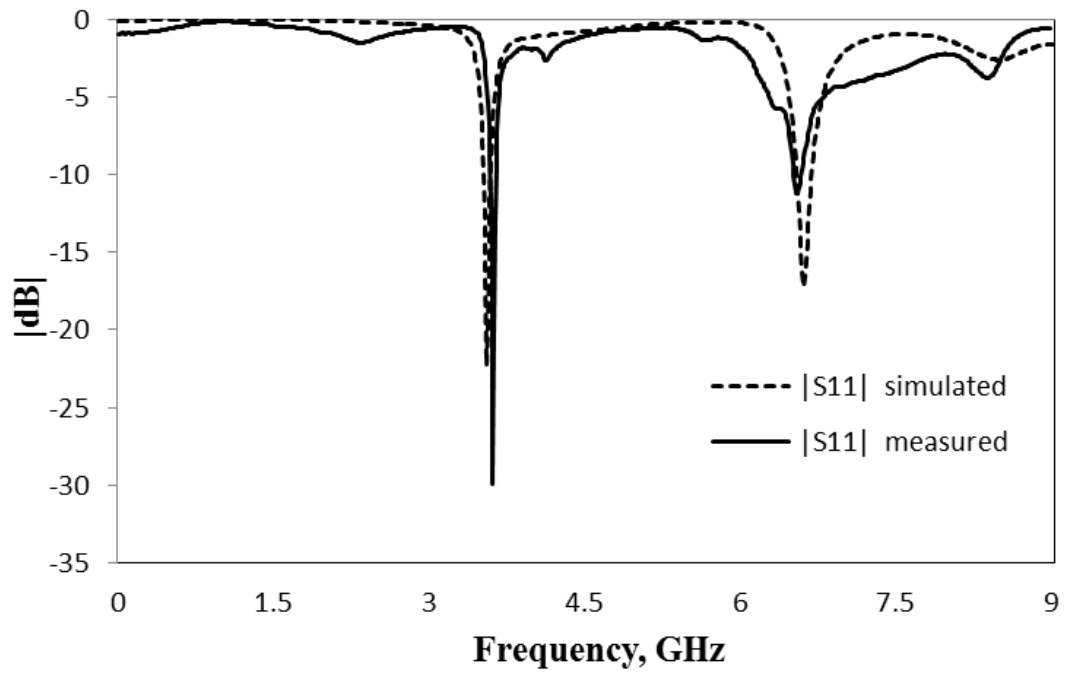
Figure 6.7 Measured and simulated return loss of the proposed antenna
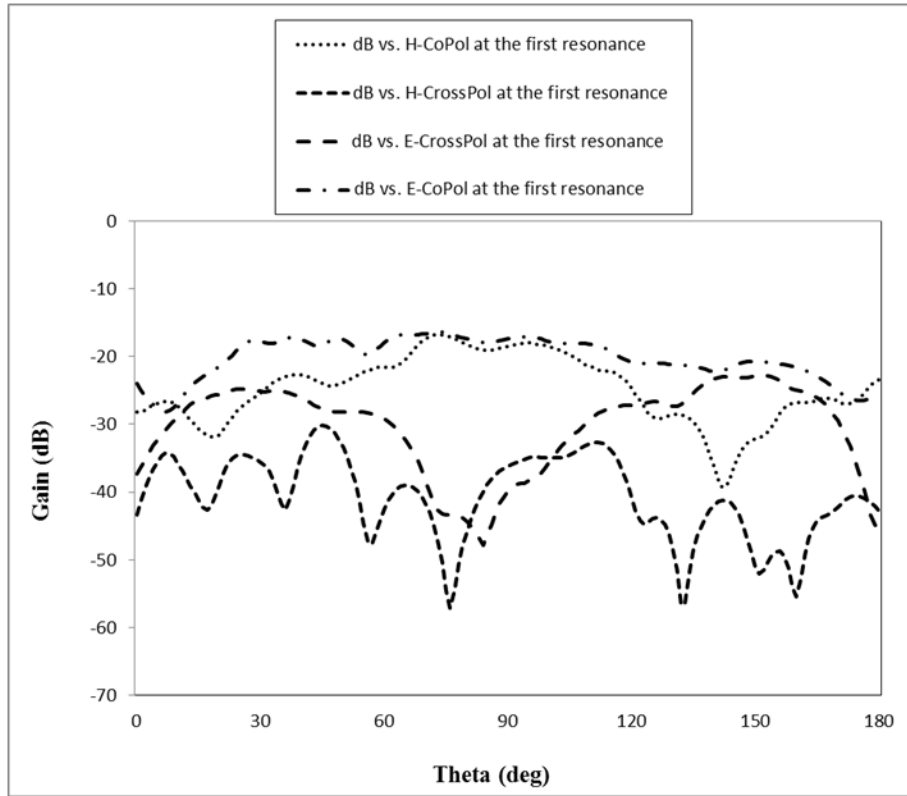
Figure 6.8 Radiation pattern of the dual-band antenna of Figure 6.6 at 3.5 GHz.
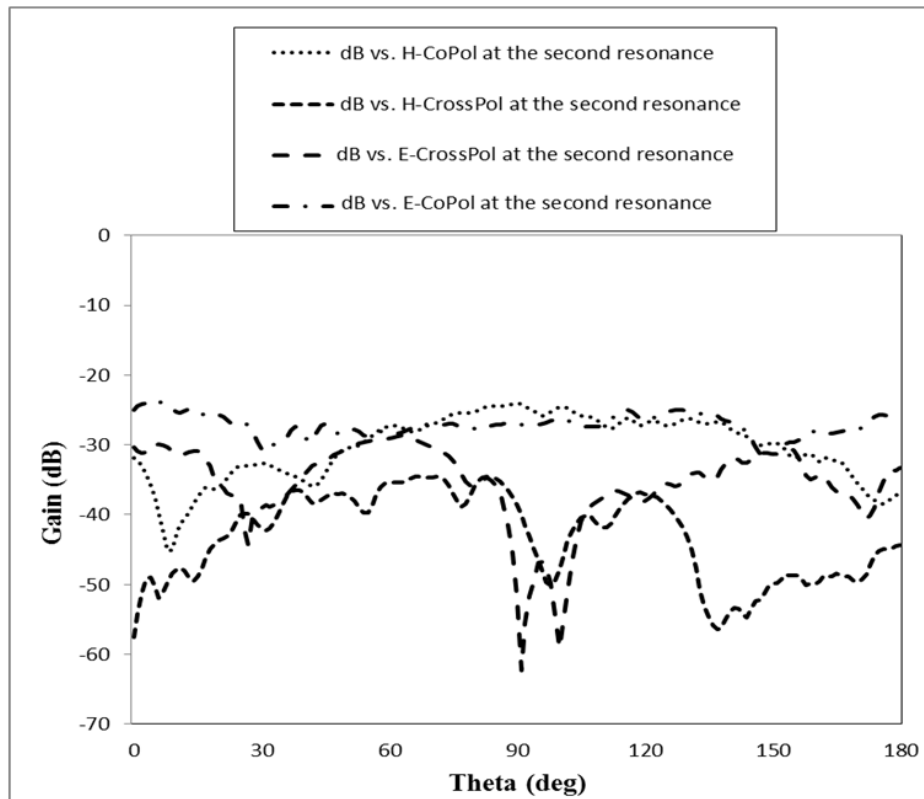
Figure 6.9 Radiation pattern of the dual-band antenna of Figure 6.6 at 6.5 GHz.

The co-polarization and cross-polarization gain patterns of the antenna in the E-plane (x-z plane) and H-plane (y-z plane) are shown in Figure 6.8 and Figure 6.9 for the two center frequencies of 3.5 and 6.5 GHz, respectively. The antenna was measured in the far-field range located in the Microwave Metrology Facility at Poly-Grames Research Center, Montreal, QC. These patterns show that the antenna possesses a linear polarization with cross polarization level more than 20 dBi lower than the co-polarization level. At 3.50 and 6.5 GHz, the antenna gain is about 4.3 dBi.

6.5.2 Dual-notched UWB antenna

Slot-type SRR loading technique has been deployed into UWB antennas in order to prevent the interference problem with other wireless systems in their vicinity [7]. In this section, the complementary geometry of the proposed inclusion is etched on the Y-shape patch of the UWB antenna proposed in [27]. This inclusion is designed to prevent interference at certain center band frequencies. Besides its Y-shape patch, the antenna has a trapezoidal ground plan printed on the back side of a 1.6 mm thick FR4 substrate having a relative permittivity of 4.5 [8]. The band-notched property of the antenna is achieved by guiding the currents at the notch frequencies concentrated in the dual-band inclusion [27]. The layout and photograph of the fabricated antenna is shown in Figure 6.10.
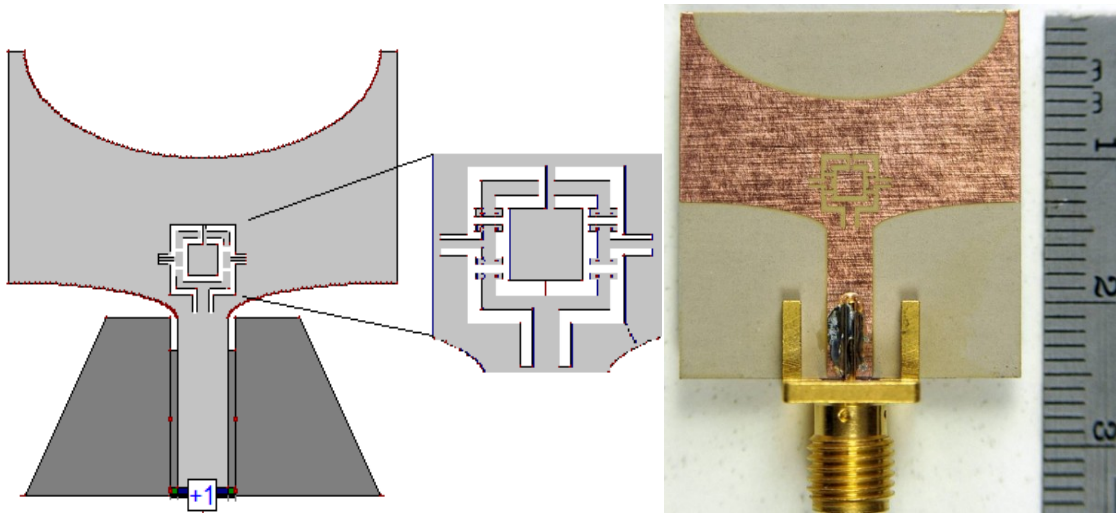
Figure 6.10 Layout and photograph of the Dual-notched UWB antenna

Figure 6.11 shows the radiation patterns at 5 GHz, 7.5 GHz and 10 GHz. The antenna has an omnidirectional radiation pattern in the H-plane (xoz-plane) and a dipole-like radiation pattern in the E-plane (yoz-plane). Fig 6.13 shows the return loss of the antenna against frequency, two gain decrements are at the two resonant frequencies of the inclusion are noticed.

(a)

(b)
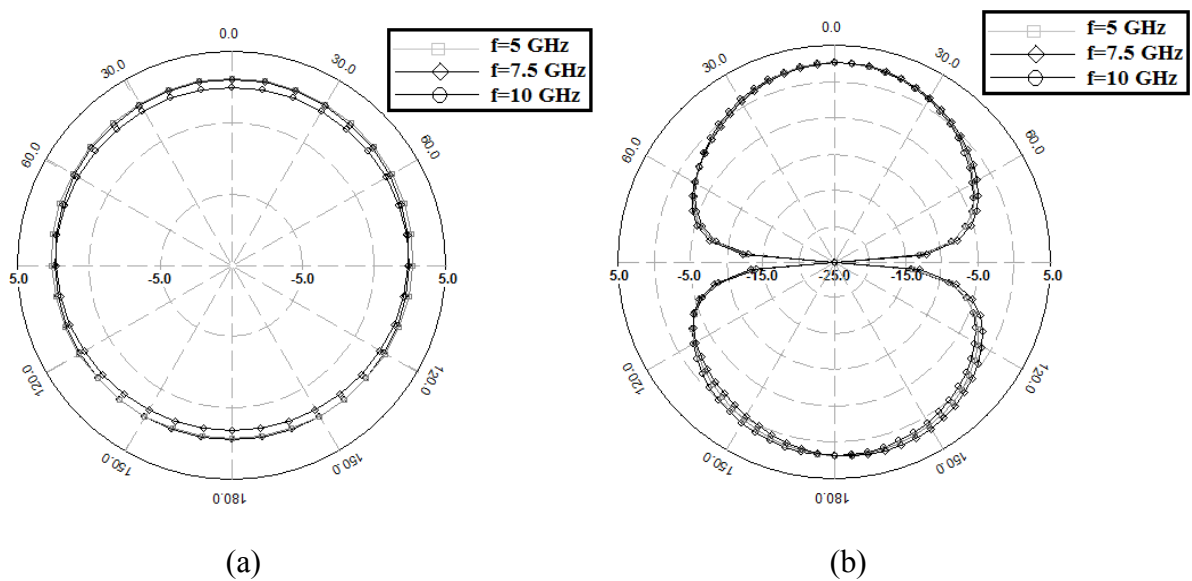
Figure 6.11   Radiation patterns against frequency: (a) H-plane (b) E-plane
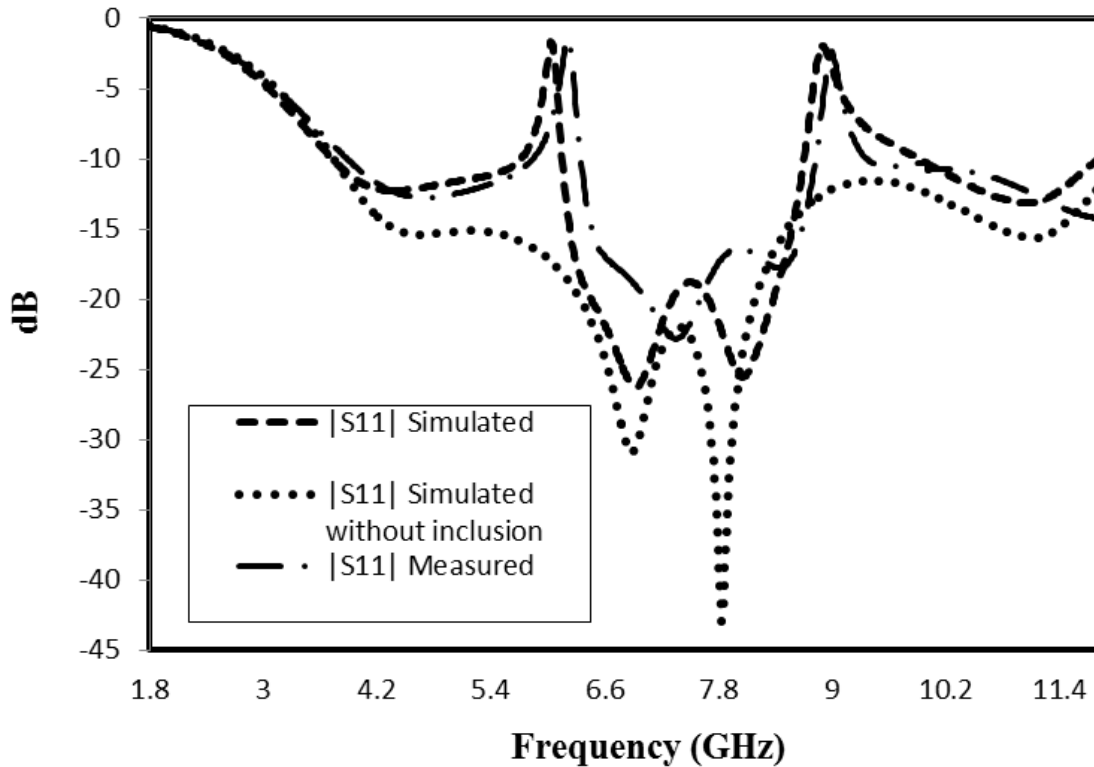
Figure 6.12 Measured and simulated return loss of the proposed antenna

Figure 6.12 shows simulated and measured return loss versus frequency for the antenna. The antenna provides a wide impedance bandwidth along the ultra-wideband range with dual notched bands at 6 GHz and 9 GHz.

6.6 Conclusion

In this chapter, a dual-resonant metamaterial inclusion having composite right/left-handed transmission line-based elements was proposed. The inclusion's design was based on a new hybrid technique which combined the two main metamaterial design approaches, the resonance-type (split ring resonators) and the composite right/left-handed transmission lines approaches, resulting in a dual-resonant response. The geometry of the inclusion was derived from the TL-based prototype inclusion, previously proposed in Section 4.1. The two resonant frequencies of the new inclusion

were controlled separately, using a proper combination of the right-handed and left-handed sections for each passive element. The new technique and design procedure for the inclusion were well established. To verify our proposed structure, it had been deployed in two antenna designs. Firstly, a dual-band CPW-fed single folded slot antenna which radiates at 3.5 GHz and 6.5 GHz. The antenna utilized the dual-band property in CRLH TLs in order to have dual-frequency radiation. Secondly, a dual-band notched ultra-wideband antenna having two narrow rejection bands at 6 GHz and 9 GHz. The complementary shape of the inclusion was patterned on the antenna's patch. Simulated and measured scattering parameters results for the inclusion were in very good agreement. Also, radiation patterns, gains, and insertion losses values for the two antennas at the resonant frequencies verified the potentiality of using the proposed inclusion in microwave circuits and antennas

Reference

[1] C. Caloz and T. Itoh, *Electromagnetic Metamaterials, Transmission Line Theory and Microwave Applications*, Wiley and IEEE Press, Hoboken, NJ, 2005.

[2] Abu Safia, O.; Talbi, L.; Hettak, K.; Kabiri, A., "CPW discontinuities-based metamaterial inclusions," *Antennas and Propagation Society International Symposium (APSURSI), 2013 IEEE* , vol., no., pp.1176,1177, 7-13 July 2013

[3] Zeland Software, Inc., "IE3D Simulator," Fremont, CA, 2002.

[4] Weller, T.M.; Katehi, L.P.B.; Rebeiz, G.M., "Single and double folded-slot antennas on semi-infinite substrates," *Antennas and Propagation, IEEE Transactions on* , vol.43, no.12, pp.1423,1428, Dec 1995.

[5] Li, L.; Zhou, Z.-L.; Hong, J.-S.; Wang, B.-Z., "Compact dual-band-notched UWB planar monopole antenna with modified SRR," *Electronics Letters*, vol.47, no.17,

pp.950, 951, August 18 2011.

[6] Gheethan, A.A.; Anagnostou, D.E., "Broadband and Dual-Band Coplanar Folded-Slot Antennas (CFSAs) [Antenna Designer's Notebook]," *Antennas and Propagation Magazine, IEEE* , vol.53, no.1, pp.80,89, Feb. 2011.

[7] Kim, J.; Cho, C.S.; Lee, J.W., "5.2 GHz notched ultra-wideband antenna using slot-type SRR," *Electronics Letters* , vol.42, no.6, pp.315,316, 16 March 2006.

[8] Li, L.; Zhou, Z.-L.; Hong, J.-S.; Wang, B.-Z., "Compact dual-band-notched UWB planar monopole antenna with modified SRR," *Electronics Letters* , vol.47, no.17, pp.950,951, August 18 2011.

CHAPTER 7

Afterword

7.1 Summary

In this thesis, coplanar waveguide transmission-line based LC resonators are utilized to produce new metamaterial inclusions (resonance-type metamaterials) and cell (CRLH TL based metamaterials). The new inclusions and cells have shared the appealing properties of CPW TL. The resonance behavior for the inclusions was modeled, simulated, measured, and tested to validate the proposed work.

All the proposed structures are applied into new microwave devices, such as filters, couplers, and antennas. Regarding the filters, our proposed inclusion gives the possibility to control the Q-factors for each passband. Moreover, the filters have very compact sizes and simple configurations compared to conventional structures. The new inclusions are deployed in HBLCs in order to reduce their sizes. A theoretical study that relates the inclusion's size and their number per transmission line with the compactness factor was proposed. The study goes through the slow/fast wave behavior related to etching our inclusions on the ground planes of the host transmission lines. Moreover, the losses related to this type of etching were estimated.

In order to investigate the possibility of designing dual-resonant inclusions, the dual-band property found in the second main metamaterial design approach (CRLH TL) was investigated thoroughly. A simple CRLH CPW cell was introduced in which its passband was controlled in a straightforward manner using a similar filter design procedure. In addition, a dual-band HBLC was introduced based on this cell.

The two aforementioned design procedures were combined together in order to have a hybrid approach. Using this hybrid approach a novel dual-resonant inclusion with controllable center band frequencies was introduced. A theoretical model that models the resonance behavior at the two frequencies and predicts the scattering parameters response was produced. Simulated and measured results match the theoretical results. Two antenna designs that utilized the dual-resonant inclusion were designed. The two antennas showed excellent responses which validate the proposed work.

7.2   Contributions

In this thesis the following contributions were reported:

- Distributed passive elements in the center strip of CPW were designed and tested. These elements include inter-digit elements and gaps in the center strip.

- The effect of undesired CPW TL discontinuities were pointed out and considered.

- Several metamaterial inclusions based on the aforementioned elements were produced. Their resonant frequencies and scattering parameters were modeled using a simple TL theory. Theoretical results were compared with simulated and measured results.

- In order, to build a hybrid approach that combines the two metamaterial design approaches, a thorough investigation of a designed CPW CRLH cell was performed. The LE values of the cell was linked to the center passband and the bandwidth of the cell, then, the dimensions of the cell's components were found based on simple closed-form formulas. After, that, the cell was utilized to build a dual-band HBLC.

- A new hybrid technique was built and utilized to build a dual-resonant metamaterial inclusion. These inclusions were deployed in to two antenna designs in order to validate the proposed inclusions.

7.3 Recommended future work

The followings are some possible future work:

- Utilize other CPW discontinuities that have capacitive and inductive responses in order to produce a better response inclusions. This includes inclusions with higher Q-factors for sensors applications.

- Study the effect of etching metamaterial inclusions at different height levels inside the host TL substrate. This includes the effect of parallel etching at two or even more height levels.

- Study the effect of etching the proposed inclusions in the center conductor of the CPW rather than in the ground plane.

- Produce relatively non-dispersive elements by utilizing the CRLH TL dual-band property to fix the LE values in the passive distributed elements at two center band frequencies.

- Investigate the possibility of producing dual-band passband and stopband filters using our CPW CRLH cell.

- Design dual-band CPW devices on the 60 GHz band. This can be achieved by finding new techniques that reduce the required number of left-handed cells for each artificial line, and to reduce the parasitic effect of the right-handed components in each left-handed element.

- Build new meshed metamaterial inclusions and related their transparency levels with their electrical responses.

Appendix

Summary of the thesis in French

Résumé de la thèse

Chapitre 2: Introduction

Les métamatériaux sont des matériaux artificiels qui ont des propriétés difficilement observables dans la nature. Ces matériaux sont synthétisés dans le but de fournir des valeurs spécifiques de la perméabilité et de la permittivité sur les gammes de fréquences micro-ondes [1]*. La structure des métamatériaux incorpore des inclusions électriquement petites devant être disposées périodiquement sur le plan de masse du milieu hôte [1]. Ces inclusions vont contribuer à modifier les propriétés électromagnétiques du milieu hôte et ce particulièrement lorsque le milieu hôte se verra excité par une onde électromagnétique de longueur d'onde supérieure à la dimension maximale des métamateriaux. Cette modification de propriétés diélectriques du matériau est essentiellement aux comportements des inclusions présent sur le métamatériau et entrainant un effet de résonance [1]. Le matériau hôte présentera à cet effet de nouvelles caractéristiques physiques et électriques inexistantes dans la nature. En principe, les structures artificielles non-homogènes des métamatériaux devront être caractérisées comme des supports homogènes décrits par des paramètres de permittivité et de perméabilité effectifs. Cette condition garantira la transmission et non la diffraction de l'onde incidente sur les parois du métamatériau [2].

---

*Les numéros de références et de figures listés dans ce résumé sont identiques à ceux des chapitres correspondant de la version anglaise de la thèse.

Deux principales approches de conception sont utilisées afin de produire des circuits métamatériaux opérationnels aux fréquences micro-ondes. A savoir, l'approche basée sur les lignes de transmission de type composite main droite/gauche (CRLH TL), celle utilisant la technologie basée sur les résonateurs (résonateurs annulaires fendus). Les métamatériaux de type CRLH TLs ont la particularité d'avoir les lignes de transmission côté main droite (RH) et celle côté main gauche (LH) adjointes afin de générer des nouvelles propriétés. La ligne située côté droit est réalisée à base d'une structure microruban classique ou d'un guide d'ondes coplanaire (CPW), tandis que la partie gauche est réalisée en utilisant une chaîne de condensateurs connectés en série associé à une chaîne d'inductances connectées en dérivation. Ces condensateurs et inductances sont mis en œuvre en utilisant soit des éléments distribués, soit des composants réalisés à l'aide de la technologie mettant en œuvre les couches surfaciques. Une combinaison équilibrée des sections de gauche et de droite assure une propagation en mode reverse (correspondant à la réponse d'un filtre passe bande) pour une large gamme de fréquences. En outre, les métamatériaux de type CRLH TL ont la particularité de générer des réponses bi-bande réglable [3]. Plusieurs dispositifs à double bande sur la base de ces lignes ont été rapportés.

Des approches hybrides qui combinent les deux techniques de conception métamatériaux ont été rapportées dans [62]-[67]. Dans [62], les lignes CPW sont chargées par les structures métamatériaux de type SRR complémentaires combinées avec des écarts série capacitifs dans la bande conductrice, située au-dessus des RRF complémentaires, dotés d'adaptateurs d'impédances inductifs reliés au plan de masse. Cette structure a été utilisée pour obtenir un filtre compact UWB [62]. Gil et al ont proposés une structure comparable réalisée sur une ligne de transmission microruban. Les structures à base de lignes artificielles ont été utilisées pour produire un diviseur de

puissance compact et un filtre passe-bande hyper sélectif [63]. Dans [64], une ligne équilibrée ayant les propriétés CRLH a été réalisée en chargeant le plan de masse de l'hôte de type CPW TL avec les résonateurs de forme carrés de type SRR, situé en dessous des positions occupées par les adaptateurs d'impédance inductifs raccordés au plan de masse. Un choix minutieux des dimensions des résonateurs ainsi que des longueurs de talons permettent l'obtention d'importantes caractéristiques de transmission. Dans [65], les inclusions capacitives sont reliées aux bagues des résonateurs SRR afin de modifier les caractéristiques de la bande à droite dans un CPW TL SRR-chargé. La structure a une large bande passante avec des taux élevés d'atténuation en dehors de la bande passante du fait de sa paire de zéros de transmission de chaque côté de la bande passante. Ces caractéristiques ont suscité un grand intérêt de ladite structure en ce qui concerne les applications dans le domaine du filtrage. Dans [66], des éléments capacités supplémentaires montés en série et en dérivation ont étés adjoints à la structure de ligne de transmission uni planaire à indice de réfraction négative initialement proposé dans [67]. Etant donné l'excellent accord entre les sections d'avance et de compensation de retard de phase, la structure se trouve équilibrée avec la capacité de généré une réponse large bande.

Chapitre 3: Recherche relative au Guide d'onde coplanaire à base de ligne de transmission de type composite main droite/gauche (CRLH TL)

Ce chapitre constitue un bref rappel en ce qui concerne l'implémentation des lignes de transmissions de type composite main droite/gauche (CRLH). Cette approche sera associée plu tard à notre modèle d'inclusion basé sur la technologie des lignes de transmission afin de réaliser une inclusion capable de résonner à deux fréquences distinctes. En outre, une nouvelle cellule CRLH guide d'ondes coplanaire distribuée est proposée. Cette dernière incorpore un résonateur monté en série associé à deux embases de dérivation reliées. Une très bonne concordance entre les résultats simulés et théoriques est observée ce qui valide la fiabilité de la cellule proposée. Au final, la propriété bi-bande de la structure CRLH TL est mise en évidence puis validée par la mise sur pied de deux coupleurs de ligne à branche hybride bi-bande.

La figure 3.14 illustre un filtre passe-bande de Chebyshev (agissant en tant que cellule de CRLH) centré à 5 GHz avec une ondulation dans la bande passante de 0,01 dB. Dans [16], les valeurs numériques des grandeurs caractérisant les éléments du prototype passe-bas de la figure 3.12 sont données par: $g0 = 1$, $g1 = 0,4488$, 0,4077 et $g2 = g3 = 1,1007$. La largeur de bande fractionnaire souhaitée du filtre passe-bande est de 0,3, c'est à dire, les largeurs de bande à ondulation égales de part et d'autre de la bande passante est de 1,5 GHz. Les valeurs des éléments localisés du BPF peuvent être trouvées en utilisant les relations (3.10) et (3.13), comme l'illustre le Tableau 3.1

La figure 3.15 montre les résultats simulés du filtre en utilisant l'outil IE3D [17]. Il est mis en évidence une concordance notoire entre les résultats découlant des différentes configurations (à savoir le modèle en éléments distribués et celui réalisé à base des composants discrets).

Un coupleur hybride de type HBLC bi-bande avec des fréquences de résonance centrées respectivement aux valeurs 0,9 GHz et 1,8 GHz est proposé dans cette section. Ces deux bandes sont adaptées pour des applications GSM / 3G.

La figure 3.19 quant à elle met en évidence le coupleur de type HBLC à base d'éléments semi discrets. Toutes les branches sont conçues selon la même procédure. La longueur électrique de la section main droite est une fonction des deux fréquences de la bande centrale ainsi que du déphasage total sur chaque bande. Dans cet exemple, la longueur électrique de la section main droite vaut 160,24° et ceci pour chacune des lignes de 35,35 Ω et 50 Ω. Par conséquent, la longueur électrique de chaque section de ligne de transmission main droite situé à côté d'une extrémité de section de lignes LH est égale à 80,12°.

L'amplitude et la phase des paramètres de diffusion du coupler hybride (HBLC) sont illustrées sur la figure 3.20. La puissance d'entrée est également répartie entre les deux ports de sortie aux deux fréquences centrales des bandes dans laquelle le dispositif fonctionne en diviseur de puissance. Le déséquilibre de phase entre les deux ports de sortie vaut à peu près 90° aux deux fréquences centrales des bandes de fréquence du coupler. La figure 3.1 permet de valider le modèle de lignes de transmission artificielles proposées pour des applications bi-bande.

Sur la figure 3.27, il est mis en évidence un léger décalage des fréquences centrales du diviseur de puissance bi-bande vers la droite de 0,094 GHz pour la première bande de fréquence respectivement de 0,01GHz pour la seconde. Les paramètres de performances relatifs au dispositif bi-bande HBLC à 1,024 GHz et 1,79 GHz sont présentés dans le tableau 3.4.

Chapitre 4: Un nouveau type de ligne de transmission-Basé sur des inclusions de type métamatériaux

Dans ce chapitre, un nouveau type de ligne de transmission basé sur des résonateurs à propriété métamatériau est proposé. Le principe consiste à modifier un résonateur uniplanaire, puis le donner une forme arrondie afin d'aboutir à une inclusion en boucle fermée de forme rectangulaire incorporant des éléments capacitifs et inductifs distribués. De nombreux avantages de cette structure comparée au résonateur de type SRR sont énumérés. Sur la base de la théorie des lignes de transmission simples, la fréquence de résonance à laquelle une bande de fréquence de réjection profonde est observée avec un taux de coupure nette avoisinant les bornes de la bande d'arrêt, due à la particularité de la structure métatmatériau à avoir une perméabilité effective négative dans la plaque diélectrique de la ligne de transmission de l'hôte au voisinage de la fréquence de résonance est calculée et comparée aux résultats de simulations et de mesures.

D'autres part, ce chapitre fait mention de deux autres variétés d'inclusions de type AMM utilisant des formes différentes de lignes de transmission à guide d'ondes coplanaires discontinues (Voir figure 4.1).

La concordance entre les résultats expérimentaux et ceux issues des mesures de ces nouvelles inclusions permet la validation de leurs concepts de réalisation.

La figure 4.1 illustre l'un des résonateurs proposé dans [5], constitué des lignes de transmission coplanaires associées à son schéma électrique équivalent. Cette structure équivaut à l'association en série d'une inclusion de type circuit ouvert à une autre de type court-circuit au niveau de la ligne conductrice centrale (conformément au schéma de la figure 4.1). D'après [5], les deux rubans métalliques situés de part et d'autre des

inclusions ouvertes et fermées au voisinage du ruban central se comportent comme un plan de masse virtuel (confère figure 4.1).

Lorsque la longueur de chaque fragment de ligne interne est inférieur ou égale à $\frac{\lambda_g}{8}$, alors elles peuvent représenter respectivement une capacité ou une inductance distribuée. Les équations (4.1) et (4.2) définissent le modèle équivalent des fragments de lignes ouvertes et fermées présents au sein du conducteur central du guide d'onde coplanaire en fonction des longueurs de ces derniers.

Par opposition aux métamatériaux de type SRR et ses dérivées AMM, la fréquence de résonance du nouveau métamatériel obtenu dépend uniquement d'une dimension (à savoir la longueur du fragment de ligne présent au sein de sa structure). En second lieu, il est intéressant de mentionner que l'accord des éléments distribués passifs peut être réalisé indépendamment du changement de longueur du fragment de ligne interne propre à la structure de l'inclusion dans laquelle ils sont présents.

De par la faculté du nouvel AMM proposé en ce qui concerne l'accord des valeurs des éléments distribués passifs, sa structure présente un net avantage comparé à ceux des métamatériaux de type SRRs (étant donné que les capacités distribuées de ces éléments sont liés ensemble par l'intermédiaire de plusieurs dimensions géométriques communes).

Par conséquent, l'usage du dispositif AMM proposé peut être contrôlé en changeant de manière indépendante les longueurs de fragments. Cette propriété permettra l'amélioration significative ainsi que le contrôle des largeurs de bande passe-bande, réjecteur de bande et fractionnelle des filtres utilisant les structures métamaériaux de type AMM.

En troisième position, la fréquence de résonance est indépendante de l'impédance caractéristique des fragments de lignes ouvertes ou fermées.

En quatrième lieu, il est à préciser que la fréquence de résonance du dispositif AMM proposé est faible comparée à celle d'une cellule similaire d'un résonateur SRR à structure carrée. C'est pour cette raison qu'il est observé une réduction significative de la taille d'une cellule AMM comparativement à celle d'une cellule SRR carrée à une fréquence de résonance identique.

En cinquième point, étant donné que la fréquence du résonateur dépend de la théorie des lignes de transmission, il serait possible de normaliser la longueur du fragment central dans le but de décaler linéairement la valeur de la fréquence de résonance. Finalement, l'expression (4.6) est simple, précise pour des fragments de lignes internes de longueur de l'ordre de $\frac{\lambda_g}{8}$.

Afin de valider les qualités du matériau proposé, un résonateur uni périodique disposé sur une structure de type CPW TL a été conçu et implémenté comme l'indique la figure 4.3.

Le substrat utilisé est de type RT/6010LM Duroid ayant une constante diélectrique de 10,02, les pertes tangente de 0,0023 et une épaisseur de 0,635 mm. La fréquence de résonance équivalente vaut 3,4 GHz. Ainsi donc, en utilisant (4.6), les fragments de lignes ouvertes et fermées au sein du résonateur valent 4,20 mm. Conduisant à $\varepsilon_{eff} = 6.89$ identique à la valeur de la permittivité propre à une structure CPWTL à masse finie et de même dimension que le fragment interne.

La figure 4.4 décrit les paramètres de mesures et simulation du matériau proposé. Le logiciel IE3D (simulateur d'ondes électromagnétique) basé sur la méthode des moments

est utilisé pour la simulation du métamatériau proposé. La fréquence de résonance est obtenue à 3,35 GHz assez proche de la valeur théorique obtenu pour f=3,4 GHz. Le léger décalage entre les mesures et la simulation est dû à l'effet parasite des discontinuités au sein de la structure CPW TLs. Cependant, cette discontinuité a un effet négligeable sur les performances du AMM. Un léger décalage de l'ordre de 0,02 GHz entre mesures et simulations de la fréquence de résonance est illustré à la figure 4.4. Ceci peut être dû aux erreurs de fabrication.

Le tableau 4.1 résume les caractéristiques simulées et mesurées de l'AMM proposé. La bande passante à 3 dB et le facteur de qualité Q peuvent être facilement contrôlés étant donné leur lien direct avec les capacités et inductances d'accord au sein de l'AMM. En plus de l'estimation précise de ses fréquences de résonance, le dispositif proposé montre de très bonnes valeurs de pertes d'insertion (> 10 dB), de pertes de retour (<2,5 dB) ainsi que celle du facteur de qualité Q (> 20). Par conséquent, il peut être un excellent candidat pour des circuits résonants micro-ondes.

Conformément à [2], la fréquence de résonance d'une cellule carrée de SRR classique ayant les mêmes dimensions que le métamatériau AMM proposé, et chargé sur le même CPW TL, est de 4,36 GHz. Par conséquent, le dispositif MSA proposé a un facteur de réduction de la taille de 23,62% par rapport au facteur découlant d'une S-RRF classiques.

Chapitre 5: Applications des Inclusions à base de ligne de transmission (TL) proposées

Dans le but d'examiner la capacité inhérente propre aux inclusions à ligne de transmission proposées dans cette étude, deux exemples d'applications ont été réalisés et décrits dans ce chapitre, il s'agit d'un filtre passe-bande bi-bande et de deux coupleurs à branche en lignes hybrides. L'inclusion génère une réponse bande étroite de type rejecteur de bande pour ce qui est du premier dispositif réalisé, tandis que pour le second, il est observé un effet de miniaturisation. Les résultats de mesures et de simulation propres à l'inclusion de type ligne de transmission et aux deux applications mentionnées plus haut sont en parfait accord. Le filtre passe-bande bi-bande (DBBS) génère une très bonne réponse fréquentielle au sein de sa bande passante avec une atténuation prononcée au voisinage de cette dernière. Concernant le coupleur hybride, lorsqu'il est associé à une paire d'inclusion par branche, ces dimensions se trouvent réduites de 16,95% afin qu'il puisse résonner à la fréquence de résonance du coupleur conventionnel. Ce qui suscite tout de suite un intérêt pour l'industrie de production des composants microondes au vue de la volonté perpétuelle de miniaturiser les appareils et dispositifs électroniques et électromécaniques indispensables dans nos tâches quotidiennes.

La figure 5.1 décrit le dispositif constituant le filtre DBBS doté de quatre résonateurs sur son substrat. Le substrat utilisé pour la fabrication de ce circuit est le RT / Duroid 6010 ayant une constante diélectrique de 10,2 et une épaisseur de 0,635 mm. La figure 5.2 présente les paramètres de dispersion simulés et mesurés du filtre. Une nette concordance est observée en ce qui concerne les résultats simulés et mesurés. Les tableaux 5.1 et 5.2 indiques entre autre la convergence entre les résultats théoriques et pratiques.

Il existe deux zéros de transmission autour des fréquences 1,6 GHz et 2,2 GHz, chacune d'elle décalées d'une valeur inférieur à 0,05 GHz par rapport à la simulation. D'autres caractéristiques telles que les pertes d'insertion (> 25 dB), les pertes de retour (<2 dB), les taux d'atténuation au voisinage de la résonance (> 200 dB / GHz), et le facteur de qualité (> 10) propres à chaque bande illustrent la haute performance du filtre proposé.

Un semblable de la structure à inclusion SRR, appelé SRR complémentaire (CSRR), présentant une permittivité négative a été introduit dans [7]. Une TL chargé par ce résonateur se comportera comme une ligne à retard, en d'autres termes, la longueur électrique d'une ligne de transmission à dimensions constantes augmente lorsqu'on effectue une gravure consistant à le charger par une structure CSRRs au niveau de son plan de masse. Par conséquent, il est utile d'employer ce type de ligne de transmission dans des circuits à micro-ondes afin de réaliser des applications de type miniaturisation des composants.

Dans cette section, nous proposons deux nouveaux coupleurs directionnels hybrides (HBLCs), qui ont la particularité d'avoir chacune de leurs branches chargée par une ou deux cellules de métamatériaux de type AMM complémentaires. Leur fréquence de résonance a été choisie pour être suffisamment loin de la bande passante des HBLCs afin d'éviter d'être dans la zone de réjection des résonateurs complémentaires disposés au niveaux des lignes desdits coupleurs. La longueur électrique de chaque branche peut être ajustée en modifiant le nombre de résonateurs chargés ainsi que la distance entre eux dans le cas où ils sont plus de deux par branche. Cette séparation détermine le couplage magnétique et électrique entre les cellules adjacentes garantissant plus de flexibilité de conception dans le contrôle du facteur de miniaturisation. Il peut être établit que plus le nombre de résonateurs chargés par branche augmente plus la

longueur électrique de la ligne de transmission augmentera et ainsi donc une réduction conséquente des dimensions du composant sera obtenue (car pour compenser l'augmentation de la ligne électrique due à la présence des métamatériaux sur le plan de masse, il faudra par compensation réduire les dimensions des lignes du dispositif conventionnel dépourvue de la charge par ceux-ci).

Chapitre 6: Inclusions de type Métamatériaux Double Résonance basées sur des Lignes de Transmission Composites de type main droite/ main gauche

Ce chapitre fait l'objet de la conception et la réalisation des nouvelles inclusions résonantes bi-bandes dotées de lignes de transmission composites de type main droite/main gauche. L'inclusion proposée repose sur une nouvelle technique hybride combinant les approches de conception de métamatériaux de type résonateur à annulaires fendues (SRR) avec celle des métamatériaux de type composite main droite/main gauche. Le fait de combiner les techniques propres à la réalisation des cellules (SRR) à celle utilisée pour les métamatériaux composites a la particularité de généré une dualité pour ce qui concerne le phénomène de résonance et ses bandes. La technologie de l'inclusion a été inspirée de celle du prototype basé sur les lignes de transmission proposé précédemment à la section 4.1. Afin de s'assurer de la non dépendance en ce qui concerne le contrôle des deux fréquences de résonance générées par la nouvelle inclusion proposée, une association spéciale des branches main droite et main gauche pour chaque élément passif faisant partie du dispositif a été entreprise. La structure proposée est ensuite utilisée pour la conception de deux types d'antennes. La première antenne est une antenne à ligne de transmission coplanaire bi-bande alimentée par un pli de coin unique rayonnant à des fréquences 3,5 et 6,5 GHz. La dualité point de vue de fréquence de rayonnement de l'antenne susmentionnée est conséquente des propriétés bi-bande qu'ont les lignes de transmission de type main droite/main gauche composites. En seconde intension, il a été conçu une antenne encochée bi-bande ultralarges bandes dotée de deux bandes de réjection étroites centrées aux fréquences respectives de 6 GHz et 9 GHz. Les mesures et les simulations des paramètres S réalisées sont en parfait accord. En plus, les diagrammes de rayonnement, les gains ainsi que les valeurs de pertes d'insertion associées auxdites antennes aux fréquences de

résonance attestent la potentialité de l'éventuelle utilisation de ces nouvelles inclusions conçues dans le domaine de fabrication des dispositifs microondes.

La figure 6.2 illustre l'effet générée par l'inclusion proposée. La partie main gauche (LH) de chaque élément de type CRLH-TL est constituée de deux condensateurs connectés en série (C_L), séparés par une inductance montée en dérivation (L_L). D'autre part, la partie main droite (RH) est réalisée à base d'une ligne de transmission classique. L'inclusion résonne donc en présence d'une excitation consistant à l'injection de deux ondes guidées subissant au préalable un déphasage respectif de 45° et 135° en présence des lignes ouverte et fermée. La paire de phase non harmonique observée aux premières et secondes fréquences de résonance a été déterminée analytiquement et comparée aux résultats expérimentaux.

La figure 6.5 illustre le comportement des paramètres S mesurés et simulés de l'inclusion proposée et la table 6.1 indique ses paramètres de performance.

Chapitre 7: Postface

Cette thèse a porté sur l'implémentation de nouveaux résonateurs de type métamatériaux par utilisation de la technologie des lignes de transmission coplanaires à structure LC. Les nouveaux modèles de métamatériaux mis sur pied ont permis l'obtention des nouvelles propriétés attrayantes dégagés par les structures en ligne de transmission CPW. Le comportement des inclusions à la fréquence de résonance a été mis en évidence par les processus de modélisation, simulation et mesure, permettant la validation du travail entrepris dans ce sens.

Une nouvelle approche de conception combinant les deux techniques mentionnées dans le précédent paragraphe a été considérée afin de mettre sur pied un résonateur hybride. Le résonateur hybride obtenu a l'avantage de présenter une dualité de bande de fréquence pour lesquelles le phénomène de résonance est observé et ajustable. Deux conceptions d'antennes qui ont utilisées l'inclusion double résonance ont été conçues. Il a également été question dans cette thèse de mettre sur pied un modèle théorique à même de permettre la prédiction des paramètres S du dispositif résonateur. Des résultats découlant dudit modèle théorique, une concordance notoire a été observée par comparaison aux mesures expérimentales ainsi qu'aux résultats découlant des simulations. Dans l'idée de mettre en applications les très satisfaisantes propriétés des cellules résonantes mises sur pied, deux antennes ont été conçues à cet effet. Les résultats intéressant ont permis de valider l'ensemble du travail proposé.